

12-2021

## **TOWARDS AUTOMATION OF ALUMINUM CELL RAMMING PROCESS**

Maryam Salem Mohamed Alkaabi

Follow this and additional works at: [https://scholarworks.uaeu.ac.ae/all\\_theses](https://scholarworks.uaeu.ac.ae/all_theses)

 Part of the [Mechanical Engineering Commons](#)

---

United Arab Emirates University

College of Engineering

Department of Mechanical and Aerospace Engineering

TOWARDS AUTOMATION OF ALUMINUM CELL RAMMING  
PROCESS

Maryam Salem Mohamed Alkaabi

This thesis is submitted in partial fulfilment of the requirements for the degree of  
Master of Science in Mechanical Engineering

Under the Supervision of Dr. Khalifa Hamad Harib

December 2021

### Declaration of Original Work

I, Maryam Salem Mohamed Alkaabi the undersigned, a graduate student at the United Arab Emirates University (UAEU), and the author of this thesis entitled “*Towards Automation of Aluminum Cell Ramming Process*”, hereby, solemnly declare that this thesis is my own original research work that has been done and prepared by me under the supervision of Dr. Khalifa Hamad Harib, in the College of Engineering at UAEU. This work has not previously been presented or published, or formed the basis for the award of any academic degree, diploma or a similar title at this or any other university. Any materials borrowed from other sources (whether published or unpublished) and relied upon or included in my thesis have been properly cited and acknowledged in accordance with appropriate academic conventions. I further declare that there is no potential conflict of interest with respect to the research, data collection, authorship, presentation and/or publication of this thesis.

Student's Signature: \_



Date: \_\_\_10/02/2022\_\_\_

Copyright © 2021 Maryam Salem Mohamed Alkaabi  
All Rights Reserved

## **Advisory Committee**

1) Advisor: Dr. Khalifa Hamad Harib

Title: Associate Professor

Department of Mechanical and Aerospace Engineering

College of Engineering

2) Co-Advisor (Member): Dr. Sangarapillai Sivaloganathan

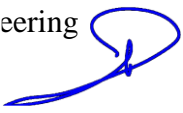
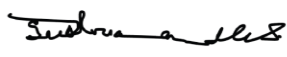

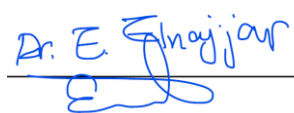
Title: Associate Professor

Department of Mechanical and Aerospace Engineering

College of Engineering

## Approval of the Master Thesis

This Master Thesis is approved by the following Examining Committee Members:

- 1) Advisor (Committee Chair): Dr. Khalifa Hamad Harib  
Title: Associate Professor  
Department of Mechanical and Aerospace Engineering  
College of Engineering  
Signature  Date 27/12/2021
  
- 2) Co-Advisor (Member): Dr. Sangarapillai Sivaloganathan  
Title: Associate Professor  
Department of Mechanical and Aerospace Engineering  
College of Engineering  
Signature  Date 10/01/2022
  
- 3) Member: Dr. Jaber Abu Qudeiri  
Title: Associate Professor  
Department of Mechanical and Aerospace Engineering  
College of Engineering  
Signature  Date 04/01/2022
  
- 4) Member (External Examiner): Prof. I. S. Jawahir  
Title: Professor  
Department of Mechanical Engineering  
Institution: University of Kentucky, Lexington, Kentucky, USA  
Signature  Date 6/1/2022

This Master Thesis is accepted by:

Acting Dean of the College of Engineering: Professor Mohamed Al-Marzouqi

Signature Mohamed AlMarzouqi Date March 31, 2022

Dean of the College of Graduate Studies: Professor Ali Al-Marzouqi

Signature Ali Hassan Date March 31, 2022

Copy \_\_\_\_ of \_\_\_\_

## Abstract

Newly installed cathode blocks in an aluminum reduction cell, expand due to rapid increase of temperature when passing high current at the start-up of the cell. High thermal stresses may result if cathode blocks are lined without gaps, and this can lead to cracking of the cathodes and failure of the cell. On the other hand, leaving gaps would cause failure due to molten metal infiltration in the gaps. To overcome these problems carbon-based ramming material is used to fill these gaps. Currently 'Filling' is carried out manually or partially automated, but this needs to be fully automated in line with Industry 4.0. Automation here means the making of an apparatus, a process, or a system to operate with minimum inputs from humans and produce consistent filling of the ramming paste. The main objective of this project was to establish the needed characteristics of ramming paste under different conditions so that one can make decisions to optimize the life of the carbon paste in the cell, while designing the automatic system. Experimental analysis was carried out to visualize and investigate the manual compaction of ramming paste in the gaps and identify forms and defects after the compaction. Building on this, characterization of ramming paste was carried out under different conditions by varying applied pressure. At room temperature it had the ability to bond and solidify under pressure with increasing young's modulus value as pressure increases. But it was observed that over-compaction initiated internal cracks in the solidified sample. Then, characterization was carried out by varying the baking temperature, so blocks were fabricated to be heated to different temperatures and then investigate their behaviors, the baking temperatures were from 200°C to 600°C. The achieved yield strength 200°C was high however similar strength was achieved at room temperature for unbaked samples as well, on the other hand, it was observed that the higher the temperature with presence of oxygen the more fragile ramming paste became. Further, to achieve consistent flow of the ramming paste into the filling, Principle of Fused Deposition Modelling was tested to extrude ramming paste using a nozzle with different nozzle profiles and various applied loads. This set of experiments concluded that ramming paste cannot be extruded using a nozzle as it gets compacted at the nozzle exit and compaction builds up on the top layers. The paste does not flow because of its strong bonding nature and the resulting consolidation under pressure. Based on the findings a machine was designed and built to extrude



ramming paste using a two-stage process comprising of, firstly a screw conveyor to positively convey the material and secondly a roller to compact the material coming out from the screw conveyor. Test runs were carried out with the machine and the results show that the machine can produce ramming paste flow, at the desired density in a consistent fashion. Based on the findings of this research and the prototype machine, industry scale machines automating the ‘Aluminum Cell Ramming Process’ can be built.

**Keywords:** Aluminum reduction cells, Ramming paste, Automation of cell ramming, Cell relining, Extrusion of ramming paste.

## Title and Abstract (in Arabic)

### نحو أتمة عملية بثق معجون الضغط (Ramming Paste) في خلية الألمنيوم

#### الملخص

تتمدد كتل الكاثود المثبتة حديثاً في خلية اختزال الألمنيوم عندما تتعرض لارتفاع في درجة الحرارة نتيجةً لمرار تيار كهربائي عالٍ عند بدء تشغيل الخلية. تنتج ضغوط حرارية عالية إذا كانت كتل الكاثود مصفوفة بدون فجواتٍ بينها، وهذا يمكن أن يؤدي إلى تشقق الكاثود وفشل الخلية. من ناحية أخرى، فإن ترك الفجوات قد يؤدي إلى فشل الخلية بسبب تسرب المعدن المنصهر في الفجوات. للتغلب على هذه المشاكل، يتم استخدام معجون قائم على الكربون لملء هذه الفجوات ويسمى معجون الضغط. حالياً يتم الملء يدوياً أو آلياً بشكل جزئي، ولكن تماشياً مع الثورة الصناعية الرابعة لا بد أن يكون ذلك مؤتمتاً بالكامل. كان الهدف العام من هذا المشروع هو تحديد خصائص عجينة الضغط في ظل ظروف مختلفة بحيث يمكن للمرء اتخاذ قرارات لتحسين عمر عجينة الكربون في الخلية. سيساعد هذا في تسريع العملية وتقليل عدد الطبقات المضغوطة. كذلك تم إجراء تحليل تجريبي لتصور وفحص كيفية انضغاط عجينة الضغط في الفجوات وتحديد هيوئتها والعيوب الناتجة. ثم، تم إجراء تجارب لتحديد خصائص معجون الضغط في ظل ظروف مختلفة عن طريق تغيير الضغط المطبق على عجينة الضغط في القوالب المستخدمة للعجينة للحصول على إعدادات التشغيل المحسنة. هذه التجارب نتجت عن قيم مرتفعة لمعامل يونج (Young's Modulus) تنتج عند ارتفاع الضغط المطبق. كذلك تتكون بداية تشققات في العينات التي تتعرض لضغط عالٍ جداً. في المرحلة التالية، تم تعريض عينات العجينة المنتجة لدرجات حرارة مختلفة وتم التحقق من سلوكها حيث كانت مقاومة عجينة الضغط للضغط المطبق عالية عند التسخين لدرجة حرارة تتراوح بين 200°C و 400°C بينما أصبحت هشّة عند الدرجات الأعلى. علاوة على ذلك، تم استخدام مبدأ الطباعة الثلاثية الأبعاد لحقن معجون الضغط باستخدام فوهة ذات رأس بأشكال مختلفة وبتغيير الضغط المستخدم لإخراج المعجون. كانت خلاصة هذه المجموعة من التجارب أنه لا يمكن حقن معجون الضغط باستخدام فوهة حيث أنه يبدأ بالتصلب عندما تقل مساحة المقطع العرضي لمسار مخرج الفوهة. وبذلك لا يتدفق المعجون بسبب طبيعته اللزجة وما ينتج عنه من تصلب نتيجة الضغط. وكان لا بد من إضافة مصدر خارجي لدفع المعجون. نتيجة لذلك، تم إجراء محاولة لبثق معجون الضغط باستخدام عملية تتكون من مرحلتين الأولى هي ناقل لولبي لنقل المواد بشكل موحد والثانية هي استخدام أسطوانة متدرجة لضغط

المادة عند الخروج. في نهاية هذه التجارب تم ضغط معجون الضغط بنجاح بالكثافة المطلوبة وبتقها عبر قناة الخروج؛ كذلك تم التحكم في كثافة المعجون للحصول على قيم مختلفة للكثافة. يمكن أن تساعد هذه النتائج في تطوير طرق الضغط الآلي لعجينة الضغط في الفجوات بين كتل الكاثود.

**مفاهيم البحث الرئيسية:** خلية اختزال الألمنيوم، معجون الضغط، أتمتة عملية التعبئة، تبطين خلية الألمنيوم، بثق معجون الضغط.

## **Acknowledgements**

I would like to express my gratefulness to my advisor Dr. Khalifa H. Harib who encouraged me to start my master's studies and welcomed the topic that I have suggested, then guided me throughout the journey despite all challenges and the emerged pandemic. I would like also to extend my gratitude to Dr. Sangarapillai Sivalogonathan for being a great mentor and for his guidance to steering the wheel of this research towards its conclusions.

I would like also to thank UAEU family for the support and guidance especially the program coordinators Dr. Tariq Darabseh and Dr. Emad Elnajjar and the testing committee.

Not to forget the support received from Emirates Global Aluminum staff in providing testing material and openly discussing the research topic and providing the required info. Special thanks goes to my direct manager and area manager for understanding my needs to fulfill the degree requirements.

I Finally would like to thank my family for all the support and the encouragement. For believing in me all the way long.

## Dedication

*To my beloved mother, the person who made me who I am today.*

*To my sisters and brothers.*

## Table of Contents

Title .....	i
Declaration of Original Work .....	ii
Copyright .....	iii
Advisory Committee .....	iv
Approval of the Master Thesis .....	v
Abstract .....	vii
Title and Abstract (in Arabic) .....	ix
Acknowledgements .....	xi
Dedication .....	xii
Table of Contents .....	xiii
List of Tables.....	xv
List of Figures .....	xvi
List of Abbreviations .....	xviii
Chapter 1: Introduction .....	1
1.1 Overview .....	1
1.1.1 Structure of the Cell .....	2
1.2 Statement of the Problem .....	3
1.3 Objectives.....	4
1.4 Scope and Organization .....	5
1.4.1 Scope .....	5
1.4.2 Organization .....	5
Chapter 2: Literature Review .....	7
2.1 General Importance of Ramming Paste .....	7
2.2 Behaviour of ramming Paste at Elevated Baking Temperatures .....	8
2.3 Physical Properties of Ramming Paste .....	8
2.4 Inputs to Test Ramming Paste Properties as Stated in other Research .....	10
Chapter 3: Manual Ramming and Material Characterization .....	12
3.1 Introduction to the Experimental Works.....	12
3.2 Investigating Manual Ramming .....	14
3.2.1 Method and Experimental Set-up.....	14
3.2.2 Observations .....	15
3.2.3 Analysis and Discussion.....	17
3.3 Characterization of Ramming Paste Under Different Applied Pressures .....	18

3.3.1 Method and Experimental Set-up.....	18
3.3.2 Observations .....	19
3.3.3 Analysis and Discussion.....	25
3.3.4 Error Analysis .....	26
3.4 Characterization of Ramming Paste at Elevated Baking Temperatures .....	27
3.4.1 Method and Experimental Set-up.....	27
3.4.2 Observations .....	27
3.4.3 Analysis and Discussion .....	31
3.4.4 Error Analysis .....	32
3.5 Ramming Paste Extrusion Through Nozzle with Different Profiles.....	33
3.5.1 Method and Experimental Set-up.....	33
3.5.2 Observations .....	34
3.5.3 Analysis and Discussion .....	38
3.5.4 Summary of the Experiments .....	39
Chapter 4: Screw Extrusion and Rolling of Ramming Material .....	41
4.1 Introduction .....	41
4.2 Method and Experimental Set-up.....	41
4.3 Motor Calibration.....	45
4.4 Mathematical Model .....	47
4.5 Observations and Results .....	56
4.5.1 Motor Calibration.....	56
4.5.2 Conveying Material without Roller.....	59
4.5.3 Error Analysis .....	60
4.5.4 Conveying Material with a Roller .....	61
4.5.5 Conveying Material with Varying Roller Height.....	67
4.5.6 Error Analysis .....	72
4.6 Summary .....	72
Chapter 5: Conclusions and Recommendations.....	74
5.1 Managerial Implications.....	77
5.2 Research Implications .....	77
References .....	79
List of Publications .....	81
Appendix .....	82

## List of Tables

Table 2.1: Selected properties of cathode ramming paste.....	9
Table 3.1: Young's modulus values at different loads .....	21
Table 3.2: Density readings for fabricated samples with different applied loads .....	22
Table 3.3: Yield for samples for corresponding applied load.....	23
Table 3.4: Yield resulting from compression test for two sets of samples (compressed with 40 kN and 45 kN).....	28
Table 4.1: Fixed parameters of the experiments .....	54
Table 4.2: Fixed parameters for roller experiments .....	55
Table 4.3: Current and torque values at speed of 50 step/s for a mass of 2 kg .....	56
Table 4.4: Current and torque values at speed of 50 step/s for a mass of 5 kg .....	56
Table 4.5: Current and torque values at a speed of 100 step/s for mass of 2 kg .....	57
Table 4.6: Current and torque values at speeds of 250 step/s for a mass of 2 kg .....	57
Table 4.7: Current and torque values at speed 500 step/s for a mass of 2 kg .....	57
Table 4.8: Current and density data obtained during compaction without the roller .....	59
Table 4.9: Density calculations for desired density of 1.2 g/cm <sup>3</sup> and screw speed of 250 step/s (2 ms step on-time) .....	65
Table 4.10: Obtained results for three samples with inputs from Table 4.9 .....	65
Table 4.11: Density calculations for desired density of 1.08 g/cm <sup>3</sup> and screw speed of 1000 step/s (0.5 ms step on-time) .....	66
Table 4.12: Obtained results for three samples with inputs from Table 4.11 .....	66
Table 4.13: Density calculations for desired density of 1.4 g/cm <sup>3</sup> and screw conveyor speed of 500 step/s .....	68
Table 4.14: Obtained values for the data presented in Table 4.13.....	68
Table 4.15: Density calculations for desired density 1.2 g/cm <sup>3</sup> and screw conveyor speed 500 step/s.....	69
Table 4.16: Obtained values for the data presented in Table 4.15.....	69
Table 4.17: Density calculations for desired density of 1.4 g/cm <sup>3</sup> and screw conveyor speed of 250 step/s .....	70
Table 4.18: Obtained values for the data presented in Table 4.17.....	70



## List of Figures

Figure 1.1: Cross-section of Hall-Herault Cell .....	2
Figure 3.1: Cathode blocks and ramming paste filling .....	12
Figure 3.2: Schematic of the mold .....	14
Figure 3.3: Manual ramming set-up with transparent mold.....	15
Figure 3.4: Grain size of ramming paste across the layers .....	16
Figure 3.5: Breaking of layers at the plane separating them.....	17
Figure 3.6: Sampling set-up fixed on MTS machine .....	18
Figure 3.7: Batch of prepared samples for testing .....	19
Figure 3.8: Sample height. ....	20
Figure 3.9: Stress-Strain curve for ramming paste compression up to 21 MPa as captured from MTS machine.....	20
Figure 3.10: Average values of young's modulus at different loads .....	21
Figure 3.11: Density values at different loads .....	23
Figure 3.12: Yield for samples at room temperature .....	24
Figure 3.13: Pattern of samples failed under compression at room temperature .....	24
Figure 3.14: Comparison of yield at different baking temperatures for samples made at 40 kN and 45 kN .....	29
Figure 3.15: Failure of samples baked at 400°C at 45 kN .....	30
Figure 3.16: Before compression test of 45 kN samples baked at 600°C .....	30
Figure 3.17: After compression test of 45 kN samples baked at 600°C .....	30
Figure 3.18: Form of failure for 40 kN samples baked at different temperatures .....	31
Figure 3.19: Set-up of extrusion experiments .....	34
Figure 3.20: Data obtained from MTS machine showing extrusion load approaching 35 kN .....	35
Figure 3.21: Result showing paste compaction in the nozzle without being extruded .....	35
Figure 3.22: Data obtained from MTS machine showing extrusion load approaching 65 kN .....	36
Figure 3.23: Result showing similar results of paste compaction in a nozzle with circular outlet without extrusion.....	36
Figure 3.24: Data obtained from MTS machine showing extrusion load approaching 31 kN .....	36
Figure 3.25: Third Trial with no extrusion up to 31 kN with nozzle of an angle of 60° and a slit outlet .....	37
Figure 3.26: Data obtained from MTS machine showing extrusion load approaching 25 kN .....	37
Figure 3.27: Forth trial with 42 mm circular outlet with no extrusion with extrusion load up reaching 25 kN .....	37

Figure 3.28: Form of ramming paste after extrusion experiments.....	38
Figure 3.29: Ramming paste at the nozzle exit sliding uncompacted.....	38
Figure 3.30: Compaction of paste comparison .....	39
Figure 4.1: Schematic of the developed extrusion and rolling machine .....	42
Figure 4.2: Circular to rectangular adaptor .....	42
Figure 4.3: Screw conveyer .....	43
Figure 4.4: Front view of two-stage compaction set-up .....	44
Figure 4.5: Side view of two-stage compaction set-up .....	44
Figure 4.6: Schematic of two-stage compaction set-up .....	45
Figure 4.7: Schematic of the motor calibration set-up.....	46
Figure 4.8: Calibration set-up showing the applied weights and the steel bar used to apply torque.....	46
Figure 4.9: Model of the screw .....	50
Figure 4.10: Side view of roller and exit channel (left), front view of roller and exit channel (right) .....	51
Figure 4.11: Plot of current change with applied loads at different motor speeds .....	58
Figure 4.12: Current readings with varying speed.....	60
Figure 4.13: Extruded ramming paste.....	62
Figure 4.14: Measurement of density for ramming paste .....	63
Figure 4.15: Current changes over time with delay of 1ms .....	63
Figure 4.16 : The inlet opening of the screw conveyer showing sample gap changes over one full revolution of the screw .....	64
Figure 4.17: Obtained densities by experiment.....	67
Figure 4.18: Density obtained with different roller height at two speeds values.....	71

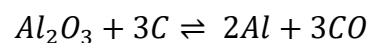
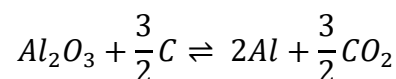
**List of Abbreviations**

ECA	Filler Materials Electrically Calcined Anthracite
FDM	Fused Deposition Modeling
G	Electrographite
GCA	Gas - Calcined Anthracite
MTS	Material Testing System
SPR	Steps Per Revolution
GR	Gear Ratio
$N_1$	Angular Velocity of the Gearbox Output Shaft (for the Screw)
$S_1$	Angular Velocity of the Screw Motor
$N_2$	Angular Velocity of the Gearbox Output Shaft (for the Roller)
$S_2$	Angular Velocity of the Roller Motor

## Chapter 1 : Introduction

### 1.1 Overview

The genesis of aluminum refining process has started with Hall-Herault electrolysis process. The process has not changed as the basic process for aluminum production over the past 100-years (Sørli & Øye, 2010). Aluminum oxide ( $Al_2O_3$ ), also called Alumina, is separated by the electrolytic process into pure Aluminum, Al and a mixture of carbon monoxide, CO, and carbon dioxide  $CO_2$ . The overall reaction could be written as



The process is implemented in an aluminum reduction cell (Pot), which consists mainly of (1) Anode, (2) Cathode, and (3) Medium “Cryolite”. In such process, high DC electricity is passed from the anode, at the top of the cell, and through the electrolyte (which is also called the bath), to the cathode at the bottom of the cell. This process causes the decomposition of Alumina (Aluminum Oxide) into molten Aluminum and carbon dioxide. During the process, aluminum anode which is hanging from the top of the cell is consumed (Clark & Duane, 1983). However, it is designed to be replaceable after being consumed with relative ease. On the other hand, the cathodes at the bottom part of the aluminum reduction cell cannot be replaced without stopping the production process and overhauling the cell. The bottom part of the cell is designed in such a way to have longer life by preventing the interaction of the

material with the cathodes and by reducing the heat losses and the over-heating in the bottom part of the cell.

### 1.1.1 Structure of the Cell

Cathodes are made in the form of blocks by mixing coke and carbon containing particles (Kucher et al., 2012; Salazar et al., 2002). The current passed through the reduction cell is directly proportional to the amount of the produced aluminum. Therefore, modern practice in aluminum production is to increase the current intensity while increasing the life cycle of the reduction cell. This is done by certain designs in the cathode region structure. The cathode region contains (1) the cathode blocks with embedded collector bars, (2) several layers of insulation materials below the cathode blocks, (3) sidewall lining, (4) steel structure, and (5) molten metal pad (Salazar et al., 2002). This structure is shown in Figure 1.1.

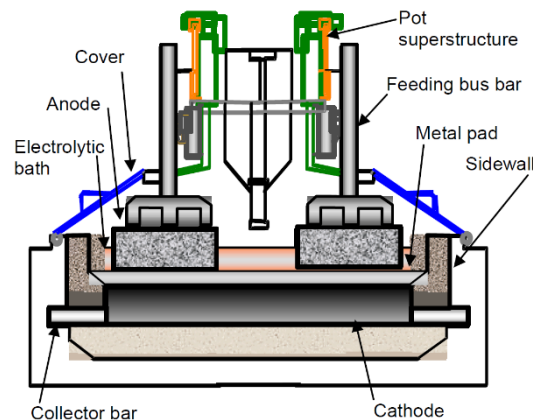


Figure 1.1: Cross-section of Hall-Herault Cell

As can be seen from Figure 1.1, the anodes are at the top and can be easily replaced from time to time. The cathode of the Aluminum cell is designed for long-term use; at least 4-10 years. During the production process, the cathodes are still

consumed and subjected to mechanical wear which is due to aluminum layer movement on the surface of the cathodes, and electrochemical corrosion, which is due to formation of carbide and sodium intercalation.

Cathode blocks expand when heated and to allow for cathode blocks expansion, the gaps between cathode blocks are filled with ramming paste consisting of carbon and graphite based on coal tar. Ramming paste serves as seal against molten constituents as well as compensating for mechanical stresses that form when cathodes expand during start-up. Since 100 to 300 electrolysis cells are connected in series, the failure and replacement of cathode blocks in one of these cells is expensive and require costly repair work (Schmitt & Christ, 2018).

In this research, 'Ramming' will be referred to the process of filling and compaction of ramming paste between the cathode blocks in the reduction cell. This process is not fully automated yet in the aluminum production industry. Hence, this is the focus of this research; to investigate issues pertaining to the automation of the ramming process.

The main tasks in the ramming process are as follows: (1) filling of the first layer, (2) compacting the filling material, (3) measuring the height of the layer, (4) cleaning the cathode block surface, and (5) filling the next layer. These steps are currently partially automated, which opens window for innovation in this area.

## **1.2 Statement of the Problem**

Development of ramming process automation requires clear understanding of (1) manual ramming process as practiced in the industry (2) the behavior of ramming

paste blocks under different operating conditions (3) the flow characteristic of ramming paste suitable for extrusions.

### **1.3 Objectives**

Main objective: The main objective of this project was to establish the characteristics of ramming paste under different conditions so that one can make decisions to improve the life of the carbon paste in the cell.

Specific objectives: To achieve the main objective the following specific objectives are identified:

1. Study the behavior of the paste, using a transparent mold with similar dimensions used by the industry, then filling and ramming the paste in layers as done in the industry.
2. Investigate the relationships between applied pressure, density of the block formed due to the pressure and formed blocks structural properties like Young's modulus and yield stress.
3. Understand and explain the behavior of the paste blocks under varying temperatures.
4. Investigate the automation of the filling using the principles of 3D-printing and other means.
5. Support the experimental work with the available knowledge on each of the topics of interest by detailed literature search.

## **1.4 Scope and Organization**

### **1.4.1 Scope**

Backed by detailed literature search and analysis, experimental investigations were carried out in the following stages:

1. Forms and defects in manual compaction were experimentally investigated by compacting the paste in a transparent mold, in a similar way as practiced in industry.
2. Characterization of ramming paste was carried out under different applied pressures on the paste, to obtain favorable operational parameters.
3. Characterization of ramming paste was carried out under varying temperature to comprehend the behavior at elevated temperatures.
4. Investigation on the ability of extruding ramming paste through a nozzle with different profiles to obtain precise material filling without waste following the concept of 3D-printing.
5. Based on the results, a prototype machine, to extrude ramming paste using a two-stage process comprising of a screw conveyor to uniformly convey the material and a roller to compact the material, was built and tested.

### **1.4.2 Organization**

The remainder chapters of this thesis are devoted to elaborating on the studies and experiments that are carried out to achieve each of the aforementioned objectives. The information that are used as baseline for this research are stated in Chapter 2, which previews relevant literature research in the aluminum process, then, the importance of ramming paste function in the aluminum cell lining, followed by



ramming paste typical behavior and properties as known today, the chapter is concluded with previous experimental works for ramming paste and how these information are used to design the required experiments for ramming paste testing. Chapter 3 is dedicated to describing the experimental works in detail. Starting with an investigation of ramming paste behavior during and after manual ramming process, which is currently the practice in the industry. This is followed by two sets of ramming paste characterization experiments with varying conditions such as applied load and baking temperature. Ramming paste samples were fabricated to perform characterization experiments. According to the obtained results, ramming paste extrusion experiment was performed at room temperature. In each experiment the method is explained, the experimental set-up, the observations and finally discussions and analysis. Chapter 4 states the steps toward development of a device to extrude ramming paste over two stages: (1) conveying of the paste with a screw conveyor, and (2) compaction with a roller. The set-up is explained, in addition to mathematical modeling, observations and discussions. The thesis is concluded with Chapter 5, where Conclusions and recommendations are presented.

## Chapter 2: Literature Review

Aluminum industry is focused on the development of pot cell technologies with higher amperages to maximize the production rate. Such developments of pot cells necessitate the development of ramming machines with better operability, process, and quality control, however a core problem for such development is ramming paste compaction (Côté & Pucella, 2015). Pot cell life ranges between 1200 to 3000 days (Prasad, 2000) which means a relining frequency of 3 to 8 years unless the cell prematurely fails because of bad sealing, cathode cracking, poor operating conditions, or lining erosion. This makes it important to enhance lining process as well as cathode blocks sealing with least. Such enhancement can be done by automation of the lining process which is the intention of this research for ramming process in specific.

### 2.1 General Importance of Ramming Paste

Ramming mixes mainly consist of metallurgical coke, petroleum coke or anthracite and tar binder (Sørli & Øye, 2010), and they are used in high temperature processes such as steel and aluminum industries. Since ramming paste can absorb deformation (Brulin et al., 2011), it is used to fill the voids between cathode blocks to absorb the expected deformation and avoid damage. That is because the thermomechanical properties of cathode blocks used in aluminum pots allow them to expand when exposed to high temperatures. This expansion will cause structural damage if cathode blocks are lined without voids between them. Ramming paste is applied to the joints between the cathode blocks and the monolithic slope and between the blocks and cell's side walls (Mirchi & Chen, 2007). The sealing of ramming paste around cathode block voids plays an important role in determining the life and energy

efficiency of reduction cells. Also, premature cell failure occurs due to molten metal infiltration into the joints filled with ramming paste (Mirchi & Chen, 2007). Infiltration can happen due to insufficient sealing of ramming paste. Furthermore, ramming paste absorbs the thermal expansion of the cathode blocks during the pre-heating and start-up process passing through series of chemical and physical changes.

## **2.2 Behaviour of ramming Paste at Elevated Baking Temperatures**

Ramming paste is initially soft and viscous due to softeners added to coal tar-based binder, then with temperature increase it swells due to devolatilization which is caused by gas reactions. Devolatilization is at its highest between 450°C to 550°C. After, during carbonization the ramming paste starts shrinking until the mass loss nearly reaches a plateau. Dehydrogenation occurs until completion of binder solidification and ramming paste is fully baked (St-Arnaud et al., 2014). This statement agrees with the observations made during sample baking.

In some studies, to avoid fume problems, cold and tepid ramming paste has been used because low ramming temperature reduce fume emissions. (Sørli & Øye, 2010).

## **2.3 Physical Properties of Ramming Paste**

Cold ramming paste is cohesive, porous, and granular, a combination of static pressure and medium frequency vibration has been determined as the best way to homogeneously compact thick layers of the paste (Côté & Pucella, 2015). Proper compaction of ramming paste will reduce the porosity of ramming paste and slow the penetration of the bath through the lining. The density of rammed layers will affect the mechanical, thermomechanical, and electrical properties of the baked paste

(Faaness & Gran, 1989). Moreover, the thickness of cathode lining in the industry is 200 mm per layer before compaction and it is suggested to perform trials with thicknesses of 300 mm and 400 mm to explore possibilities of decreasing the number of layers and to reduce lining duration thus cost (Côté & Pucella, 2015).

In addition, ramming paste is characterised as hot, tepid (room temperature) and cold type ramming paste based on the softening of the binders which are normally based on coal tar with softeners added. The use of cold and tepid ramming paste has been adopted for hygienic workplace and less environmental effect; that is low ramming temperature reduces most of fume problems (Sørli & Øye, 2010). Table 2.1 shows selected properties of the three types of ramming paste.

Table 2.1: Selected properties of cathode ramming paste

	<b>Hot Paste</b>	<b>Cold or Tepid Paste</b>	
<b>Aggregate</b>	<b>ECA, GCA</b>	<b>ECA, GCA</b>	<b>G</b>
Green Properties:			
Temperature window (°C)	140 – 180	10 – 30 or 30 – 50	10 – 30 Or 30 – 50
Green Density ( $\text{kg}/\text{m}^3$ )	1500 – 1600	1500 – 1600	1550 – 1750
Baked Properties:			
Real Density ( $\text{kg}/\text{m}^3$ )	1800 – 1900	1800 – 1900	2000 – 2200
Bulk Density ( $\text{kg}/\text{m}^3$ )	1400 – 1600	1400 – 1550	1300 – 1650
Porosity (%)	15 – 25	15 – 30	20 – 40
Crushing Strength (MPa)	25 – 40	15 – 40	5 – 25
Electrical Resistivity ( $\mu\Omega\text{m}$ )	60 – 80	60 – 90	30 – 60
Ash content (%)	4 – 10	4 – 10	0.5 – 2

Rammability of aluminum paste is also an important measure for optimum paste baking. Dry paste is subject to grain crushing risk before reaching the asymptotic paste green density<sup>1</sup>. And wet paste will cause rapid increase in green density. The normal paste is between the two extremes (Allard et al., 2016; Côté and Pucella, 2015; Støre, 2015).

Hot Ramming paste is hazardous material as it contains polycyclic aromatic hydrocarbons (PAH) which are considered carcinogenic to people exposed to it. New ramming pastes with decreased carcinogenic products are developed (Allard et al., 2011).

#### **2.4 Inputs to Test Ramming Paste Properties as Stated in Other Research**

To test ramming paste properties, Cylindrical laboratory samples of 50 mm diameter and 50 mm height are used under compaction load of 20 MPa to obtain densities between 1.35 – 1.77 g/cm<sup>3</sup> as accepted density range (Orangi et al., 2011). During testing the samples were covered with coke to avoid oxidation according to the standard ISO20202 (St-Arnaud et al., 2014). Ramming paste that is heated in a container and tested for strength found to be with less ductility as the temperature increases (Orangi, 2014). It is also difficult to model the mechanical behavior of ramming paste as it is a complex material, but simple modeling showed that it is also important to study the relation between gas induces swelling during heating and the confinement of the material (Richard et al., 2005).

---

<sup>1</sup> Green density is a density that neither result in extensive particle crushing nor liquefaction of the paste

To achieve automation of ramming paste compaction process, it is important to start with understanding the behavior of ramming paste when manually rammed. To the best of authors' knowledge, there is no such information in the literature; so, this study is initiated with an experiment to visually illustrate the manual compaction of the ramming paste. In the next stage, to study the material, ramming paste samples were fabricated using MTS machine and then tested. The physical properties of the material were studied by varying the applied load to the samples and the baking temperature of the samples. Following these studies, the concept of Fused Deposition Modeling (FDM) is adopted to extrude the material by using a nozzle (Nerella et al., 2019). In FDM, the material is passed through a heated nozzle converting it to molten state as it reaches the melting temperature (Awasthi & Banerjee, 2021). To apply FDM, it is important to study how the material behaves when heated to determine the best temperature for extrusion if required. Therefore, experiments that involve baking of samples under controlled conditions were conducted at UAEU labs as mentioned earlier. Extrusion experiments however were conducted at room temperature since dehydrogenation of the samples was observed during baking. An important conclusion was drawn; that ramming paste does not flow as expected through a nozzle. So finally, to transport ramming paste at a steady flow and with a controlled rate, a screw conveyor was used to provide flow as it is best for granular material (Owen & Cleary, 2009).

### Chapter 3: Manual Ramming and Material Characterization

This Chapter consists of 5 sections describing the experimental methods and the investigations carried out in this research. It starts with (1) an overview of all experiments then, (2) describes investigation of manual ramming process, followed by characterization of ramming paste physical behavior at (3) different applied pressures, and at (4) different baking temperatures, and finally an experiment to (5) extrude compacted ramming paste through a nozzle. Each section describes the observations and results analysis for easy comprehension.

#### 3.1 Introduction to the Experimental Works

To carry out this study, it is important to refer to the current practice of ramming paste application in the industry, the process can be described as shown in Figure 3.1. As illustrated in the figure, insulation material is first lined, followed by cathode blocks lining. The joints (gaps) between the cathode blocks are filled with ramming paste and similarly the gaps between the blocks and the side walls. Ramming paste is then compacted to seal the joints.

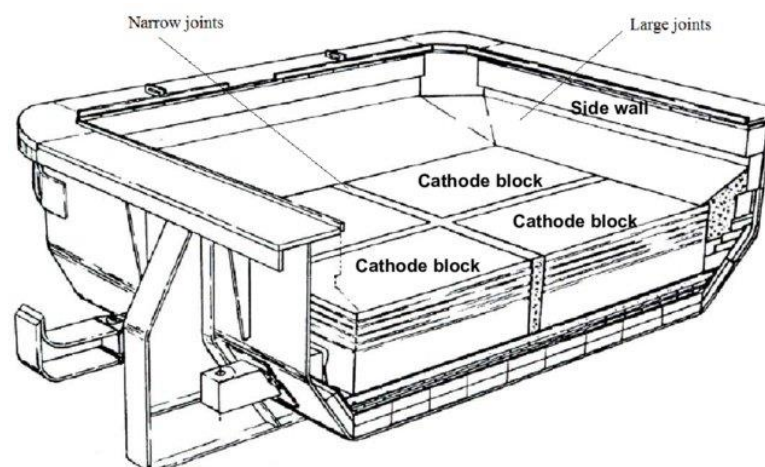


Figure 3.1: Cathode blocks and ramming paste filling

Pot dimensions of  $1320 \times 4350 \times 14896$  mm and cathode blocks of dimensions  $3800 \times 445 \times 480$  mm requiring 28 cathodes, which are considered in this research. The joints therefore are of dimensions  $40 \pm 2$  mm. The joints are made up of ramming paste filled and rammed in five layers. The objective of the first experiment is to see the filling and its characteristics.

In addition, according to literature Thickness of cathode lining in the industry is 100 mm per layer before compaction and the acceptable density range is  $1.35 - 1.77$  g/cm<sup>3</sup>.

After investigation of manual ramming, another set of experiments is designed to characterize ramming paste. To perform the experiment, ramming paste laboratory samples were fabricated in accordance with literature review findings which stated that laboratory samples can be created by using a cylindrical mold of 50 mm diameter and 50 mm height with compaction load of 20 MPa (approximately 40 kN), these inputs result in density within the acceptable range of  $1.35 - 1.77$  g/cm<sup>3</sup>. After samples fabrication, the first set of experiments was carried out to study the characteristics of ramming paste with changing applied loads. Tensile test was performed, young's modulus was calculated as well as the density of the obtained samples.

After testing of ramming paste with varied loads at room temperature, experiments for characterization of heated ramming paste samples were also carried out. But as stated in Chapter 1, according to ISO20202 standards, the samples should be covered with coke to avoid oxidation. However, in these tests the material was not covered during heating to observe the effect of baking on the samples. Finally, the strength of heated samples was tested.



The next experiment is designed with adoption of 3D-printing Fused Deposition Modeling (FDM), in which a nozzle is used to extrude ramming paste. Since ramming paste is deposited between the cathode blocks then rammed with a rammer; a precise extrusion of compacted ramming paste is assumed to be achievable by FDM. However, the extrusion was decided to be done without baking based on obtained results from the previous experiments, this is explained in the coming sections.

## 3.2 Investigating Manual Ramming

### 3.2.1 Method and Experimental Set-up

A mold was built using a transparent material, a steel rammer was also fabricated to manually compress the ramming paste. The ramming process was designed to have 5 layers of 100 mm height, at after-ramming density of  $1.4 \text{ g/cm}^3$  shown in Figure 3.2.

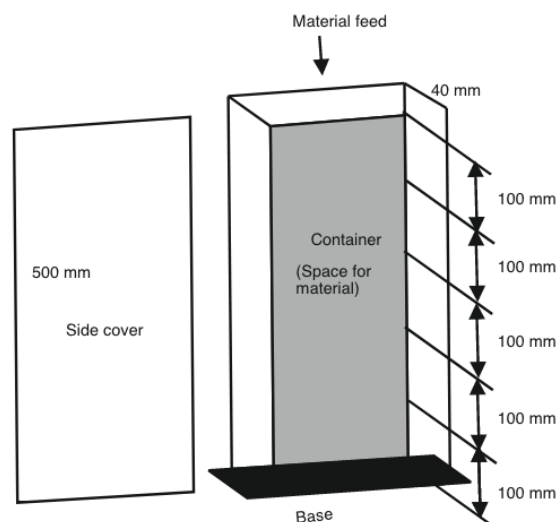


Figure 3.2: Schematic of the mold

One face is removable and secured with C-clamps as shown in Figure 3.3 to allow the extraction of the compressed ramming paste from the mold after ramming. Three layers of ramming paste were compacted manually using a steel rammer, three layers were only tested instead of five for demonstration purposes. Each layer was compacted to a height of 100 mm using 950 g of bulk material. The height of each layer is marked before the manual ramming to trace the layer movement as another is added, the first and second layers are shown in Figure 3.3.

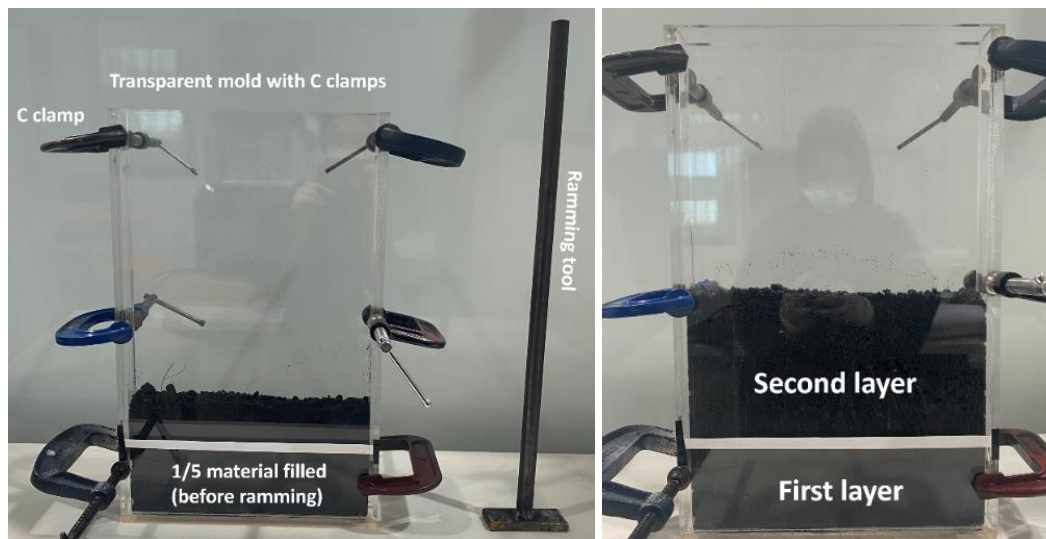


Figure 3.3: Manual ramming set-up with transparent mold showing (a) first layer filling (b) second layer filling

### 3.2.2 Observations

The densities of the layers from bottom to top were 1.57, 1.55 and 1.41  $\frac{g}{cm^3}$  respectively with manual ramming.

The number of strokes varied with varying applied force; the strokes were 95, 39 and 50 for each layer as ramming process was controlled by the resulting height of each layer.

Lower rammed layers continued to compact as other layers are added and rammed. As illustrated in Figure 3.4, it is visually noticed that the ramming paste grain size varied across the layers showing finer grains at the bottom layers compared to the top.

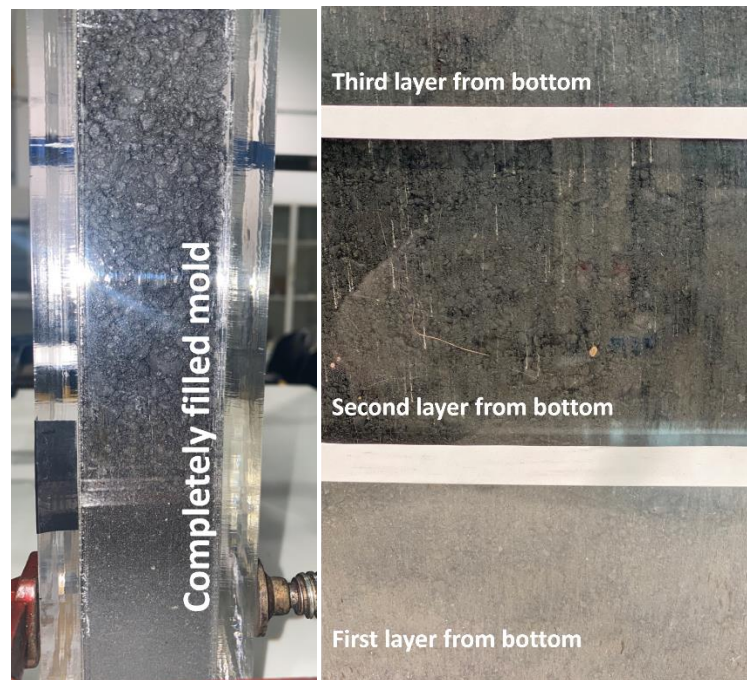


Figure 3.4: Grain size of ramming paste across the layers

Compacted ramming paste layers remained separated at the plane between each compacted layer and the following; namely the layers did not bond. Separation line was visible on the surface of rammed paste as shown in Figure 3.5. It was easy to break the layers at the plane that separate the layers.

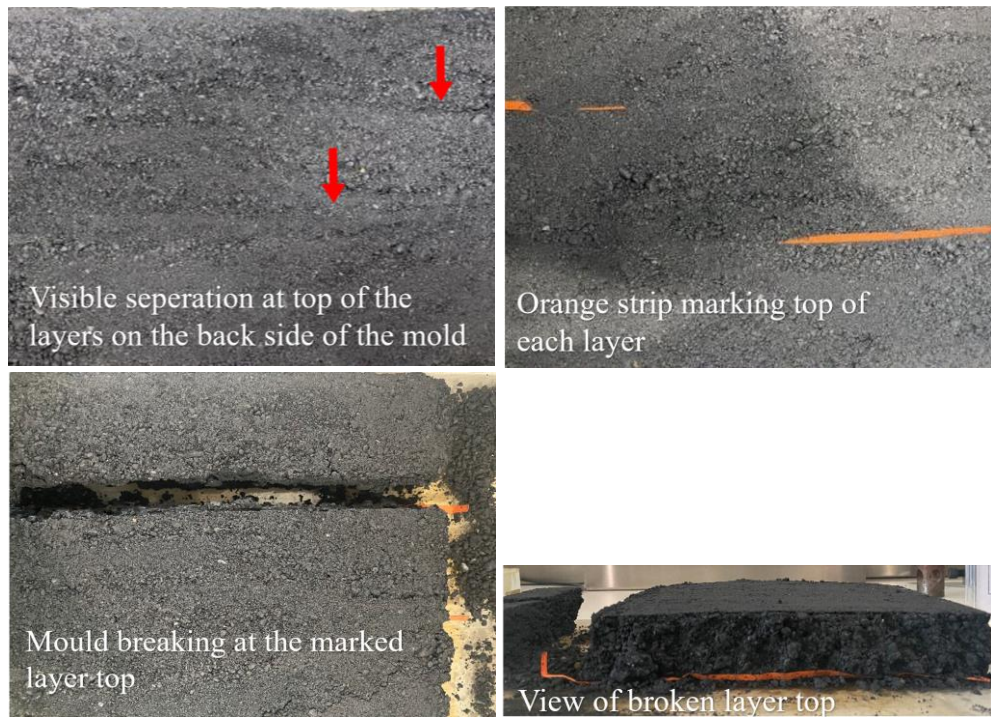


Figure 3.5: Breaking of layers at the plane separating them

### 3.2.3 Analysis and Discussion

Applied force to achieve the same level of compaction varies according to the strength of the person, which is a source of error in manual ramming.

As the ramming paste continues to compact with added pressure, different level of compaction might be required to achieve uniform density across the layers at the end of the ramming process.

At the separation plane between the layers, the grain size is different affecting the material's ability to bond and merge. Separation lines present a potential to speed up the metal infiltration and thus cause the premature failure of aluminum cell. Therefore, reducing the number of ramming paste layers will result in enhancing the life of aluminum pot.

Addition of layers adds pressure on the bottom layers which result in varying grain size across the layers and therefore the overall resultant ramming paste filling becomes heterogeneous.

### 3.3 Characterization of Ramming Paste Under Different Applied Pressures

#### 3.3.1 Method and Experimental Set-up

Set-up to fabricate ramming paste samples was designed consisting of a rammer and a steel piston with a disc inserted in the piston to facilitate taking out the rammed sample from the mold. Figure 3.6 shows the experimental set up where MTS machine was used to ram the material. All samples were produced using the same procedure that is explained in the following sections.

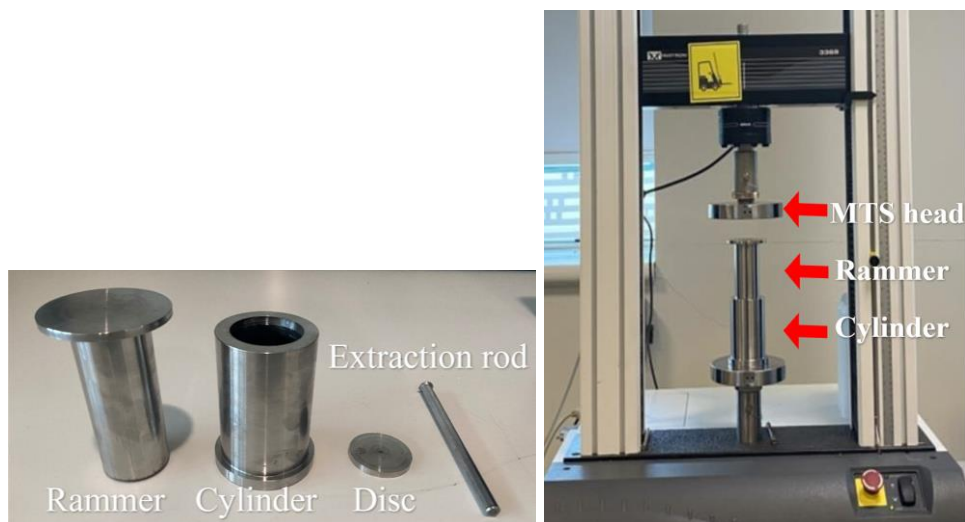


Figure 3.6: Sampling set-up fixed on MTS machine

The desired sample was obtained over two trials. In the first trial a known material quantity was used to obtain a sample and measure its height, then the result was used in the second trial to extrapolate the material quantity that is required to



obtain a sample of 50 mm height with a mold of 50 mm diameter. The obtained samples are shown in Figure 3.7.



Figure 3.7: Batch of prepared samples for testing

Compression tests were conducted on the produced samples at a rate of 1 mm/min, and the stress-strain curve was obtained to determine ramming paste's young's modulus value at different compression loads

Then, the density was calculated for 20 cylindrical samples at different loads using four samples per load. The loads to make the samples are 25 kN, 30 kN, 35 kN, 40 kN and 45 kN This is followed by the testing of the strength of the samples at room temperature.

### 3.3.2 Observations

Material with an initial weight of 85.6 g at a load of 45 kN resulted in a sample of 26.62 mm height at a compaction rate of 0.5 mm/min. to obtain the desired sample, 160.8 g of bulk material was used and resulted in a height 50.1 mm as per Figure 3.8. The obtained density in this trial is  $1.59 \text{ g/cm}^3$  which falls in the accepted range.



Figure 3.8: Sample height.

A Stress-Strain curve for compression test of unbaked samples is obtained from the MTS machine as shown in Figure 3.9. The graph shows a rapid change in the displacement at the beginning of the compaction process and then as the ramming paste is more compacted the resistance to deformation increases reaches nearly a linear relation.

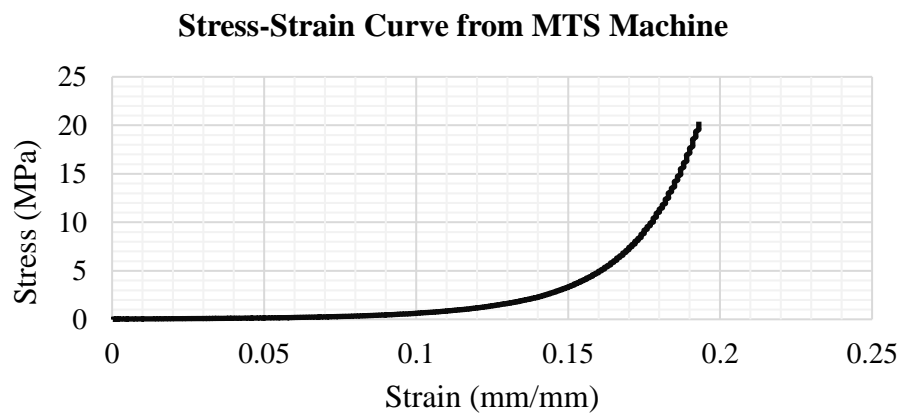


Figure 3.9: Stress-Strain curve for ramming paste compression up to 21 MPa as captured from MTS machine

The value of young's modulus was calculated at the slope of the tangent of the linear region by obtaining the slope to the tangent of the curve for each load and found between 6.5 – 12.7 MPa, the obtained values are shown in Table 3.1. The average value of young's modulus is obtained and plotted as shown in Figure 3.10.

Table 3.1: Young's modulus values at different loads

Sample No.	Load	Youngs Modulus (MPa)
1	25	6.69
2	25	6.69
3	25	6.71
4	25	6.21
1	30	8.35
2	30	8.34
3	30	8.52
4	30	8.67
1	35	10.26
2	35	10.19
3	35	9.6
4	35	10.36
1	40	11.7
2	40	12.2
3	40	11.79
4	40	11.53
5	40	10.7
6	40	10.7
7	40	11.02
8	40	10.98
9	45	12.48
10	45	12.53
11	45	12.25
12	45	12.6

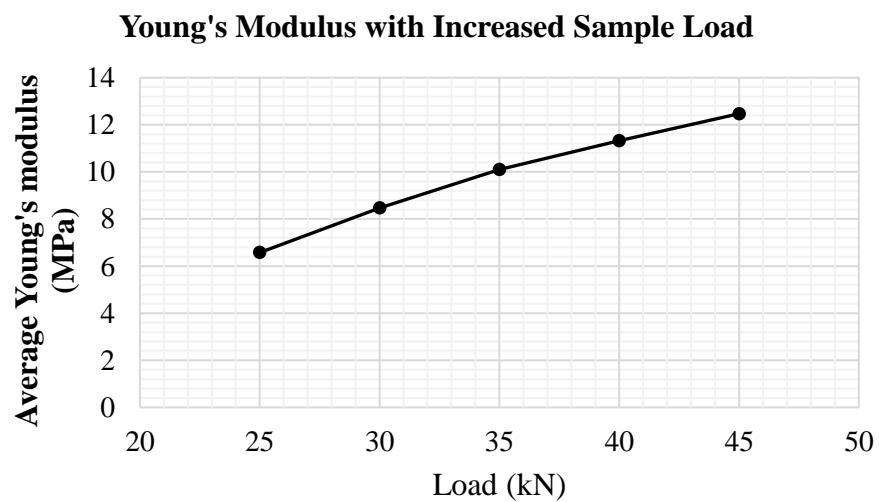


Figure 3.10: Average values of young's modulus at different loads



In addition, the density of ramming paste was calculated for the fabricated samples and shown in Table 3.2. the average density readings per load were found to be between 1.57 – 1.6 g/cm<sup>3</sup> which is acceptable. Figure 3.11 shows average densities where each value is obtained using four readings per load. The density drops between 30 – 35 kN and then increases again; however, the change is very small and still within the acceptable range.

Table 3.2: Density readings for fabricated samples with different applied loads

Applied Load	Sample No.	Height (cm)	weight (g)	Volume (cm <sup>3</sup> )	Density (cm <sup>3</sup> /g)
45	1	5.1	158.9	100.1	1.59
45	2	5.16	160.7	101.3	1.59
45	3	5.16	160.5	101.3	1.58
45	4	5.12	160.7	100.5	1.60
40	21	5.1	158.1	100.1	1.58
40	22	5.13	158.7	100.7	1.58
40	23	5.124	158	100.6	1.57
40	24	5.128	158.5	100.7	1.57
35	17	5.18	159.8	101.7	1.57
35	18	5.16	159	101.3	1.57
35	19	5.18	160.2	101.7	1.58
35	20	5.14	158	100.9	1.57
30	13	5.13	158.5	100.7	1.57
30	14	5.13	158.6	100.7	1.57
30	15	5.14	159.5	100.9	1.58
30	15	5.11	158.2	100.3	1.58
25	25	5.13	158.8	100.7	1.58
25	26	5.16	160.4	101.3	1.58
25	27	5.11	158.6	100.3	1.58
25	28	5.12	158.6	100.5	1.58

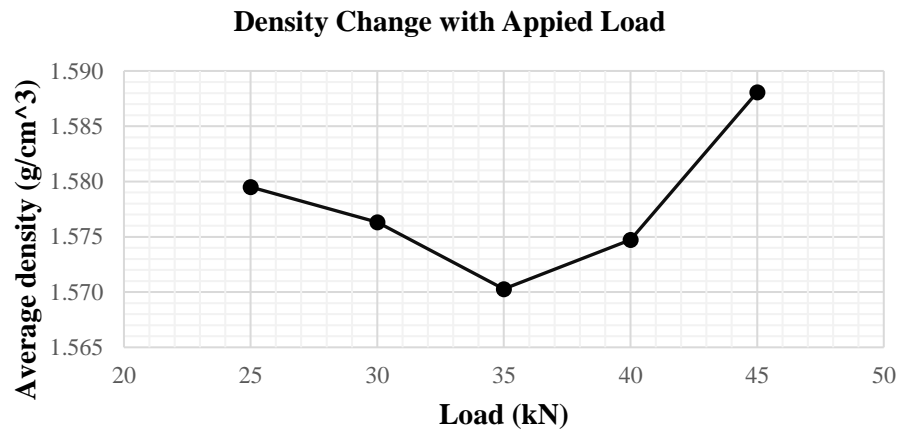


Figure 3.11: Density values at different loads

The average yield for the samples which are compressed at room temperature are obtained from MTS machine where the test stepped once cracks start initiation and load value started dropping, the max value (yield) is listed in Table 3.3 per load.

Table 3.3: Yield for samples for corresponding applied load

Applied load (kN)	Maximum load (MPa)
25	0.52
25	0.56
25	0.59
25	0.60
30	0.58
30	0.61
30	0.64
30	0.66
35	0.70
35	0.73
35	0.73
35	0.76
40	0.70
40	0.75
40	0.76
40	0.78
45	0.69
45	0.71
45	0.73
45	0.73

The average yield is shown in Figure 3.12 at each corresponding compression load. From the figure; it is observed that the samples compressed at 35 kN and 40 kN failed at higher applied loads showing higher strength than others. Whereas the sample compressed at 45 kN failed earlier than the previous sample which might mean initiation of internal crack and over-compaction of the sample.

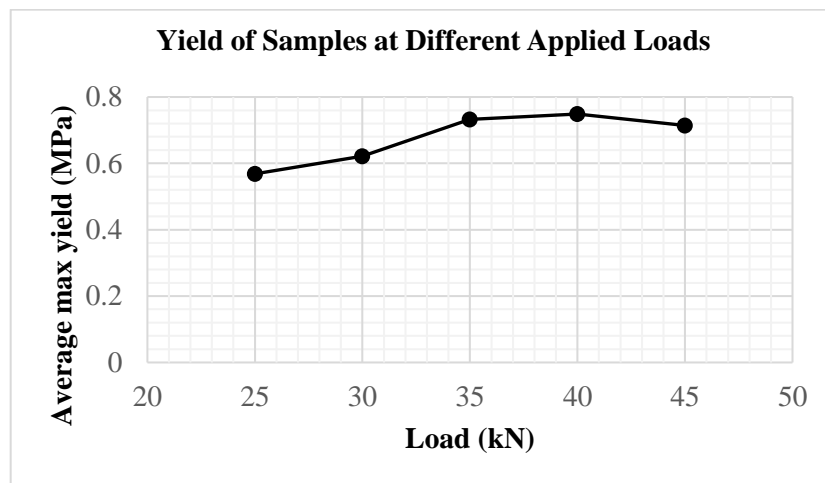


Figure 3.12: Yield for samples at room temperature

Also, the samples compressed at room temperature crack in random directions which sometimes is called failure like a matrix or concrete matrix. Typical failure pattern of ramming paste samples at room temperature is shown in Figure 3.13.

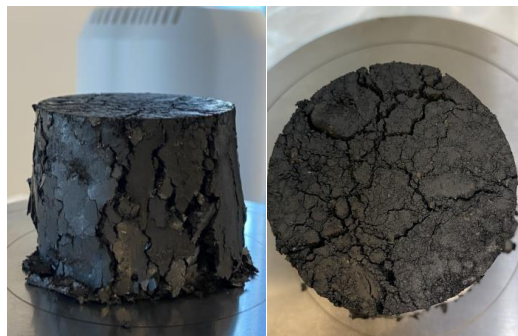


Figure 3.13: Pattern of samples failed under compression at room temperature

### 3.3.3 Analysis and Discussion

At the beginning of the compaction there is rapid change in the height. Then as the ramming paste is more compacted the resistance increases, and the force increases rapidly with a smaller change in height and starts to become linearly increasing where Hook's law can be applied to obtain the modulus of elasticity.

As expected, with higher loads applied to compact the material, young's modulus average value has increased, which means the material is getting less flexible at higher loads. According to these results it is best to use lower compression loads for better flexibility of ramming paste in case the paste was to be extruded through a nozzle

As 45 kN is the highest load that can be achieved with the set-up, the possibility of obtaining acceptable density values at higher loads was not tested. Nevertheless, obtaining such density at lower loads is preferable for lower power consumption and to avoid internal defects in the samples. The desired density can be achieved at an applied load of 35 kN. Also, the flexibility will be achieved as mentioned earlier.

Young's modulus increases as density increases. This means physical behavior of ramming paste changes as density change, therefore having different densities across the layers will also affect young's modulus values and the homogeneity of the material

In addition, the samples compressed at a load of 45 kN might have cracked internally during compaction which resulted in less strength than those at 40 kN.

### 3.3.4 Error Analysis

Error analysis for the obtained data is carried out and the results are as follows:

a. Young's Modulus calculations

Average value of young's modulus obtained for samples made with load of 25 kN is 6.58 with standard deviation of 0.2, hence the young's modulus is  $6.58 \pm 0.2$ .

Similarly for samples compressed at 30 kN the average young's modulus is 8.47 and standard deviation is 0.2 as well, so the value can be represented as  $8.47 \pm 0.2$ .

For samples compressed at 35 kN and 40 kN, the standard deviation is 0.3 for both sets and the average is 10.10 and 11.33 respectively, young's modulus in this case varies as  $10.10 \pm 0.3$  for 35 kN samples and  $11.33 \pm 0.3$  for 40 kN samples.

Finally for the samples compressed at 45 kN the average is 12.47 and standard deviation is 0.15, has young's modulus of  $12.74 \pm 0.15$ .

The values of standard deviation are smaller for samples compressed at 25 kN, 30 kN and 45 kN compared to the samples compressed at 35 kN and 40 kN which showed wider spread of the data around the mean value.

b. Density measurements

The average density obtained for measured density of all fabricated samples is  $1.58 \text{ g/cm}^3$  with standard deviation of 0.0081, the density can be represented as  $1.58 \pm 0.0081$  which is very small deviation indication repeatability of the values with narrow distribution around the mean value.

c. Yield of samples

For the compression test that is done for samples which are fabricated with load of 25 kN the obtained average yield was 1.1 with a standard deviation of 0.06, hence represented as  $1.1 \pm 0.06$ . Whereas the yield for samples compressed at 30 kN can be represented as  $1.2 \pm 0.09$  with average yield of 1.2 and standard deviation of 0.09. For samples fabricated at 35 kN, had yield with standard deviation of 0.05 and the average is 1.4, so the yield is  $1.4 \pm 0.05$ . Samples fabricated at 40 kN reached average yield of 1.5 kN with standard deviation of 0.08; hence the yield is  $1.5 \pm 0.08$ . The last compression test for samples made at 45 kN yielded at an average of 1.4 with standard deviation of 0.04, therefore the yield is  $1.4 \pm 0.04$ .

The values of standard deviations are generally small for all samples indicating spread of data over a narrow range around the mean value.

### **3.4 Characterization of Ramming Paste at Elevated Baking Temperatures**

#### **3.4.1 Method and Experimental Set-up**

Two sets of experiments for baked samples were carried out. One set of 12 samples were baked and compressed at loads of 45 kN and the second set was of 16 samples compressed at 40 kN. The strength of the samples is then tested after baking at different temperatures: 200°C, 400°C, 500°C (only for 40 kN samples) and 600°C; that is four samples per temperature with a heating rate of 2°C/min. The samples were not covered with coke to test heating effect on ramming paste characteristics.

#### **3.4.2 Observations**

The yield that is obtained at different loads for samples that are baked at various temperatures is shown in Table 3.4. The average yield is calculated at each temperature reading and then a plot is made to represent the trends.

Table 3.4: Yield resulting from compression test for two sets of samples (compressed with 40 kN and 45 kN)

Temperature (°C)	Yield for 40 kN samples (MPa)	Yield for 45 kN samples (MPa)
200	9.679	1.4
200	10.662	1.4
200	10.789	1.4
200	10.645	1.4
400	19.288	17.1
400	20.609	16.3
400	18.450	14.3
400	19.095	17.4
500	15.003	-
500	9.907	-
500	10.611	-
500	7.683	-
600	9.480	11.5
600	10.025	13.9
600	8.244	10.7
600	6.710	7.8

Figure 3.14 shows the plot of average yield against temperature for two sets of samples as mentioned previously; a comparison of the results of the strength test for heated samples at loads 40 kN and 45 kN is presented. The yield at 500°C is not shown in the plot as it was not obtained for samples compressed at 45 kN.

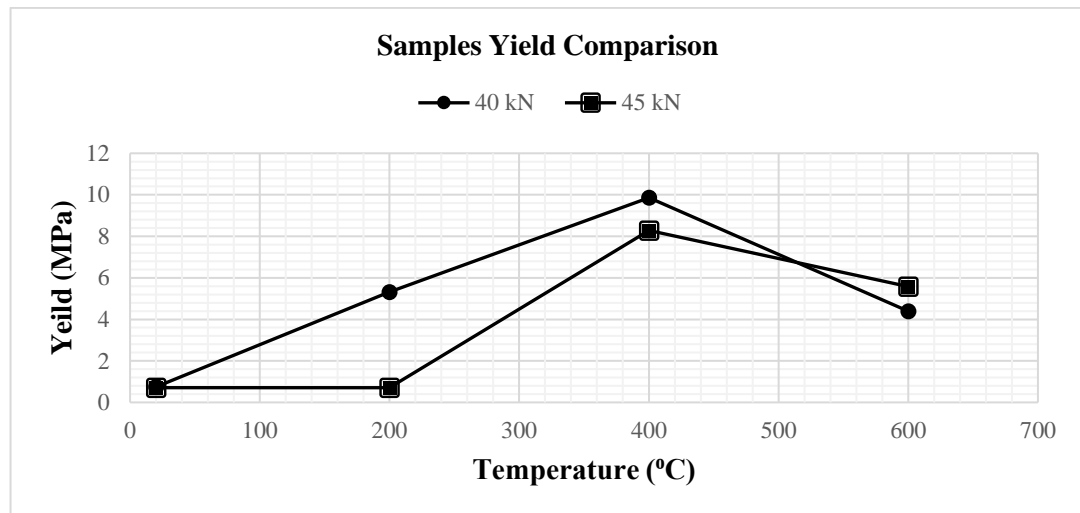


Figure 3.14: Comparison of yield at different baking temperatures for samples made at 40 kN and 45 kN

It is observed that the strength increases as the sample is baked at higher temperature, however the strength started reducing with temperature further increased beyond 400°C. For both set of samples, the samples which are heated to 400°C can withstand loads higher than those at 200°C and 600°C.; that is because the material is solidified when heated from room temperature to 200°C then further to 400°C, whilst it starts oxidizing above 400°C causing material failure prematurely. Furthermore, comparing the results at each temperature shows that the material possesses higher strength at lower compression loads, this also supports the assumption of internal crack initiation a higher compression loads.

Also, for both loads (40 kN and 45 kN), similar mode of failure was observed when the samples were baked at 400°C as shown in Figure 3.15; where the samples failed in conical shape due to shear stresses. Such failure happens when the material bonds and solidifies.



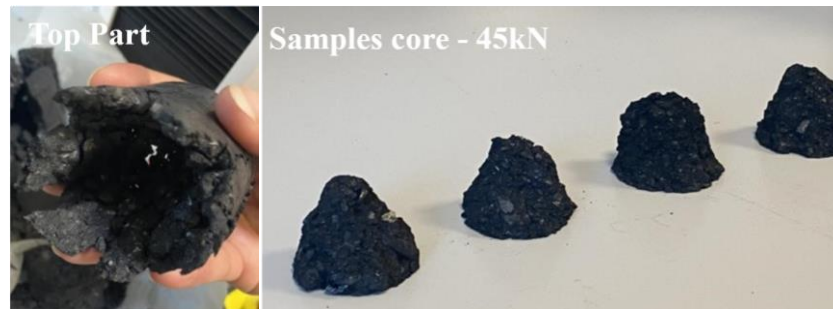


Figure 3.15: Failure of samples baked at 400°C at 45 kN

On the other hand, samples baked at 600°C were powdery and brittle as shown in Figures 3.16 and 3.17. The density for the samples ranged between 1.54 – 1.57 g/cm<sup>3</sup>. Similar results were observed for samples compressed at 40 kN as shown in Figure 3.18; the samples oxidized and became brittle.



Figure 3.16: Before compression test of 45 kN samples baked at 600°C



Figure 3.17: After compression test of 45 kN samples baked at 600°C

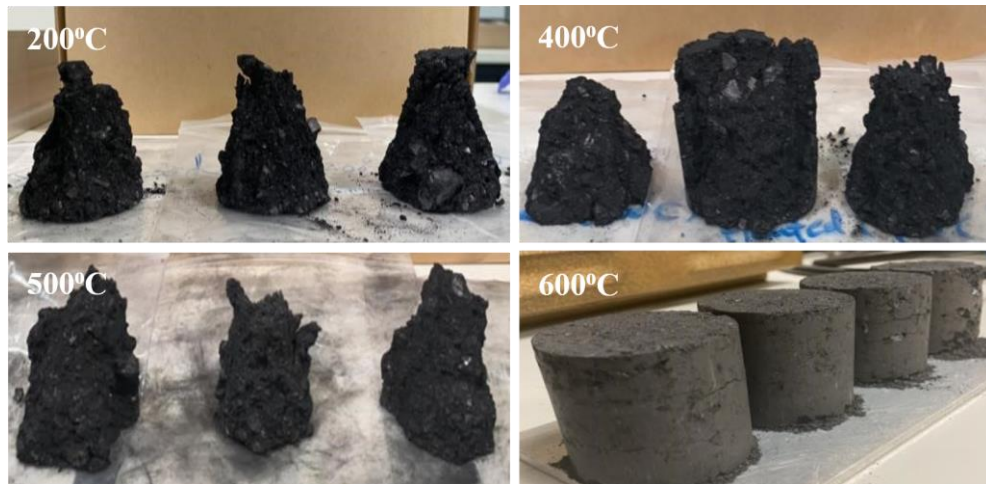


Figure 3.18: Form of failure for 40 kN samples baked at different temperatures

### 3.4.3 Analysis and Discussion

Ramming paste at room temperature behaved as a granular nonhomogeneous material similar to the behavior of cement.

The baked material showed less strength due to oxidation at 600°C where the samples became very soft and powdery on the surface. On the other hand, the samples at lower temperatures were still solid as they failed due to shear stresses similar to the solid material.

The material started to expand and bond however, it lost its strength once the oxidation took place. Both sets of samples result in similar outcomes in terms of strength and texture, the samples failed under shear stresses from 200°C to 400°C and oxidized at temperatures 500°C – 600°C. At 600°C, the samples were too fragile and powdery at the surface, the samples failed as a matrix in the test.

The yield value that was achieved at baking temperature of 200°C was also obtained at room temperature without baking meaning that samples with high strength can be achieved at room temperature as well.

These results show that the samples can be compacted at lower compression loads and at room temperature. Thus, a nozzle can be tested at room temperature for feasibility of extrusion of compacted material.

#### 3.4.4 Error Analysis

Error analysis for the obtained data is carried out and the results are as follows:

a. Yield for samples fabricated with 40 kN load

The average yield obtained for samples baked at 200°C is 5.32 MPa with a standard deviation of 0.51, hence represented as  $5.32 \pm 0.51$ . Also, the samples baked at 400°C yielded at an average of 9.86 MPa with a standard deviation of 0.91, so the value can be expressed as  $9.86 \pm 0.91$ . On the other hand, samples baked at 500°C yielded at an average of 5.5 MPa with a standard deviation of 1.56, so yield can be expressed as  $5.5 \pm 1.56$ . Finally, the samples that are baked at 600°C yielded at an average of 4.39 MPa with a standard deviation of 1.47, the yield is  $4.39 \pm 1.47$

b. Yield for samples fabricated with 45 kN load

Average yield obtained for samples baked at 200°C is 0.71 MPa with a standard deviation of 0.04, hence represented as  $0.71 \pm 0.04$ . whereas the samples that are baked at 400°C yielded at an average of 8.3 MPa with a standard deviation of 1.4, so the value can be expressed as  $8.3 \pm 1.4$  and those baked at 600°C yielded at an average of 5.6 MPa with a standard deviation of 2.53, the yield is  $5.6 \pm 2.53$

The data distribution varies over wide range and narrow range around the average yield for all baked samples. Such wide deviation might be due to the phases that ramming paste passes through during heating and due to occurrence of oxidation.

### **3.5 Ramming Paste Extrusion Through Nozzle with Different Profiles**

#### **3.5.1 Method and Experimental Set-up**

Based on the observations obtained from the previous experiments, the following is considered when extrusion with a nozzle is performed.

- a. Manual compaction observed to be creating heterogeneous material distribution with different levels of compaction across layers, which might lead to over compaction on the layers at the bottom causing internal cracks.
- b. Yield strength value can be obtained for unbaked compacted ramming paste at room temperature as high as a value that is obtained at baking temperature up to 200°C.
- c. Ramming paste is fragile when heated with presence of oxygen so extrusion experiment can be carried out without baking.

The experiment is designed to attempt extrusion of ramming material through a nozzle with the desired density. The set-up as shown in Figure 3.19 and consists of a piston as rammer, cylinder, changeable nozzle, base, and a slide to consistently convey the extruded material. Two different nozzles were made: (a) a slit outlet to extrude the material with the full length of the gap at one run and (b) a circular outlet where filling can be done with several runs.



Figure 3.19: Set-up of extrusion experiments

In this experiment four trials were carried out with different nozzle profiles. The material was filled in the cylinder and the target was to extrude compacted ramming paste with no more than 25 kN force.

The nozzle in the first trial was made with an angle of  $90^\circ$  and an outlet with a  $40 \times 20$  mm slit which has the dimension of the gap width between the cathode blocks in the considered aluminum pot, 1096 g of material was used, and the pressure was applied in such a way that the paste was rammed at a rate of 5 mm/min.

In the second trial the nozzle outlet was changed to a 20 mm circular nozzle. The degree of inclination remained on an angle of  $90^\circ$ , amount of material was fixed as well as rate of compaction.

After that, a steeper nozzle angle was used to provide a downward material flow with a nozzle of  $60^\circ$  angle and slit outlet with similar dimensions.

The final trial was done to confirm the results of extrusion tests, with a  $60^\circ$  angle nozzle having circular outlet of 42 mm diameter.

### 3.5.2 Observations

In the first trial the applied force by MTS machine was gradually increased but no material was extruded at the targeted load of 25 kN, so it was further increased

to 35 kN, ramming paste started to compact when experienced reduction in the cross-sectional area of the path. It was rammed and it took the shape of the mold as shown in Figures 3.20 and 3.21.

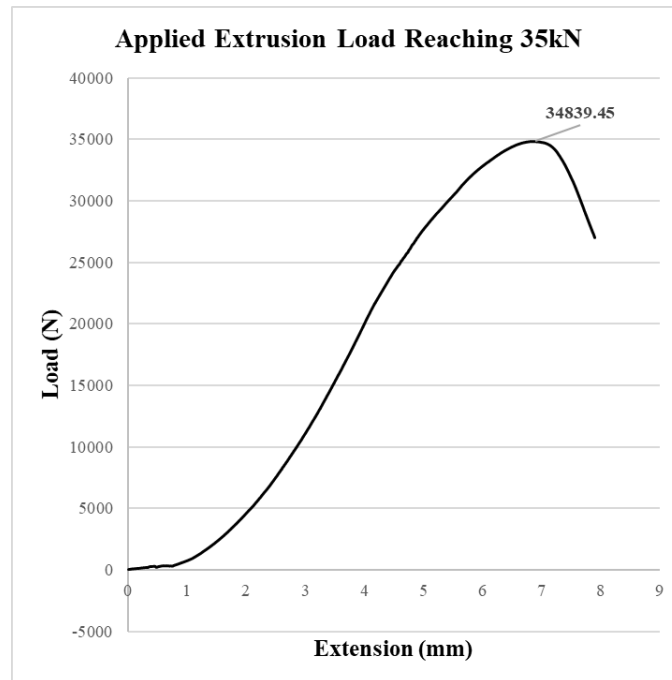


Figure 3.20: Data obtained from MTS machine showing extrusion load approaching 35 kN

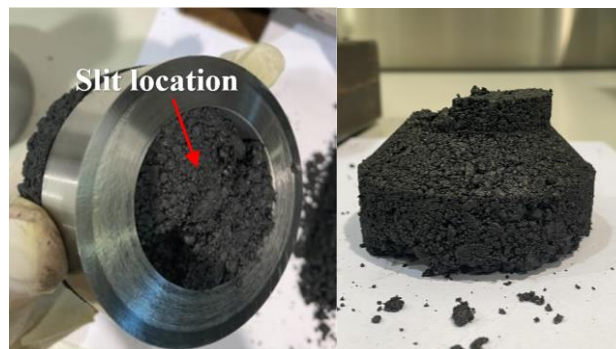


Figure 3.21: Result showing paste compaction in the nozzle without being extruded

The same scenario was repeated for the next three trials, namely the load was gradually increased, and the test was performed until the load reached 25 kN then

further increased to higher loads. However, there was no flow of ramming paste, and the material compacted taking the shape of the mold as shown in Figures 3.23 to 3.28.

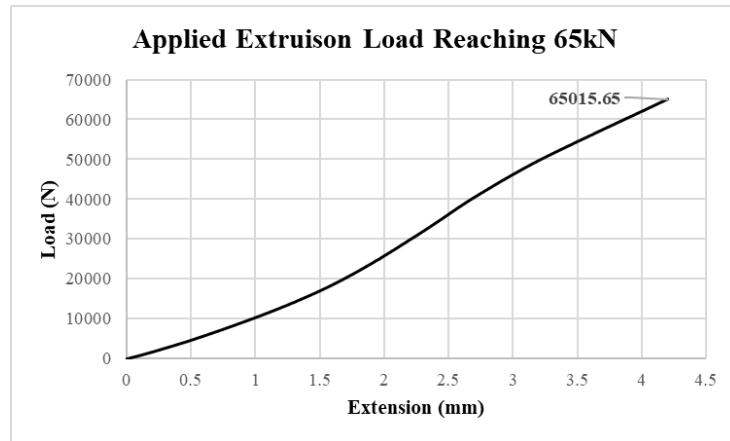


Figure 3.22: Data obtained from MTS machine showing extrusion load approaching 65 kN

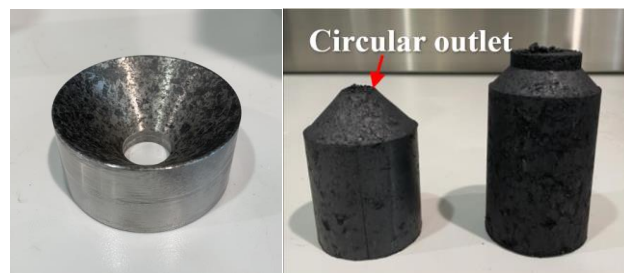


Figure 3.23: Result showing similar results of paste compaction in a nozzle with circular outlet without extrusion

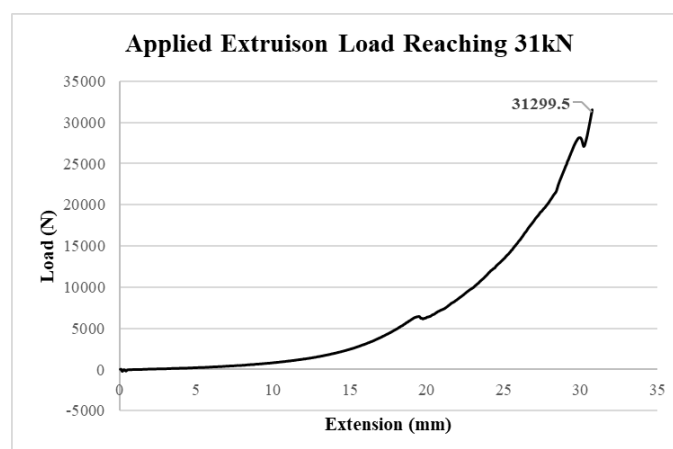


Figure 3.24: Data obtained from MTS machine showing extrusion load approaching 31 kN



Figure 3.25: Third Trial with no extrusion up to 31 kN with nozzle of an angle of 60° and a slit outlet

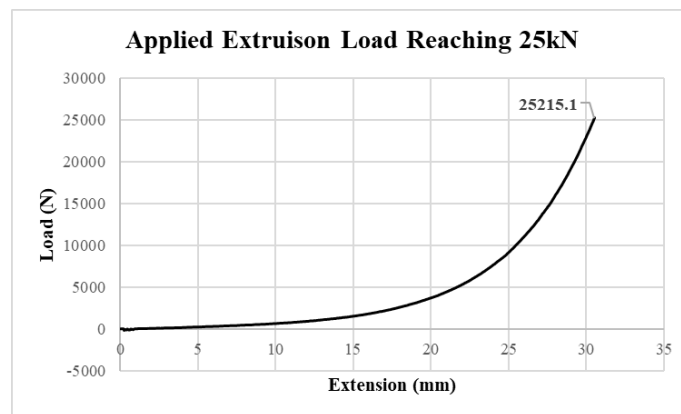


Figure 3.26: Data obtained from MTS machine showing extrusion load approaching 25 kN



Figure 3.27: Forth trial with 42 mm circular outlet with no extrusion with extrusion load up reaching 25 kN



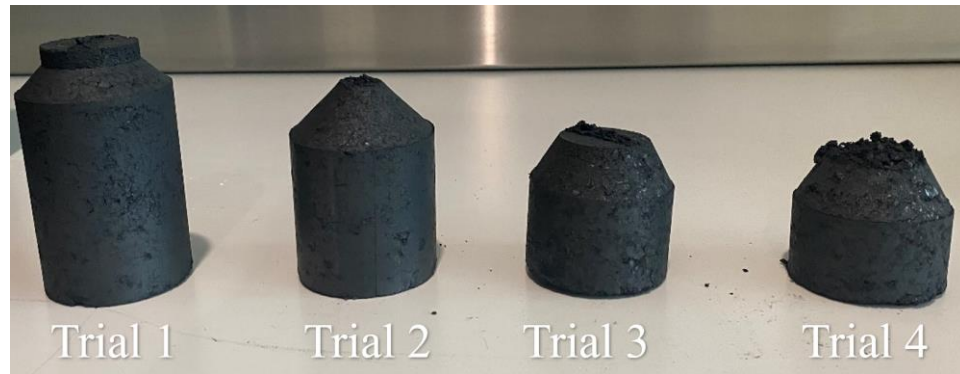


Figure 3.28: Form of ramming paste after extrusion experiments

The material at the free end was not compacted as accumulation occurred at the top layers only leaving the below layer loose and falling as loose material as shown in Figure 3.29.



Figure 3.29: Ramming paste at the nozzle exit sliding uncompact

### 3.5.3 Analysis and Discussion

This set of experiments showed that the characteristics of ramming paste does not apply to the 3D-printing approach of FDM, as the ramming paste lacks flow at room temperature and immediately compacts with the reduction in the path area. Ramming paste started compacting only when a significant change in cross-sectional

area is encountered. The material accumulated in the nozzle and then compacted without flowing out of the nozzle causing an increase in the resistance and thus the value of the applied load when compaction built up to the top.

Also, a comparison of extrusion results with the manual compaction experiments shows that the paste compacted at the bottom layers first then at the top layers when rammed in the manual compaction experiments whereas its behavior was completely opposite in extrusion experiments and the ramming paste compacted at the top layers in the nozzle leaving the bottom layers less compacted. Figure 3.30 shows that the ramming paste behaves differently when passed through a nozzle.



Figure 3.30: Compaction of paste comparison: in a nozzle (left) and manual ramming (right)

### 3.5.4 Summary of the Experiments

In summary, manual ramming can result in the desired density, however, the produced layers are heterogeneous and bottom layers are prone to initiation of internal crack due to over compaction. Uniform and controlled compaction needs to be implemented in this process.

Ramming paste samples are produced with density within accepted range, but lower loads of compaction as 25 kN is sufficient to produce sample with high yield

strengths, also at higher loads ramming paste has higher young's modulus which makes is stiffer and over compacted.

Ramming paste at elevated temperatures and with presence of oxygen becomes fragile and loses flexibility, also, when baked at 200°C the yield value is similar to that at room temperature. Hence, extrusion of ramming paste can be done at room temperature.

It is evident that the characteristics of ramming paste does not allow smooth flow of the material when extruded through a nozzle. It is viscosity and tendency to compact in restricted areas, initiated compaction at the instance of cross-sectional area reduction in the nozzle. In this case an external means to provide positive displacement is required.

## **Chapter 4: Screw Extrusion and Rolling of Ramming Material**

### **4.1 Introduction**

Following the results obtained in the extrusion experiments described in Chapter 3, it was concluded that adding flow to ramming paste was necessary to achieve extrusion. Moreover, combining compaction with flow is also required to achieve a desired density. Thus, a machine to enable flow, compaction and filling at the same time was developed, evaluated, and is presented in this chapter. The process was split into two stages: (a) an extrusion stage using a screw conveyor, followed by (b) a compaction stage using a roller. Performance analysis for the system is carried out using the obtained experimental data as outlined in the next sections

This chapter describes the machine setup developed to carry out experimental work related to extrusion and compaction of aluminum cell ramming material. The details of the developed experimental setup are described also in the next section. This is followed by analyses pertaining to the designed screw-roller machine.

### **4.2 Method and Experimental Set-up**

It was concluded from the results of the experiments that are performed in Chapter 3 that there is a necessity for external means to provide the flow of the ramming paste, and then to compact it while the paste is flowing. A plan is pursued to achieve this objective using two stages: a screw conveyor and a roller. As shown in the schematic drawing of Figure 4.1, a machine is conceptualized with two stages. In the first stage the ramming materials is fed into a screw conveyer from a hopper. It is conveyed through a screw conveyer to a circular to rectangular adapter that is shown in Figure 4.2. The material that is converted to have a rectangular cross-section is

passed through a roller stage to further compact the material to the desired density. A model is developed to predict the density by varying the parameters of the process. These include the speed of the motors and the height of the roller from the lower surface of the exit channel. The mathematical model to predict the behavior is presented in Section 4.3.

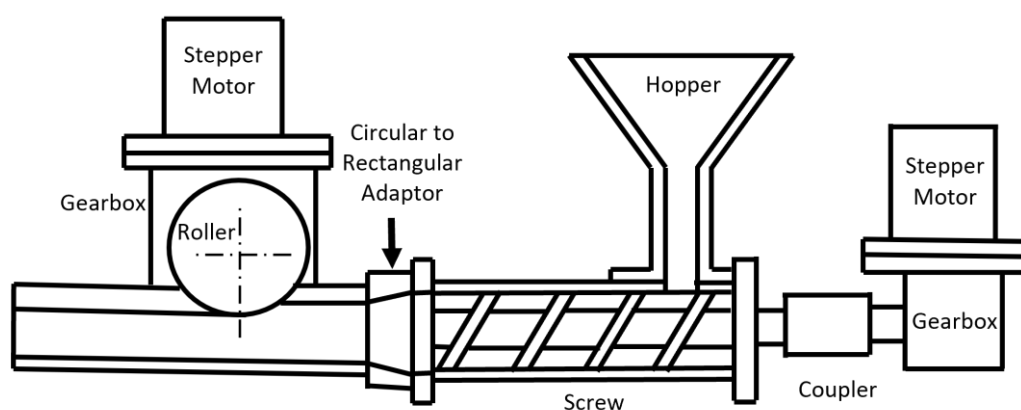


Figure 4.1: Schematic of the developed extrusion and rolling machine

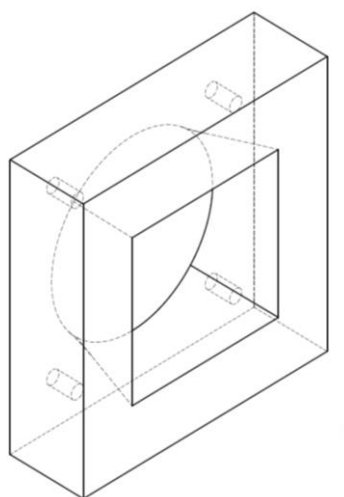


Figure 4.2: Circular to rectangular adaptor

The mechanical components of the set-up consist mainly of the screw conveyor stage and the roller stage; these components are manufactured in the UAEU workshop. The screw conveyor, shown in Figure 4.3 (A), was machined from a steel bar using a CNC turning center and on conventional lathe. It is installed inside a cylindrical tube that is capped by steel plates at the two ends as shown in Figure 4.3 (B). Four threaded tie rods are used to hold the whole assembly together with tightening nuts on both ends of the tube. All engineering drawings for the set-up are included in the Appendix.

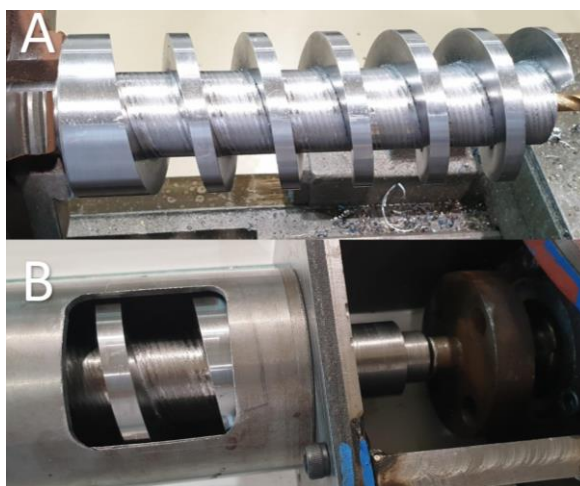


Figure 4.3: Screw conveyor (A) manufacturing lathe machine, (B) inside the cylindrical tube and connected to the motor

Figure 4.4 shows the front view of the overall assembled set-up, while Figure 4.5 provides a side view perspective. As shown in the figures, the vertical entrance tube and hopper are attached to the screw tube to provide the entrance for the material into the setup. The pressure throughout the screw conveyor seemed sufficient to transfer the ramming material through the circular to rectangular adapter that changes the exit cross-sectional area. The adapter is machined from steel stock using a 3-axis CNC milling machine on two steps. At the end of the adapter, a rectangular cross-

section channel is added to guide the extruded material and pass it through the rolling stage. In this stage, a roller that with a provision to move vertically by removal and addition of spacers below the roller is mounted at the top of the channel to reduce the exit area as desired, and thus to provide material compaction to the system; the roller height from the floor is adjusted relative to the lower surface of the flowing channel.

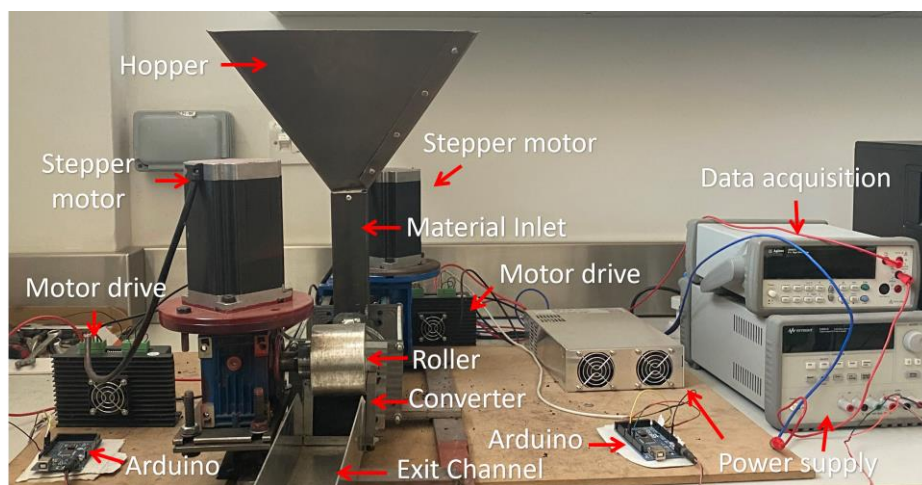


Figure 4.4: Front view of two-stage compaction set-up

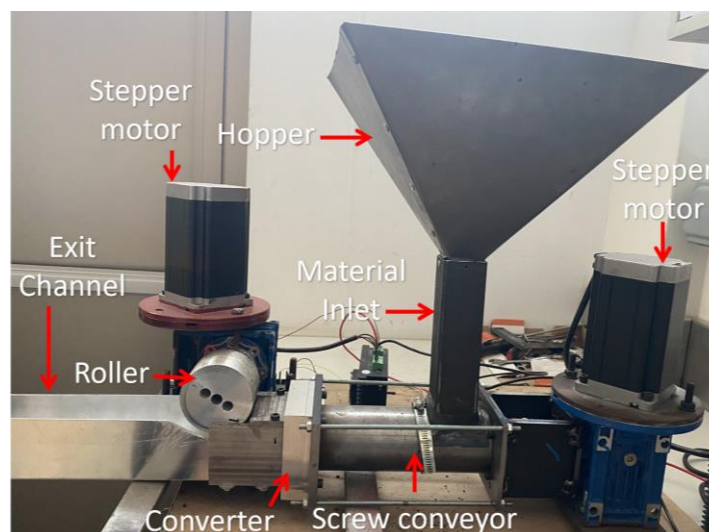


Figure 4.5: Side view of two-stage compaction set-up

A schematic of the electronic and the mechanical component of the set-up is shown in Figure 4.6. This includes the two motors, their drives, the power supply, and the data acquisition hardware. The two stages are actuated by stepper motors with gearheads that have gear ratio of 10:1 for the screw conveyor and 30:1 for the roller. The stepper motor drives were commanded by Arduino microcontroller boards that generate required pulse trains to move the motors with desired speeds and directions. The microcontroller controls the material flow rate by outputting a pulse train signal with desired frequency. Finally, a multimeter with data acquisition capability is used to measure and store the motor current data.

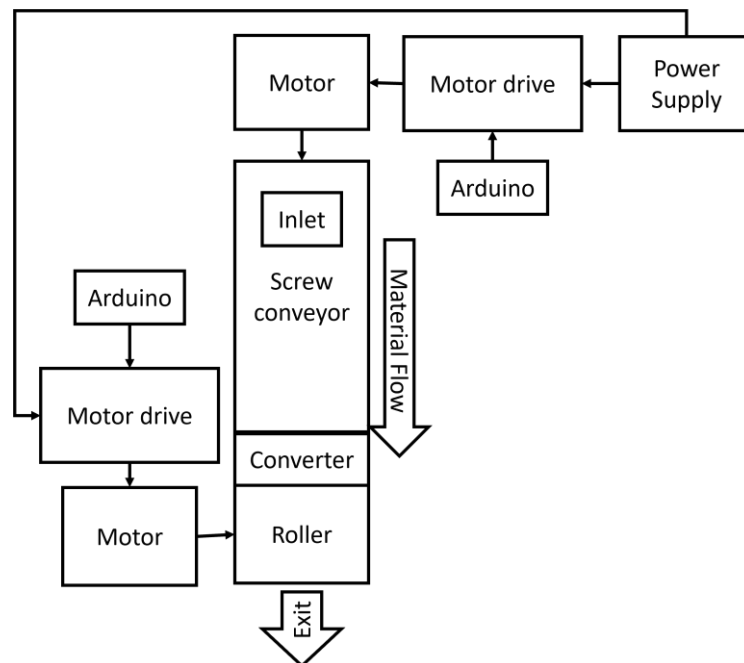


Figure 4.6: Schematic of two-stage compaction set-up

### 4.3 Motor Calibration

To estimate the motor torque that the motor exerts on the screw during extrusion, a calibration procedure was carried out on the motor to establish the relationship



between the applied motor torque, through the gearbox, and the measured motor current. A schematic drawing and a photo of the calibration set-up that was implemented are shown in Figures 4.7 and 4.8.

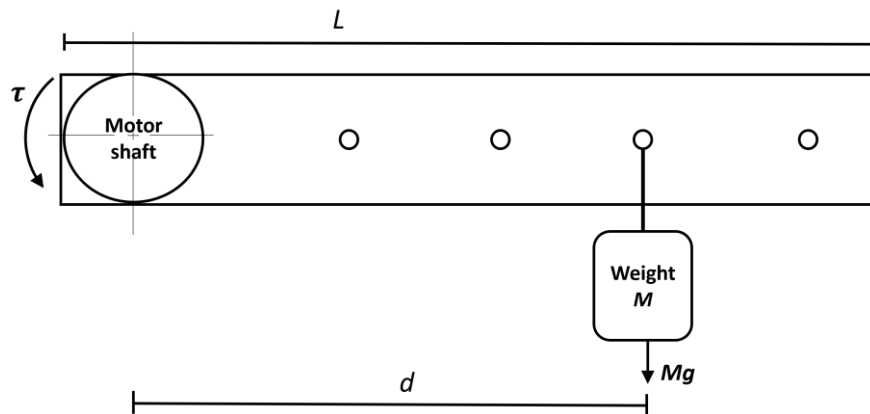


Figure 4.7: Schematic of the motor calibration set-up

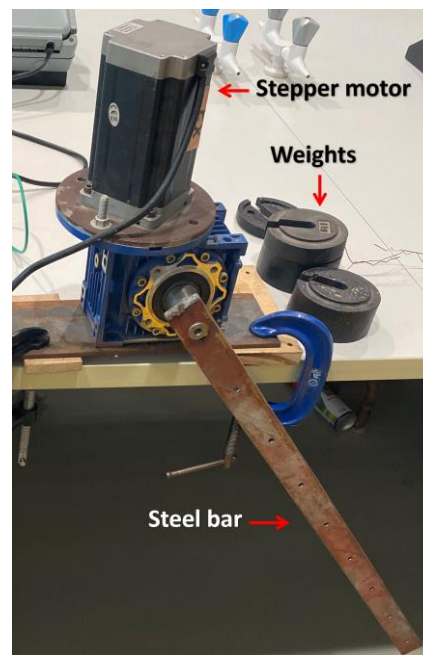


Figure 4.8: Calibration set-up showing the applied weights and the steel bar used to apply torque

The figure shows a steel bar with mass  $m$ , in kilograms fixed on the motor shaft with multiple holes drilled at fixed intervals. The holes are used to hook a standard

known load with mass  $M$  in kilograms at a distance  $d$ , in meter. The mass  $M$  and the distance  $d$  are used to get variety of torque values. The overall torque  $\tau$ , would be computed though as the sum of the torque resulting from the weight of the bar, which is represented by a concentrated force in the middle of the bar at  $L/2$ , and the hooked weight at one of the holes at a respective distance  $d$ . The overall torque is therefore expressed as:

$$\tau = \frac{1}{2}mgL + Mgd \quad (4.1)$$

A digital multimeter with data acquisition capability was connected in series with the drive on the DC power line. The current values against the corresponding torque were obtained and recorded when the motor passes through a horizontal position of the bar while moving in the upward direction (i.e against gravity).

#### **4.4 Mathematical Model**

The ramming material is fed into the screw conveyer from the hopper with a calculated homogenous density. Inside the conveyer tube, the material cross section is calculated using the screw geometry. Since the rotational speeds of the screw and the roller are considered to be known parameters, the material flow rates at these locations can be obtained from the geometry of the setup. The continuity equation is then used to calculate the output density of the material at the exit of the circular-to-rectangular adapter, as well as after passing through the compaction stage with the roller.

The continuity equation is employed as indicated below. A mass balance of the flow at the inlet and exit of the control volume is given as indicated in Equation (4.1).

$$A_1 v_1 \rho_1 = A_2 v_2 \rho_2 \quad (4.2)$$

Here, the parameters in Equation (4.2) are defined as listed below.

$A_1$  Cross-sectional area of the ramming material inside the screw conveyor,  $mm^2$

$v_1$  Axial velocity component of the screw, mm/s

$\rho_1$  Green density material entering the screw conveyor,  $g/cm^3$

$A_2$  Cross sectional area at the exit,  $mm^2$

$v_2$  Exit speed of the ramming material, mm/s

$\rho_2$  Exit density of the ramming material,  $g/cm^3$

The axial velocity component  $v_1$  is related to the angular velocity of the gearbox output shaft  $N_1$ , in revolutions/second, by the following relation

$$v_1 = P N_1 \quad (4.3)$$

where,

$P$  is the pitch of the screw

The angular velocity of the gearbox output shaft  $N_1$ , in revolution per second, and the angular velocity of the motor  $S_1$ , in number of steps per second, are related by the following relation

$$N_1 = S_1 / SPR / GR \quad (4.4)$$

where,

$SPR$  is the number of steps per revolution (400 steps per revolution)

$GR$  is the gear ratio (10:1).

The cross-sectional area  $A_1$  of the material inside the screw conveyer tube is shown in Figure 4.9. The material fills the area that results from subtracting the circular area of the root circle of the screw that has diameter  $d$ , from the inner circular area of the tube that has diameter  $D$ . The cross-sectional area of the screw flank that is perpendicular to the screw axis is also subtracted. As depicted by Figure 4.9 this area will be approximately equal to one quarter of the circular ring made by the circles  $d$  and  $D$ . In the following paragraphs, an accurate estimation of this area is performed.

The arc tangent of angle  $\psi$  can be obtained as a ratio of  $P/2$  to the diameter  $D$  as indicated in the following equation, where  $P$  is the pitch of the screw.

$$\tan \psi = \frac{P}{2D} \quad (4.5)$$

As also shown in the figure, the arc tangent of angle  $\psi$  can be obtained as indicated in the following relation.

$$\tan \psi = \frac{F}{W} \quad (4.6)$$

where,  $F$  is the flank thickness in mm, and  $W$  is the width of the flank in the perpendicular cross-sectional area of the screw in mm.

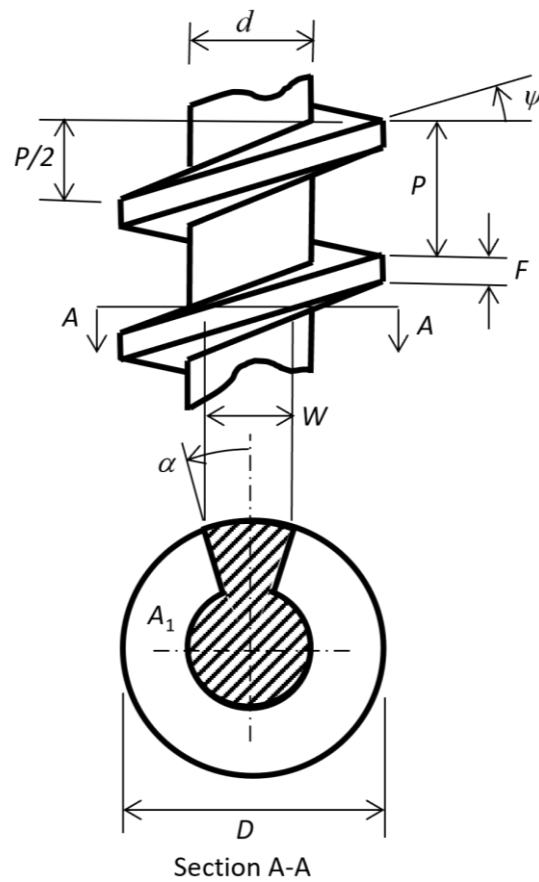


Figure 4.9: Model of the screw

Combining (4.5) and (4.6), the width  $W$  can be obtained using the following relation.

$$W = 2DF/P \quad (4.7)$$

Once  $W$  is found, angle  $\alpha$  can then be found from the following geometric relation

$$\sin \alpha = W/D \quad (4.8)$$

Now the area  $A_1$  can be derived in terms of the angle  $\alpha$  as

$$A_1 = \frac{1}{4}(\pi - \alpha)(D^2 - d^2) \quad (4.9)$$

For the following numerical values of the setup:  $d = 35$  mm,  $D = 56$  mm,  $F = 8$  mm, and  $P = 30$  mm, angle  $\alpha$  is determined as  $\alpha = 32.3^\circ$ , and therefore the area  $A_1$  is computed as

$$A_1 = 2017.8 \text{ mm}^2.$$

Development of the relations to compute the ramming material density after compaction by the roller at the exit of the conveyor is presented next. The adopted model for such computation is shown in Figure 4.10.

Where the parameters are written as indicated below.

$\omega_2$  Roller rotational speed, rev/s

$R$  Roller radius, mm

$W_2$  Width of exit channel below the roller, mm

$H_R$  Height of the roller, mm

$H$  Height of exit channel, mm

$L$  Length of exit channel below the roller, mm

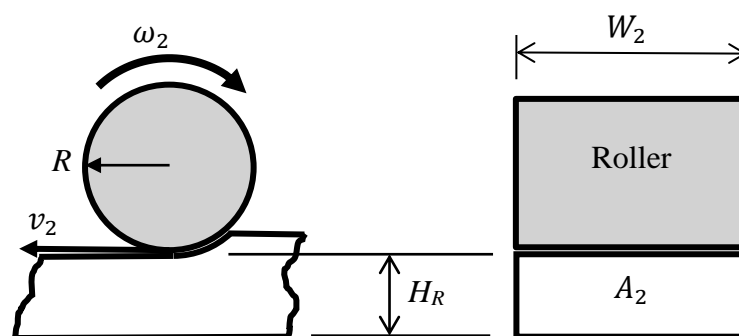


Figure 4.10: Side view of roller and exit channel (left), front view of roller and exit channel (right)

As shown in Figure 4.10, the tangential velocity component of a point on the circumference of the roller  $v_2$ , in mm/s, is obtained from the rotational speed of the roller  $\omega_2$ , in radians per second, using the radius of the roller, in mm, as indicated below.

$$v_2 = \omega_2 R \quad (4.10)$$

This tangential velocity component is used to approximate the ramming material flow velocity assuming no sliding is taking place between the roller and the ramming material. On the other hand, the ramming material is assumed to slide on the lower surface and the sides of the rectangular channel without losses. Therefore,  $v_2$ , as given by Equation (4.10), will be taken as the flow velocity of the material at the exit of the rolling stage.

In order to obtain a desired exit density  $\rho_2$ , the continuity equation is used as mentioned before. This requires availability of the exit velocity  $v_2$ . Likewise, the exit density  $\rho_2$  should be available in order to compute the exit velocity  $v_2$  using the continuity equation. This is done when a desired exit density  $\rho_2$  is sought. For this case, Equation (4.10) is used to find the corresponding angular velocity of the roller  $\omega_2$ , which is then used in programming the controller to move the roller at the required speed. The angular velocity of the motor that actuates the roller in steps per second is determined from the angular velocity of the roller as explained next. Since Equation (4.10) yields the angular velocity  $\omega_2$  in radians per second, the units can be converted to revolutions per second by dividing by  $2\pi$ . This yields the angular velocity  $S_2$  at the exit in revolutions per second as indicated below.

$$S_2 = \frac{\omega_2}{2\pi} \quad (4.11)$$

The result from Equation (4.11) is then used to find the angular velocity of the second motor  $N_2$ , in steps per second as indicated by Equation (4.12) below.

$$N_2 = S_2/SPR/GR \quad (4.12)$$

Using the calculated angular velocity, the exit velocity of the ramming paste  $v_2$  for a desired exit density  $\rho_2$ , is found by using the continuity Equation (4.2). In the preceding implementation of the continuity equation, the axial speed of the screw conveyor  $v_1$ , the density of the ramming paste at the inlet  $\rho_1$  and the cross-sectional areas at the inlet and the exit  $A_1$  and  $A_2$  respectively, are considered as known variables.

The density of the ramming paste at the inlet,  $\rho_1$  is easily estimated experimentally. The procedure is done by measuring the mass  $m_1$  in grams for the bulk ramming paste of a given controlled volume  $V_1$  in  $cm^3$ . The density  $\rho_1$  is then estimated in  $g/cm^3$  as the ratio of the mass  $m_1$  to the volume  $V_1$ .

The maximum density of the ramming paste at the exit was determined first for the case when there is no roller stage (i.e., without compaction). This was done by blocking the channel exit channel. The purpose of this is to test the screw conveyor's capability by determining the maximum density that can be achieved using extrusion alone (horizontal compaction). The density as measured for a continuous material flow without the rolling stage was found to have an average of  $1.2 g/cm^3$ .

Calculating the density of the ramming paste with the roller in place shifts the exit area to be the cross-sectional area below the roller through which the material passes and continues toward the exit. This cross-sectional area is represented by the width of the exit channel (or the width of the roller) and the height of the roller from



the floor of the exit channel. This is shown in Figure 4.10. A provision to allow this height to be adjusted on demand is made. The mass and the volume of the extruded material were obtained by measuring the mass using a material weighing scale and by using a Vernier calliper to measure the height and width of the extruded material.

The parameters in Table 4.1 are fixed parameters during all performed experiments and therefore will only be calculated once as presented in the table.

Table 4.1: Fixed parameters of the experiments

Mass of a given volume of the material at the inlet $m_1$	127 g
Volume of the material at the inlet $V_1$	146.16 cm <sup>3</sup>
Inlet density $\rho_1$	0.84 g/cm <sup>3</sup>
Channel width $W_2$	58 mm
Exit height H	59 mm
Exit area $A_2$	3422 mm <sup>2</sup>

Given the values listed in Table 4.1, the required parameters to be tested were obtained by using the continuity equation as given by Equation (4.2). A desired density of 1.2 g/cm<sup>3</sup> which is within the acceptable range, and screw conveyor motor speed set at 250 steps/s, which means a speed of  $v_1 = 1.875$  mm/s, would result in a material extrusion speed of  $v_2 = 0.76$  mm/s. This means that the screw conveyor is providing positive flow to the material and the purpose of this machine is initially fulfilled. After that, when the roller is added, the area at the exit,  $A_2$  in mm<sup>2</sup> is obtained as explained before, and accordingly the required speeds and motor input can be calculated. Table 4.2 shows the fixed parameters to be used in the calculations with added roller stage.

Table 4.2: Fixed parameters for roller experiments

Roller Radius $R$	39.5 mm
Gear Ratio GR	30
Steps Per Revolution SPR	400

Setting a roller height of  $H_R = 52$  mm, results in an exit area of  $A_2 = 3016 \text{ mm}^2$ . With desired density of  $\rho_2 = 1.2 \text{ g/cm}^3$ , and the continuity Equation (4.2), the value of the axial speed of the material at the exit  $v_2 = 0.88 \text{ mm/s}$  is achieved, and therefore the rotational speed of the roller, as calculated using (9), is obtained as  $\omega_2 = 0.022 \text{ rad/s}$ , and the angular velocity  $S_2$  as determined by Equation (4.11), will be  $S_2 = 3.5 \times 10^{-3} \text{ rev/s}$ . Hence, the speed of the motor of the roller will be  $N_2 = 11.89 \text{ step/s}$ .

These analyses show that, by setting a speed of 250 step/s as an input for the motor of the screw conveyor and approximately 12 step/s for the motor of the roller, a desired density of  $1.2 \text{ g/cm}^3$  can be obtained.

Following a similar procedure, setting the motor speed as 1000 step/s for the screw conveyor and a speed of 100 step/s for the roller motor will result in a density of  $1.08 \text{ g/cm}^3$ . The mentioned desired density values were determined experimentally by finding the material mass  $m_2$  using a weight scale, and the volume of the material  $V_2$  by measuring the dimensions of the taken sample. The density is therefore calculated as the ratio  $m_2/V_2$ . Using the assumed parameters in the previous analysis as inputs for the extrusion experiment, the obtained results were found to be close to the assumed parameters in the analysis confirming the validity of the above analysis.

## 4.5 Observations and Results

### 4.5.1 Motor Calibration

During motor calibration, the tests were performed at various motor speeds. The obtained data were listed in Tables 4.3 through 4.7. The data is then plotted in Figure 4.11, which shows the obtained relation between current and applied load for various motor speed. As depicted by the figure the current and the torque exhibit linear relations for given motor velocities.

Table 4.3: Current and torque values at speed of 50 step/s for a mass of 2 kg

<b>Distance (m)</b>	<b>Current (A)</b>	<b>Torque (N.m)</b>
0.1	0.31	2.292
0.2	0.32	4.254
0.3	0.33	6.216
0.4	0.33	8.178
0.5	0.34	10.14
0.6	0.34	12.102
0.7	0.35	14.064
0.8	0.35	16.026

Table 4.4: Current and torque values at speed of 50 step/s for a mass of 5 kg

<b>Distance (m)</b>	<b>Current (A)</b>	<b>Torque (N.m)</b>
0.2	0.34	10.14
0.4	0.36	19.95
0.5	trip	24.855
0.6	trip	29.76

Table 4.5: Current and torque values at a speed of 100 step/s for mass of 2 kg

<b>Distance (m)</b>	<b>Current (A)</b>	<b>Torque (Nm)</b>
0.1	0.38	2.292
0.2	0.39	4.254
0.3	0.4	6.216
0.4	0.41	8.178
0.5	0.42	10.14
0.6	0.43	12.102
0.7	0.44	14.064
0.8	0.45	16.026

Table 4.6: Current and torque values at speeds of 250 step/s for a mass of 2 kg

<b>Distance (m)</b>	<b>Current (A)</b>	<b>Torque (Nm)</b>
0.1	0.55	2.292
0.2	0.57	4.254
0.3	0.6	6.216
0.4	0.62	8.178
0.5	0.63	10.14
0.6	0.66	12.102
0.7	0.68	14.064
0.8	0.71	16.026

Table 4.7: Current and torque values at speed 500 step/s for a mass of 2 kg

<b>Distance (m)</b>	<b>Current (A)</b>	<b>Torque (Nm)</b>
0.1	0.71	2.292
0.2	0.74	4.254
0.3	0.76	6.216
0.5	0.77	10.14

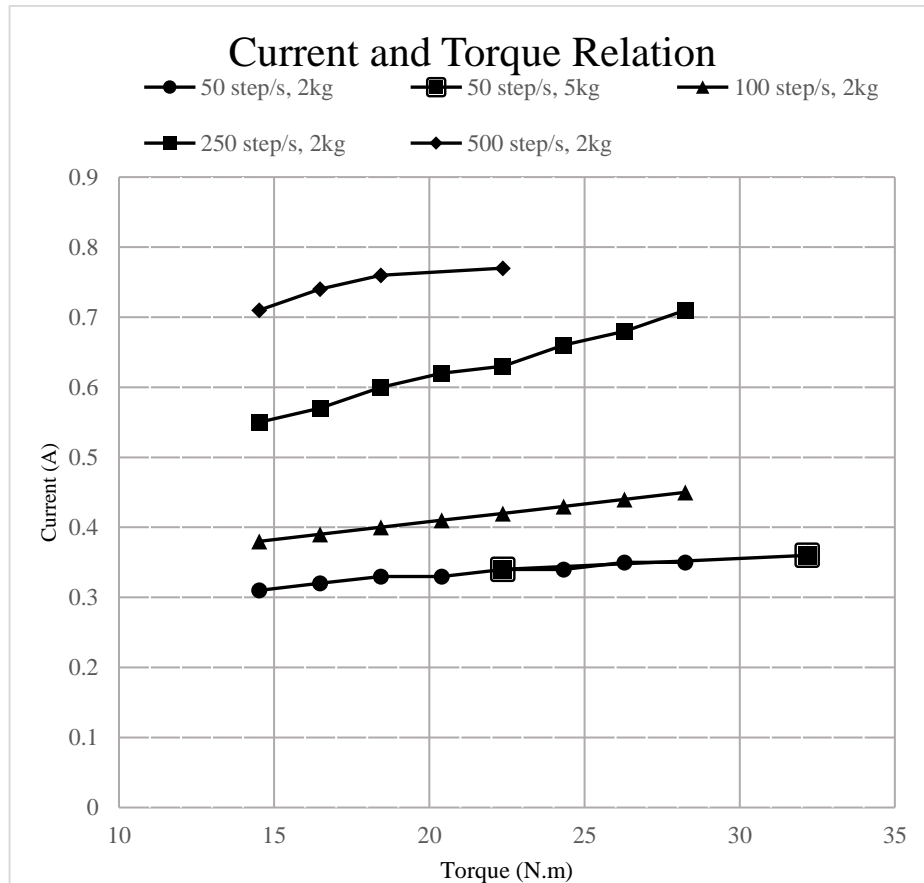


Figure 4.11: Plot of current change with applied loads at different motor speeds

As shown in the graph, linear relationship between the applied torque and the motor current for different motor speeds is notable. In addition, the capacity limits for the motor using the 2 and 5 kg weights were determined in the experiment for considered motor speeds. The indication that the motor is reaching its maximum capacity is when the stepper motor starts to slip. As indicated in Figure 4.11 using a weight of 2 kg, the maximum torque that the motor could deliver is 22.4 N.m at 0.77 A and a speed of 500 step/s. For 5 kg, the motor experienced slipping at a torque of 32.2 N.m, with a current of 0.36 A and a speed of 50 step/s. Although the motor sustained higher torque when load of 5 kg was applied, the allowable speed was only 50 step/s, whereas with an applied load of 2 kg the motor had wider speed range between 50 – 500 step/s.

#### 4.5.2 Conveying Material without Roller

To analyse screw conveyor functionality, a set of experiments were carried out on the screw conveyor stage without the roller. The test was done by blocking the exit channel immediately after passing the circular to rectangular adaptor. The material was conveyed until it is compacted due to the blockage of the exit, and the motor is tripped eventually as torque increases. The test is repeated for different speeds of screw motor. The obtained data is listed in Table 4.8.

Table 4.8: Current and density data obtained during compaction without the roller

Measured Weight (g)	Measured Volume (cm <sup>3</sup> )	Density (g/cm <sup>3</sup> )	Current (A)
Speed of 500 step/s (1 ms Step On-time)			
136.7	146.16	0.94	0.73
141.2	146.16	0.97	0.83
156.8	146.16	1.07	0.93
161.63	146.16	1.11	1.03
Speed of 250 step/s (2 ms Step On-time)			
146.32	146.16	1.00	0.7
166.53	146.16	1.14	0.75
173.4	146.16	1.19	0.8
186.2	146.16	1.27	0.85
149.4	146.16	1.02	0.62
157.4	146.16	1.08	0.67
158.3	146.16	1.08	0.72
170	146.16	1.16	0.77
158	146.00	1.08	0.67

The maximum limit on the speed was found to be at motor speed of 1000 step/s, where the screw conveyor had very small torque and was unable of further conveying of the material. This resulted in system trip, and the system was unable to capture any data. Therefore 500 step/s was considered as the highest speed that could

be used. On the other hand, a speed of less than 167 step/s was observed to be too low to convey enough amount of material to reach to appreciable compaction level. The optimum motor speed for the hardware used was found to be 250 step/s, where a density of  $1.27 \text{ g/cm}^3$  is obtained as shown in Figure 4.12.

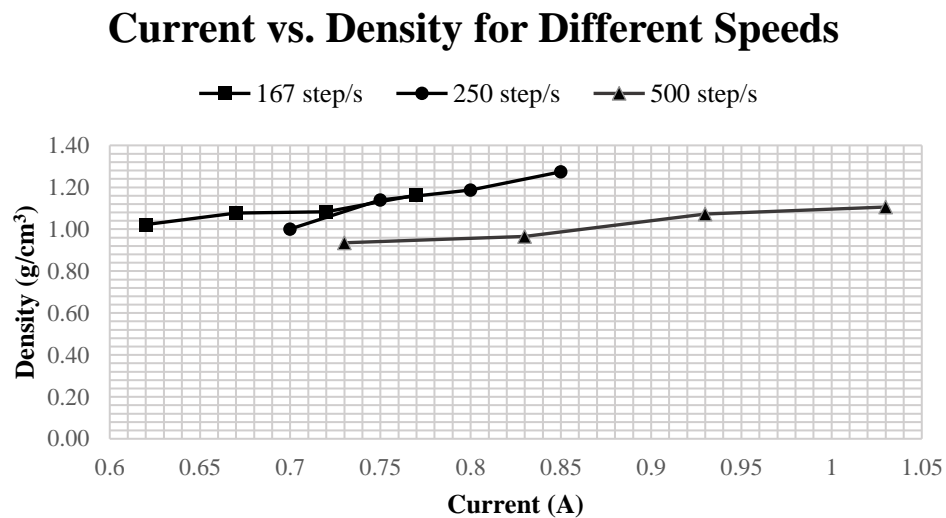


Figure 4.12: Current readings with varying speed

### 4.5.3 Error Analysis

Error analysis for the obtained data is carried out and the results are as follows:

a. Density at speed of 167 step/s

Average density obtained is  $1.09 \text{ g/cm}^3$  with a standard deviation of 0.1, the density therefore can be represented as  $1.09 \pm 0.1$ .

b. Density at speed of 250 step/s

Average density obtained is  $1.15 \text{ g/cm}^3$  with a standard deviation of 0.1, the density can be represented as  $1.15 \pm 0.1$ .

c. Density at speed of 500 step/s

Average density obtained is  $1.02 \text{ g/cm}^3$  with a standard deviation of 0.1, the density can be represented as  $1.02 \pm 0.1$ .

The standard deviation of the obtained data is almost similar showing narrow data spread from the mean and with densities with small variation showing precision with the obtained data.

#### 4.5.4 Conveying Material with a Roller

In the last set of experiments the roller was added at the exit of the screw conveyor. The calculated density of the extruded material was estimated using the continuity equation  $A_1 v_1 \rho_1 = A_2 v_2 \rho_2$  and was compared to the density that it measured in the experiment. Since the inlet and exit areas are fixed, one could obtain a desired density by setting the two motor speeds (i.e., by choosing  $v_1$  and  $v_2$ ). These theoretical predictions were experimentally verified. For instance, in the first experimental work done using the screw conveyor with the roller in place, a motor speed of 500 step/s is set as an input for the screw conveyor, which gives a velocity  $v_1$  of 3.75 mm/s for the ramming paste material. As was introduced earlier in Table 4.1, the density of the ramming material at the inlet  $\rho_1$  is  $0.84 \text{ g/cm}^3$  when it enters the screw conveyor. To obtain a desired density  $\rho_2$  of  $1.2 \text{ g/cm}^3$  at the exit, Equation (4.2) is used first to determine the equivalent roller motor speed. The cross-sectional area of the inlet  $A_1$  is  $2019.2 \text{ mm}^2$ , as calculated before, was used. The exit cross sectional area for the material under the roller was set to be  $A_2 = 2389.6 \text{ mm}^2$ . Then, using the continuity Equation (4.2), the required speed of the motor driving the roller was determined analytically as 214.5 step/s, which is equivalent to a velocity  $v_2$  of 2.2 mm/s. This speed was estimated to yield a desired ramming paste density at the exit of  $1.2 \text{ g/cm}^3$ . The density value that was obtained experimentally for the compacted



ramming paste after leaving the roller stage, as depicted by Figure 4.13, when the same input parameters are used was found to be similar to the predicted value.

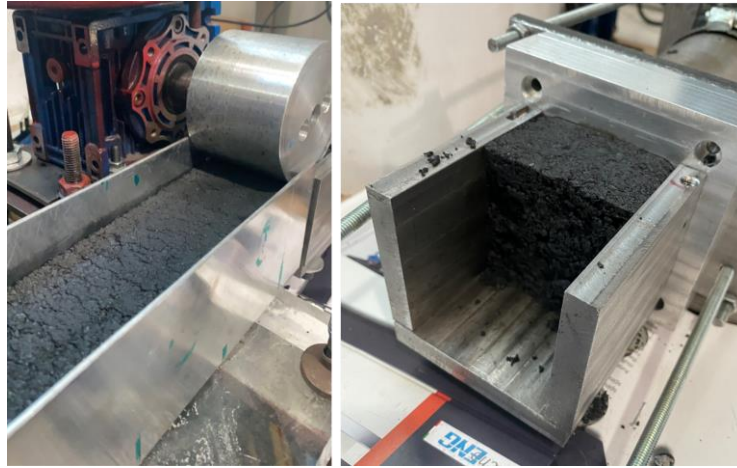


Figure 4.13: Extruded ramming paste (left) in the exit channel after the roller and compaction stage, (right) compacted material under the roller after removal of the exit channel and the roller

The experimental calculations are done by slicing a piece with rectangular shape from the compacted ramming paste after passing the roller, as shown in Figure 4.13. The density  $\rho_2$  is estimated from the measured volume and mass of the collected ramming material. The rectangular shape is further broken into smaller pieces and the average density was calculated. Figure 4.14 shows the steps for density measurement of the obtained samples and the motor current readings were recorded at real-time using the data acquisition as shown in Figure 4.15.

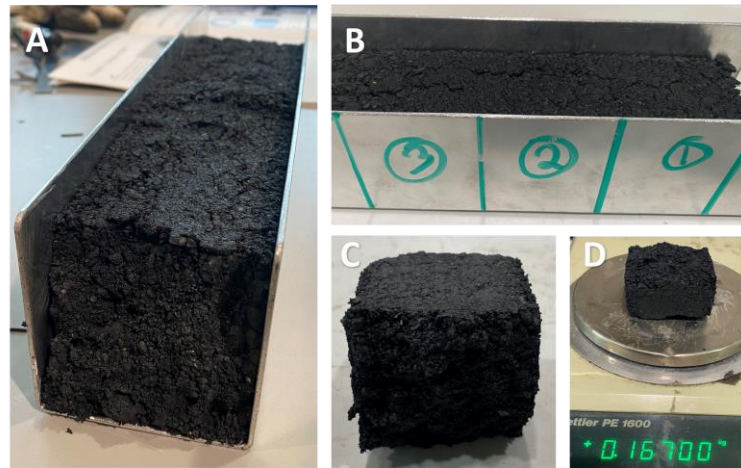


Figure 4.14: Measurement of density for ramming paste (A) material compacted in the exit channel, (B) dividing the paste into equal rectangular cuboids, (C) obtained sample, and (D) weight measuring

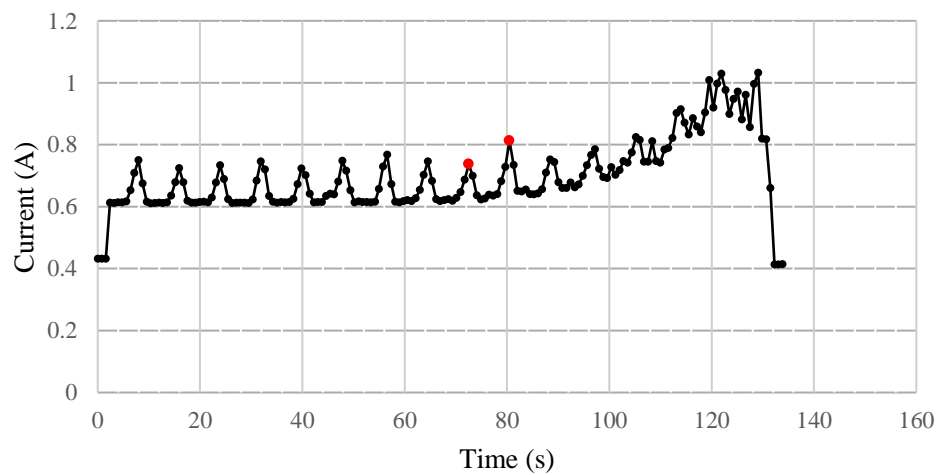


Figure 4.15: Current changes over time with delay of 1ms

As depicted by Figure 4.15 which shows the results, a repetitive pattern is noted in the graph. The fundamental frequency in the experimentally generated graph was found to match the frequency of the rotation of the screw and suggested that the material entering the screw from the hopper is not delivered consistently but rather has an intermittent pattern. This could be associated with the design of the inlet opening which is placed at the motor end of the screw (see Figure 4.16). The inlet opening,

through which the ramming material passes into the screw conveyer cavity, varies over one full rotation of the screw. Referring back to Figure 4.15, the marked peaks at time instances 72.5 and 80.4 seconds indicates a period of 7.9 seconds. A simple calculation considering a motor gear ratio GR of 10, a resolution of the drive of 400 steps per revolution, and a motor speed of 500 step per second was commanded, yields a screw speed of 1.25 revolution per second or a period of 8 second per revolution. This matches the noted period of 7.9 seconds.

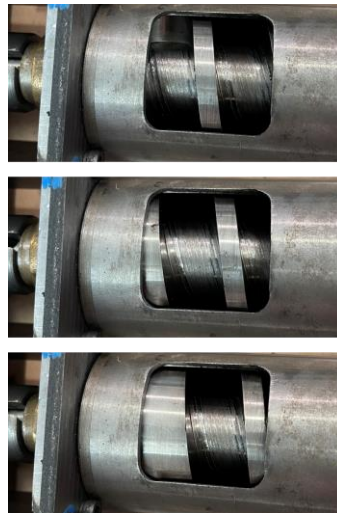


Figure 4.16 : The inlet opening of the screw conveyer showing sample gap changes over one full revolution of the screw

The parameters which are used as an input in the previous analysis were used as inputs to the experimental work as well and the obtained outputs from the experiments agreed with the analysis. Tables 4.7 through 4.10 show the parameters used in the analysis and the obtained data.

Table 4.9: Density calculations for desired density of  $1.2 \text{ g/cm}^3$  and screw speed of 250 step/s (2 ms step on-time)

Parameter	Value
Roller Diameter (mm)	79
$A_1 \text{ (mm}^2\text{)}$	2017.8
$\rho_1 \text{ (g/cm}^3\text{)}$	0.84
Step On-time for screw motor (ms)	2
$v_1 \text{ (rev/s)}$	0.0625
$v_1 \text{ (mm/s)}$	1.875
$A_2 \text{ (mm}^2\text{)}$	3016
$\rho_2 \text{ (g/cm}^3\text{)}$	1.2
$v_2 \text{ (mm/s)}$	0.88
$w_2 \text{ (rad/s)}$	0.022
$v_2 \text{ (rev/s)-gear ratio:30}$	0.106
Period for Roller (ms/step)	23.55
Step On-time for roller motor (ms)	11.78

Table 4.10: Obtained results for three samples with inputs from Table 4.9

Sample No.	Weight (g)	Volume ( $\text{cm}^3$ )	Density ( $\text{g/cm}^3$ )
1	259	226.20	1.15
2	269	223.18	1.21
3	286	241.28	1.19

Table 4.11: Density calculations for desired density of  $1.08 \text{ g/cm}^3$  and screw speed of 1000 step/s (0.5 ms step on-time)

Parameter	Value
Roller Diameter (mm)	79
$A_1 \text{ (mm}^2\text{)}$	2019.2
$\rho_1 \text{ (g/cm}^3\text{)}$	0.84
Step On-time for screw motor (ms)	0.5
$v_1 \text{ (rev/s)}$	0.25
$v_1 \text{ (mm/s)}$	7.5
$A_2 \text{ (mm}^2\text{)}$	3016
$\rho_2 \text{ (g/cm}^3\text{)}$	1.08
$v_2 \text{ (mm/s)}$	3.905
$v_2 \text{ (rev/s)-gear ratio:30}$	0.472
Period for roller (ms/step)	5.296
Step On-time for roller motor (ms)	2.648

Table 4.12: Obtained results for three samples with inputs from Table 4.11

Sample No.	Weight (g)	Volume ( $\text{cm}^3$ )	Density ( $\text{g/cm}^3$ )
1	188.4	180.96	1.04
2	183.3	180.96	1.01
3	195	180.96	1.08

Figure 4.17 shows a plot of the obtained density values from Tables 4.9 to 4.12 for three samples at each parameter settings and also shows that the obtained densities were as predicted by theory.

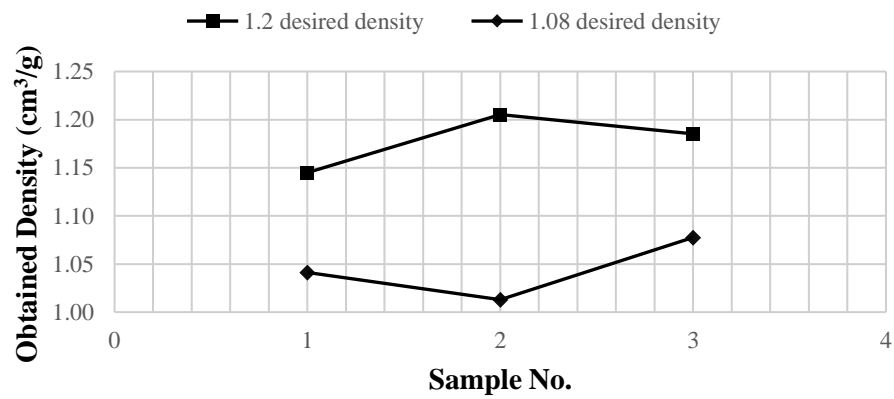


Figure 4.17: Obtained densities by experiment

#### 4.5.5 Conveying Material with Varying Roller Height

This stage of the experiments started after achieving density of  $1.2 \text{ g/cm}^3$ . For further optimization, the roller height is varied with objective to reach a desired density of  $1.4 \text{ g/cm}^3$ . By varying the speed and height of the roller a set of experiments were carried out to determine the corresponding density experimentally. The system was operated at two speeds values 250 and 500 step/s. Tables 4.13 through 4.18 list the parameters used and the obtained data, while Figure 4.18 shows the density values plotted against different roller heights.

Table 4.13: Density calculations for desired density of  $1.4 \text{ g/cm}^3$  and screw conveyor speed of 500 step/s

Parameter	Value
$A_1 \text{ (mm}^2\text{)}$	2019.176
$\rho_1 \text{ (g/cm}^3\text{)}$	0.84
Screw Delay (ms)	1
$v_1 \text{ (rev/s)}$	0.125
$v_1 \text{ (mm/s)}$	3.75
Roller Diameter (mm)	79
$A_2 \text{ (mm}^2\text{)}$	2813
$\rho_2 \text{ (g/cm}^3\text{)}$	1.4
$v_2 \text{ (mm/s)}$	1.615
$w_2 \text{ (rad/s)}$	0.041
$v_2 \text{ (rev/s)-gear ratio:30}$	0.195
Period (ms/step)	12.806
Roller Delay (ms/Step)	6.403
Roller speed (step/s)	156.2

Table 4.14: Obtained values for the data presented in Table 4.13

Weight (g)	Roller Height (cm)	Layer Length (cm)	$A_2 \text{ (cm}^2\text{)}$	Volume (cm <sup>3</sup> )	Density (g/cm <sup>3</sup> )
336	5.2	10	30.16	301.60	1.11
336	5.2	10	30.16	301.60	1.11
197.5	4.85	7	28.13	196.91	1.00
181	4.85	7	28.13	196.91	0.92
200	4.85	7	28.13	196.91	1.02
100.4	4.85	2.75	28.13	77.36	1.30

Table 4.15: Density calculations for desired density  $1.2 \text{ g/cm}^3$  and screw conveyor speed 500 step/s

Parameter	Value
$A_1 \text{ (mm}^2\text{)}$	2019.2
$\rho_1 \text{ (g/cm}^3\text{)}$	0.84
Screw Delay (ms)	1
$v_1 \text{ (rev/s)}$	0.125
$v_1 \text{ (mm/s)}$	3.75
Roller Diameter (mm)	79
$A_2 \text{ (mm}^2\text{)}$	2389.6
$\rho_2 \text{ (g/cm}^3\text{)}$	1.2
$v_2 \text{ (mm/s)}$	2.218
$w_2 \text{ (rad/s)}$	0.056
$v_2 \text{ (rev/s)-gear ratio:30}$	0.268
Period (ms/step)	9.324
Roller Delay (ms/step)	4.662
Roller speed (step/s)	214.5

Table 4.16: Obtained values for the data presented in Table 4.15

Weight (g)	Roller Height (cm)	Layer Length (cm)	$A_2 \text{ (cm}^2\text{)}$	Volume (cm <sup>3</sup> )	Density (g/cm <sup>3</sup> )
233	4.12	8	23.9	191.17	1.22
259.4	4.12	8	23.9	191.17	1.36
254.3	4.12	8	23.9	191.17	1.33
279.2	4.12	5.5	34.2	188.10	1.48 <sup>2</sup>

---

<sup>2</sup> The value is taken from the compacted material below the roller, hence not included in the plot



Table 4.17: Density calculations for desired density of  $1.4 \text{ g/cm}^3$  and screw conveyor speed of 250 step/s

Parameter	Value
$A_1 \text{ (mm}^2\text{)}$	2019.2
$\rho_1 \text{ (g/cm}^3\text{)}$	0.84
Screw Delay (ms)	2
$v_1 \text{ (rev/s)}$	0.0625
$v_1 \text{ (mm/s)}$	1.875
Roller Diameter (mm)	79
$A_2 \text{ (cm}^2\text{)}$	4160
$\rho_2 \text{ (g/cm}^3\text{)}$	1.4
$v_2 \text{ (mm/s)}$	0.546
$w_2 \text{ (rad/s)}$	0.014
$v_2 \text{ (rev/s)-gear ratio:30}$	0.066
Period (ms/step)	37.88
Roller Delay (ms/Step)	18.93
Roller speed (step/s)	52.8

Table 4.18: Obtained values for the data presented in Table 4.17

Weight (g)	Roller Height (cm)	Layer Length (cm)	$A_2 \text{ (cm}^2\text{)}$	Volume (cm <sup>3</sup> )	Density (g/cm <sup>3</sup> )
336	5.2	10	30.16	301.60	1.11
336	5.2	10	30.16	301.60	1.11

## Density Obtained with Varied Roller Height

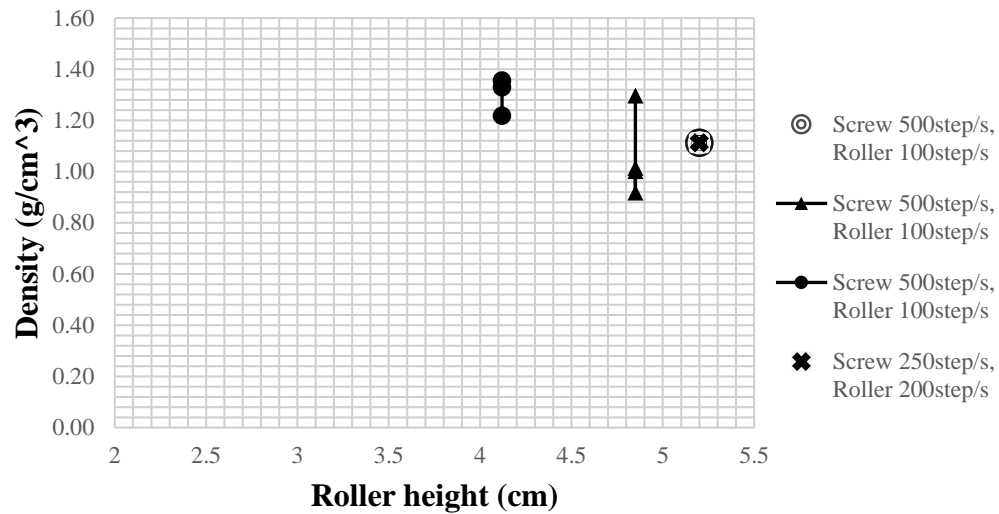


Figure 4.18: Density obtained with different roller height at two speeds values

Figure 4.18 shows that using speed of 250 step/s was not enough to obtain the desired density with the added compaction with a roller, as the amount of material delivered to the roller was not sufficient. A maximum density of 1.11 g/cm<sup>3</sup> was obtained at speed of 250 step/s with exit area  $A_2 = 3016 \text{ mm}^2$ . The roller speed was increased to 500 step/s with maintaining the same exit area nevertheless the achieved density was the same. Next with maintaining the roller speed at 500 step/s, the roller was further lowered making the exit area  $A_2 = 2813 \text{ mm}^2$ , the maximum achieved density was  $\rho_2 = 1.3 \text{ g/cm}^3$ . Finally, the roller was positioned at its lowest height (i.e using minimum  $A_2$ ) where exit area became  $2390 \text{ mm}^2$ , at this position the desired density was achieved as a maximum density of 1.48 g/cm<sup>3</sup> was obtained. This experiment concluded that with varying  $A_2$  the density ranged from 1.22 to 1.48 g/cm<sup>3</sup>, which means that the desired density is achievable.

#### 4.5.6 Error Analysis

Error analysis for the obtained data is carried out and the results are as follows:

- a. Density at screw speed of 500 step/s and roller speed of 100 step/s
  - With a roller height of 4.1cm, an average density of 1.3 g/cm<sup>3</sup> is obtained with a standard deviation of 0.1, the density therefore can be represented as  $1.3 \pm 0.1$ .
  - With a roller height of 4.9cm, an average density of 1.1 g/cm<sup>3</sup> is obtained with a standard deviation of 0.2, the density can be represented as  $1.1 \pm 0.2$
  - A roller height of 5.2cm, resulted in an average density of 1.1 g/cm<sup>3</sup> and a standard deviation of 0.0, the density can be represented as  $1.1 \pm 0.0$ , similar results are obtained when the speed of screw is changed to 250 step/s and the roller speed to 200 step/s

Small deviation is presented for the obtained data showing precision of the system in repeating the same values. Also some accuracy was presented with the system achieving the desired density after fine tuning.

#### 4.6 Summary

In this section, screw conveyor machine was designed and built as a result of the outcomes of the previous experiments, as flow was required to be established for ramming paste in order to extrude it. The setup of the machine is presented and explained as well as the calibration procedure used for relating the motor torque and the motor current. Mathematical relations that model the flow and the density were derived. The derivation and the analysis were presented first. The experimental

methods were also explained followed by the observations and the results. It was found out that flow the material established as expected, and it was successfully extruded through the exit of the screw and was pushed throughout the exit channel. As the screw itself however was not sufficient to provide the desired density, adding a rolling stage was necessary. With the addition of the rolling stage, and the variation of the motors' speeds and the exit area, the machine capability in providing desired density values was demonstrated.

## Chapter 5: Conclusions and Recommendations

The conclusions that are drawn from this study are based on the obtained results from each set of experiments. Below are the conclusions per experiment.

### a. Investigation of Manual ramming

Manual ramming can produce layers of acceptable compaction and result densities in the acceptable range. This is confirmed by the experiment where layers of 100 mm height after compaction resulting in densities with values of 1.41, 1.55, and 1.57 g/cm<sup>3</sup>. However, ramming paste continues to compact with addition of more layers until fully solidified resulting in more compaction at the bottom layers as pressure is added to the top, this might cause over-compaction of ramming paste and initiation of internal cracks. Hence, varied level of compaction needs to be considered across layers to avoid such variance in compaction and consequently a heterogeneous distribution across the layers.

Compacted ramming paste layers do not bond at the plane that separates each layer from the next. This might be due to different grain sizes of the rammed layer and the following ramming material to be compacted. Such separation might be potential source of failure for compacted layers of ramming paste, which makes it important to reduce the number the separation planes namely the number of laid layers.

### b. Characterization of Ramming paste with Different Applied Pressure

Ramming paste blocks representing the ramming paste fillings in the pot were tested for their properties such as density and young's modulus. Ramming paste samples were fabricated as cylindrical samples with 50 mm diameter and 50 mm height, with acceptable density ranging between 1.57 – 1.6 g/cm<sup>3</sup> and strength as high

as 0.75 MPa without baking. Pressures ranging from 6.5 MPa to 11.3 MPa with applied loads ranging 25 kN to 40 kN were tested. Load higher than 40 kN is not advisable as it initiates internal cracks within the material. Nevertheless, material with strength of 0.57 MPa can be achieved with a load as low as 25 kN at which ramming paste found to be having lower young's modulus value of 6.5 MPa compared to 11.3 MPa at 40 kN, this shows an advantage of having flexible ramming paste that is easier to deform at lower loads and thus preventing cathode damage.

c. Characterization of Ramming paste at Elevated Baking Temperatures

Ramming paste solidifies and fails under shear stresses when heated to temperatures ranging between 200°C and 400°C. At higher baking temperature above 500°C the ramming paste starts losing its form, then as heated to 600°C it oxidizes and turns into a soft brittle material in the presence of oxygen. Such scenario repeats itself regardless of the value of the compaction load or the level of compaction.

In addition, with heating of the samples the yield ranged between 5.3 and 4.4 MPa for samples compressed with a load of 40 kN, and a range of 0.71 and 5.5 MPa for those compresses with a load of 45 kN, showing lower strength and supporting the conclusion of internal cracks initiation. As the samples are heated (baked), a yield as high as 9.8 MPa was achieved for 40 kN samples compared to yield of 0.75 MPa for unbaked samples. Furthermore, 45 kN samples yielded at 0.71 MPa at room temperature and at 200°C, which means similar strength is obtained for unbaked samples and for samples that are baked at 200°C. As a key takeaway, in the next experiment ramming paste samples will be extruded without baking.

d. Extrusion Through a Nozzle

Extrusion through a hole by applying pressure is not feasible with the ramming paste. When ramming paste is passed through a nozzle it does not flow smoothly due to its viscosity, instead it accumulates and gets compacted with reduction in cross sectional area of the material path. As the material gets compacted without flowing, the exit of the nozzle starts clogging causing the compaction to continue in the top layers and leaving any material that passed the exit uncompacted. This happened regardless of the nozzle angle that pushes the material downwards angles of  $90^\circ$  and a steeper angle of  $60^\circ$  were used and same results were obtained. The exit opening also does not affect the result as the compacted material does not reach the exit opening, the biggest was circular outlet with 20 mm diameter, in which no extrusion occurs. Such behavior repeated regardless of the shape and size of the nozzle. Hence adopting the 3D-printing concept of injecting while heating in FDM is not feasible for ramming paste. In addition, the extrusion of ramming paste requires introduction of flow to the system by external means. Hence, a screw conveyor and a roller are planned to be tested next.

#### e. Screw Extrusion and Rolling of Ramming Paste

In continuation to the previous results, a device was designed and built to introduce positive flow and pressure as well as controlling the density of the material. This device consisted of two stage compactions: a screw conveyor as first stage and a roller as a second stage. The two stages are followed by a channel to guide the material as it flows out of the screw-roller stages. In this experiment, ramming paste was successfully extruded with the flow provided with the screw conveyor that was running at speed of 500 steps/s and a roller at height of 4.12 cm running at a speed of 100 steps/s. Ramming paste was compacted to the desired density of  $1.4 \text{ g/cm}^3$ . The

device also compacted ramming paste to different density values that are expected analytically with an assumed parameter, an example of that is achieving density of  $1.2 \text{ g/cm}^3$  with screw conveyor at speed of 500 steps/s and roller speed of 215 approximately. The device allowed the control of the material density by changing input parameters for the screw conveyor and the roller.

### **5.1 Managerial Implications**

This research showed the feasibility of controlled extrusion of ramming paste and resulted in a device that can perform such task. Additional research can be done to further optimize this device. It is suggested to do the following to fine tune the device and optimize the process:

- a. Different configuration of the rollers by adding additional roller at the bottom to minimize the discrepancies in material homogeneity across the layers.
- b. Use DC motor instead of stepper motor
- c. Use motor with higher power rating

### **5.2 Research Implications**

This research is dedicated to developing methods for automation of the ramming process in aluminum cell lining. For this purpose, the concept of 3D-printing FDM was adopted in addition to the use of screw conveyor as an alternative for ramming paste extrusion. This approach necessitated investigation of manual ramming process followed by characterization of ramming paste, with different loads and temperatures. These experiments led to the invention of device that utilizes screw conveyor for provision of material flow and a roller to compact the material to layers



with a desired density. The expected impact for this study on the aluminum industry is (1) increased safety of the ramming process, (2) reduction of cell relining shutdown duration, (3) cost saving, (4) ability to select operating parameters, (5) improved compaction of ramming paste, and (6) the study will set the basis for full automation of ramming machines.

## References

- Allard, B., Paulus, R., Billat, G., Savoie, C., & Savoie, C. (2011). A new ramming paste with improved potlining working conditions. 2, 1091 - 1096.
- Allard, B., Tawfik, M., & Kumar, A. (2016). Performances of Green and Eco-Friendly Ramming Pastes in EGA Pots. *Metals*, 6(5), 112.  
<https://doi.org/10.3390/met6050112>
- Awasthi, P., & Banerjee, S. S. (2021). Fused deposition modeling of thermoplastic elastomeric materials: Challenges and opportunities. *Additive Manufacturing*, 46, 102177. <https://doi.org/10.1016/j.addma.2021.102177>
- Brulin, J., Rezik, A., Josserand, L., Blond, E., Gasser, A., & Roulet, F. (2011). Characterization and modelling of a carbon ramming mix used in high-temperature industry. *International Journal of Solids and Structures*, 48(5), 854 - 864. <https://doi.org/10.1016/j.ijsolstr.2010.11.024>
- Clark, J., & Duane, S. (1983). *Method of manufacturing aluminum in a Hall-Heroult cell* (Patent No. US4379033).
- Côté, P., & Pucella, G. (2015). An innovative pot ramming machine. *Light Metals*, 699 - 704.
- Discrete Element Method (DEM). (2009). *Powder Technology* 193. 274 - 288
- Faanes, B. M., & Gran, H. (1989). Ramming paste related failures in cathode linings. *Light Metals*, 633 - 639.
- Kucher, M., Tomala, J., & Hiltmann, F. (2012). *Process for Producing a Cathode Block for Aluminum Electrolysis Cell and a Cathode Block* (Patent No. CA2805729C).
- Mirchi, A. A., & Chen, W. (2007). *High swelling ramming paste for aluminum electrolysis cell* (Patent No. US 7186357 B2).
- Nerella, V. N., Näther, M., Iqbal, A., Butler, M., & Mechtcherine, V. (2019). Inline quantification of extrudability of cementitious materials for digital construction. *Cement and Concrete Composites*, 95, 260 - 270.  
<https://doi.org/10.1016/j.cemconcomp.2018.09.015>
- Orangi, S. (2014). Time-dependant behaviour of ramming paste used in hall-héroult cell: Characterization and constitutive law [Thesis for Ph.D, Laval University]. <https://www.researchgate.net/publication/270278717>

- Orangi, S., Picard, D., Alamdari, H., Ziegler, D., & Fafard, M. (2011). Development of representative assembly for the fabrication of cold ramming paste samples at laboratory. 13, 47 - 58.
- Owen, P. J., & Cleary, P. W. (2009). Prediction of screw conveyor performance using the Discrete Element Method (DEM). *Powder Technology*, 193(3), 274 - 288. <https://doi.org/10.1016/j.powtec.2009.03.012>
- Prasad, S. (2000). Studies on the Hall-Heroult aluminum electrowinning process. *Journal of the Brazilian Chemical Society*, 11(3), 245 - 251. <https://doi.org/10.1590/S0103-50532000000300008>
- Richard, D., D'Amours, G., Fafard, M., Gakwaya, A., & Désilets, M. (2005). Development and Validation of a Thermo-Chemo-Mechanical Model of the Baking of Ramming Paste. 7, 733 - 738
- Salazar, J. E., Márquez, G., Imery, J., & Mendoza, J. (2002). Design of aluminum reduction cells sidewall linings based on the use of silicon carbide. Proceedings of ESDA2002, Turkey, 1-10.
- Schmitt, R., & Christ, M. (2018). *Cathode Bottom for Producing Aluminum* (Patent No. US20180282888A1).
- Sørli, M., & Øye, H. (2010). *Cathodes in Aluminium Electrolysis* (3rd ed.). Aluminium-Verlag Marketing & Kommunikation GmbH.
- St-Arnaud, P.-O., Picard, D., Alamdari, H., Ziegler, D., & Fafard, M. (2014). Room temperature creep behaviour of ramming paste baked at different temperatures. 2, 1221 - 1226
- Støre, A. (2015). *Carbon Materials Testing Rammability of Paste* (p. 2). The Norwegian University of Science and Technology, SINTEF Materials and Chemistry.

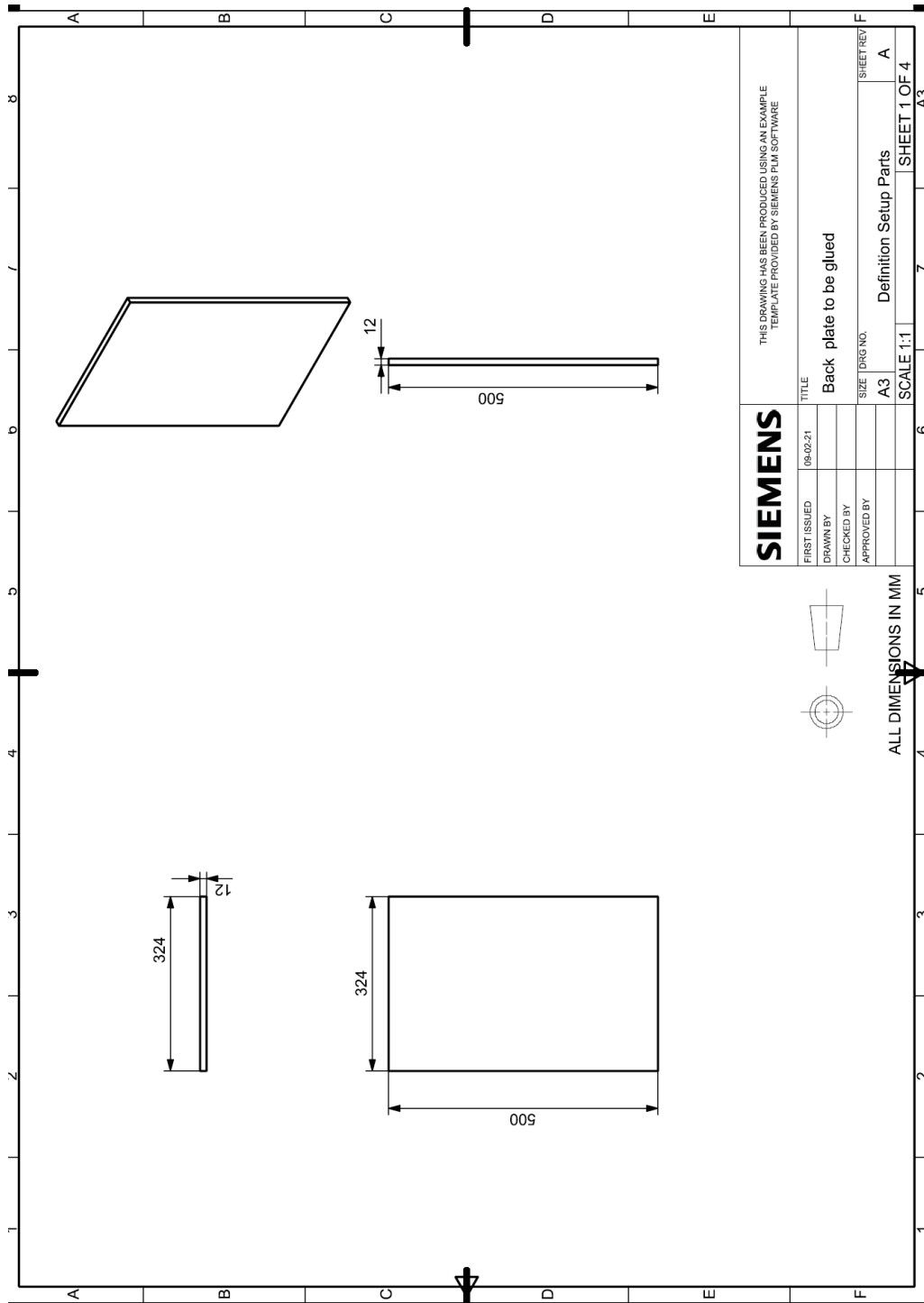
## List of Publications

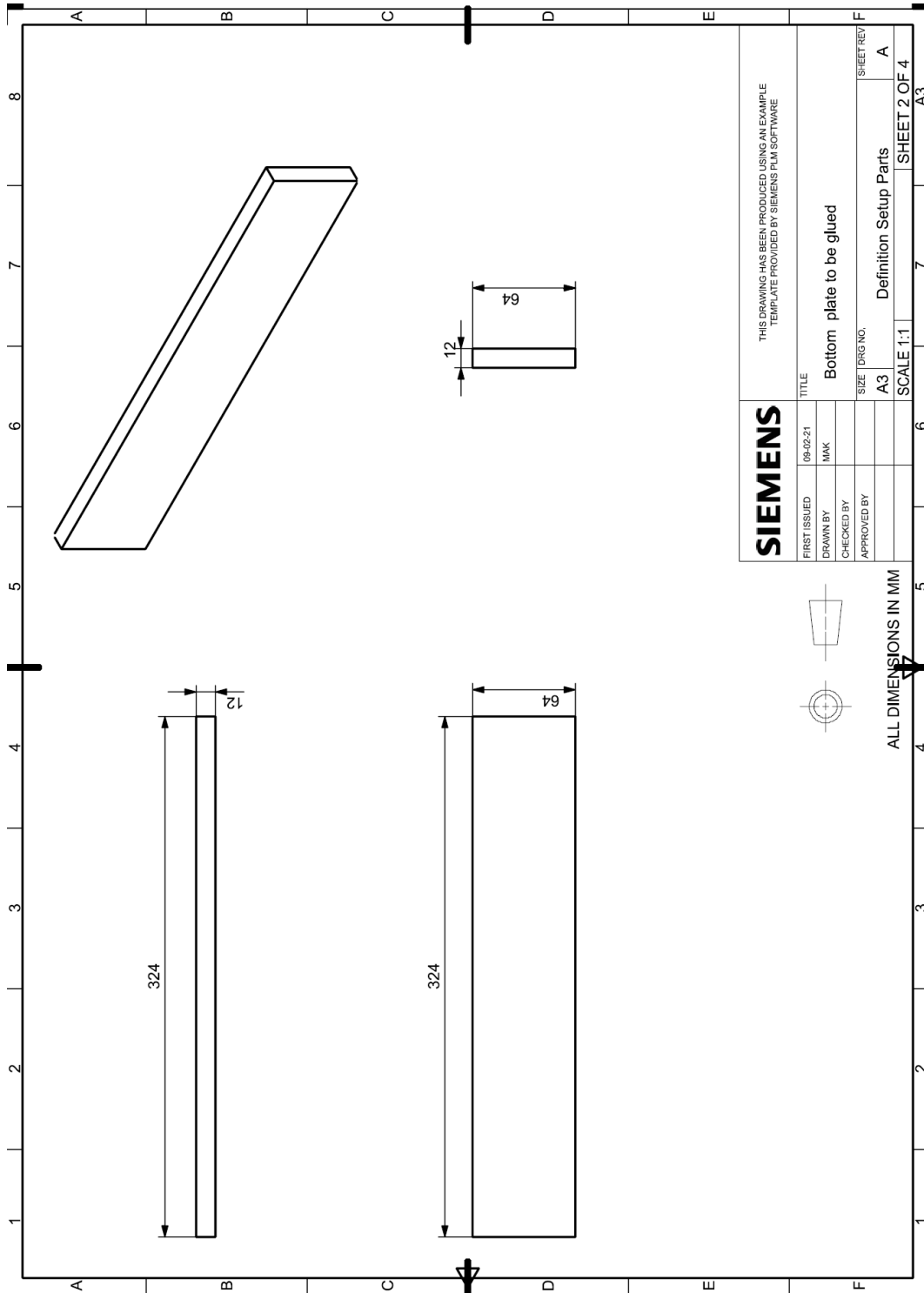
Alkaabi, M., Harib, K., Sivaloganathan, S., Sureshkumar, V., & Oseni, A. (2021). *Automation of Ramming Process for Aluminum Reduction Cell*. Proceedings of the 39th International ICSOBA Conference .16.

# Appendix

## Design Drawings for the Set-ups

### 1- Manual Ramming





**SIEMENS**

THIS DRAWING HAS BEEN PRODUCED USING AN EXAMPLE  
TEMPLATE PROVIDED BY SIEMENS PLM SOFTWARE

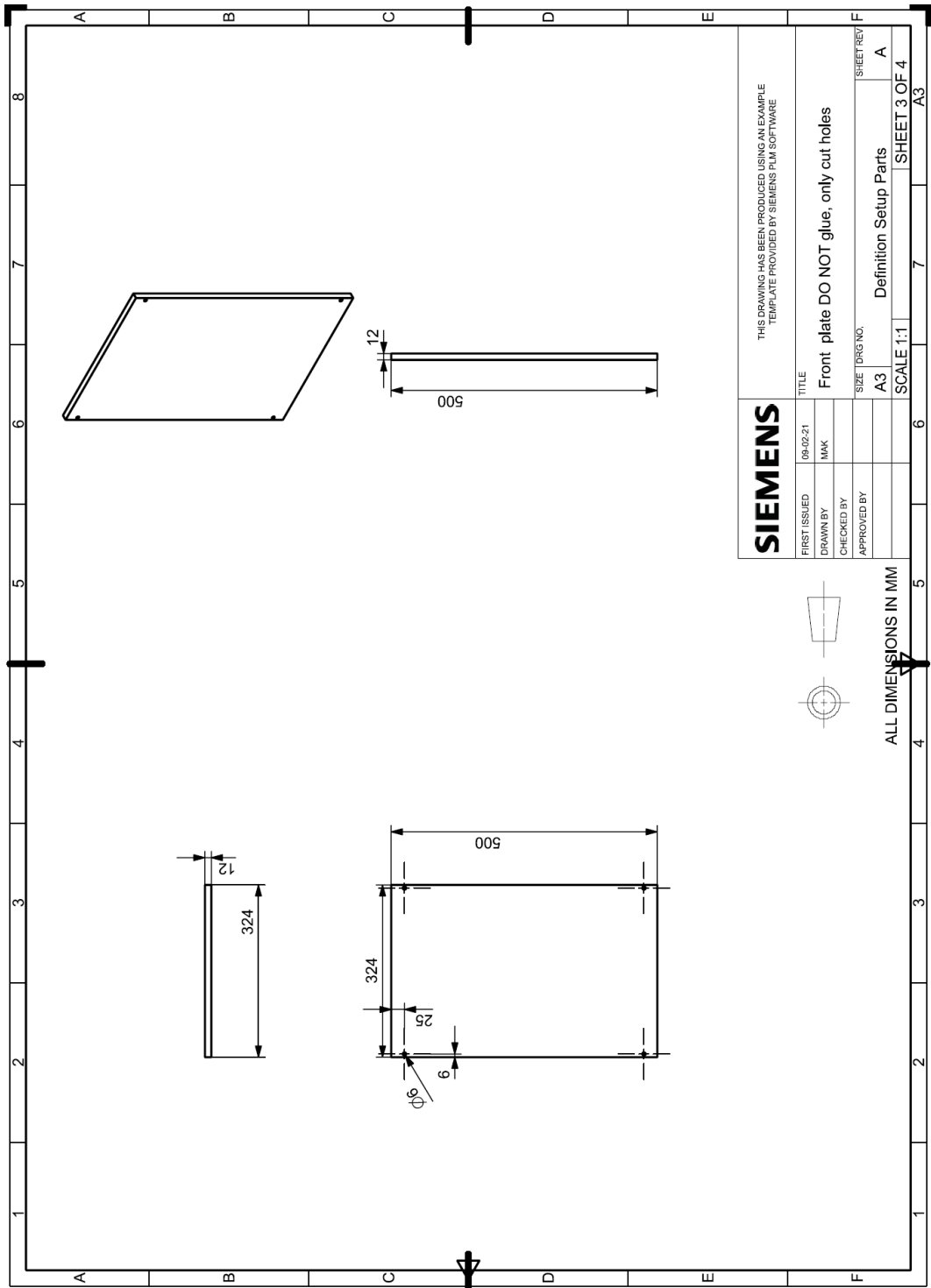
FIRST ISSUED 08-02-21  
DRAWN BY MKK  
CHECKED BY  
APPROVED BY

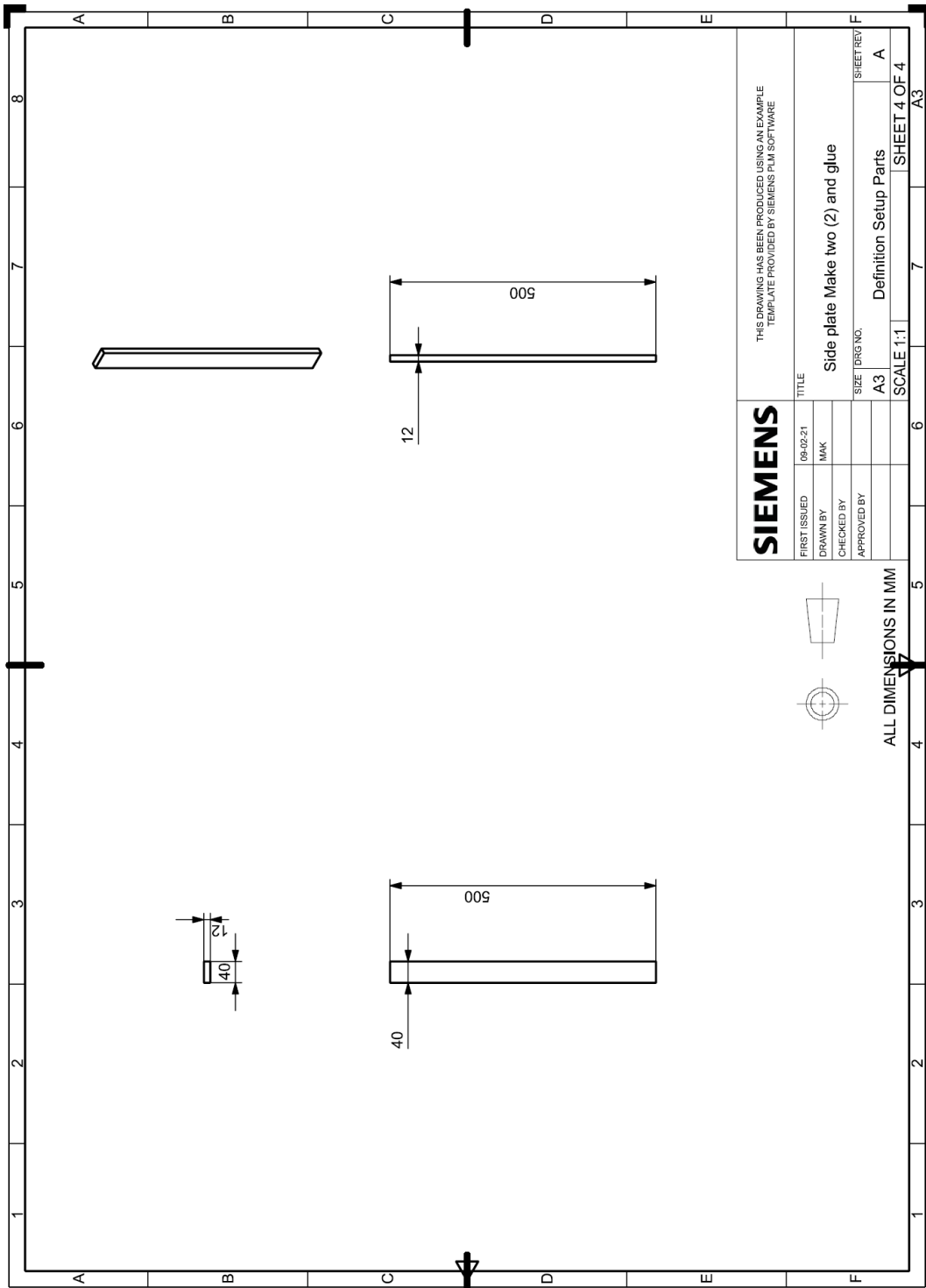
TITLE  
Bottom plate to be glued  
SIZE DRG NO. A3  
SCALE 1:1  
SHEET REV. A



ALL DIMENSIONS IN MM

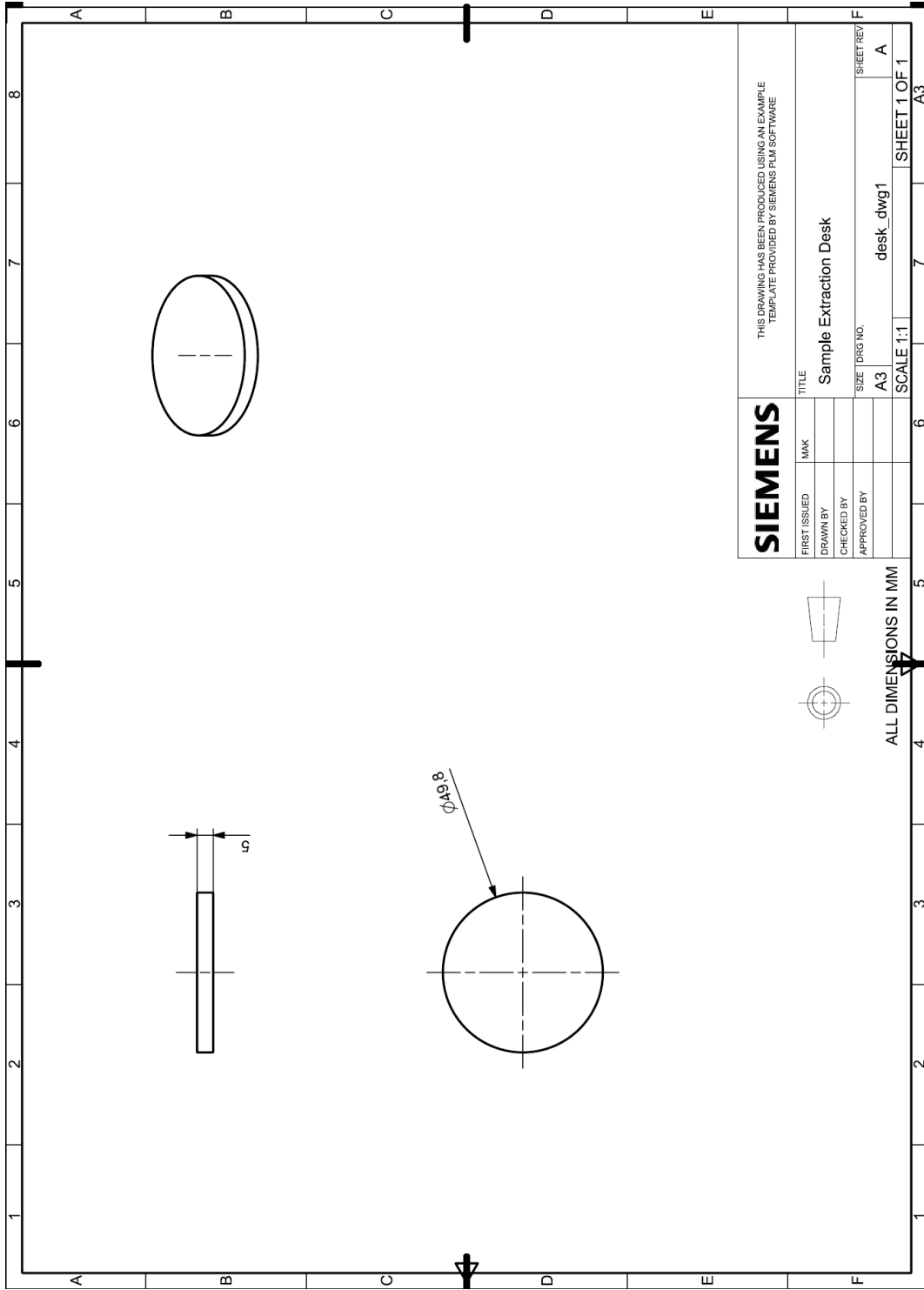
Definition Setup Parts  
SHEET 2 OF 4  
A3







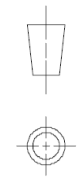




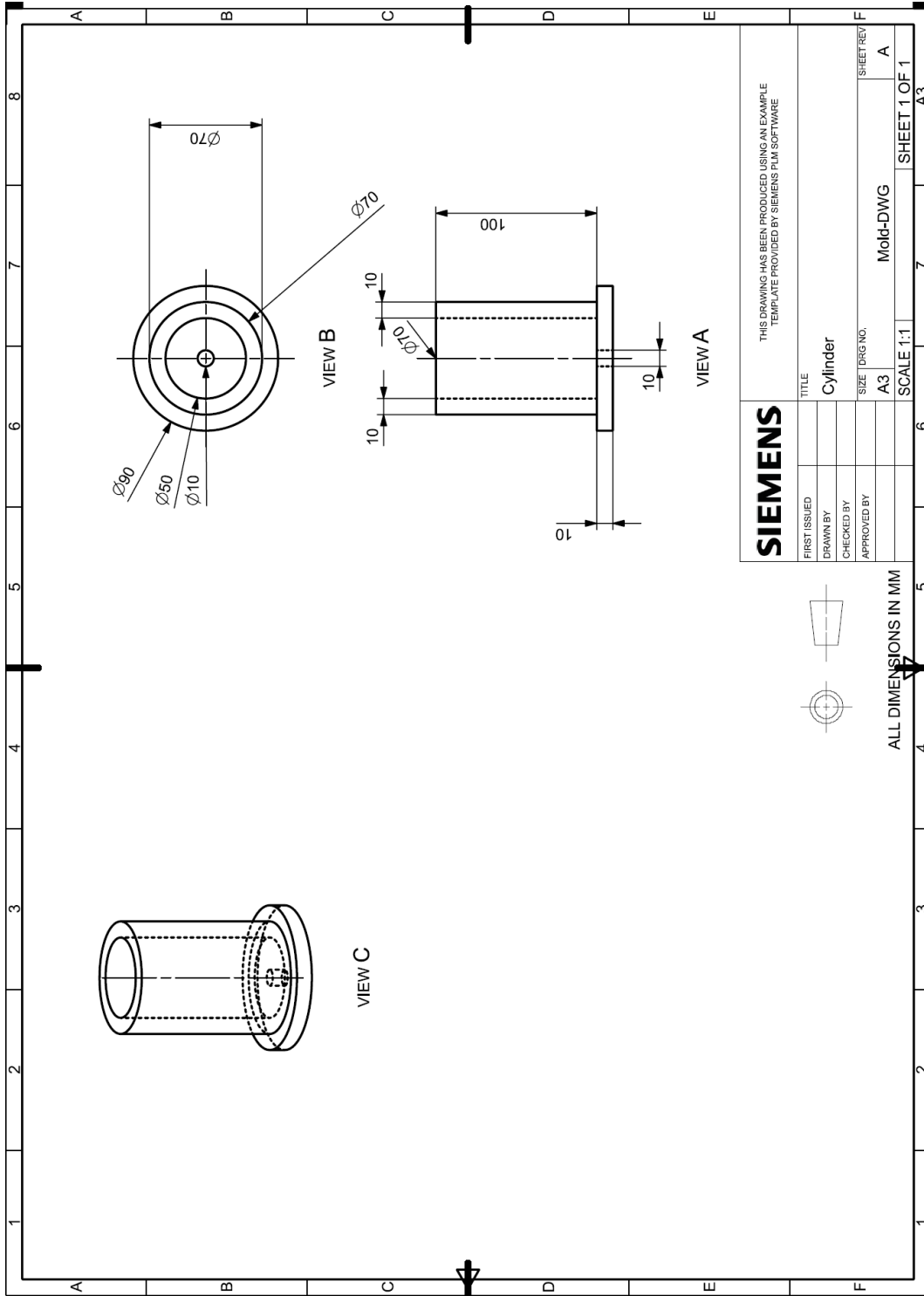
**SIEMENS**

THIS DRAWING HAS BEEN PRODUCED USING AN EXAMPLE  
TEMPLATE PROVIDED BY SIEMENS PLM SOFTWARE

FIRST ISSUED	IMAK	TITLE	Sample Extraction Desk
DRAWN BY		SIZE	A3
CHECKED BY		DRG NO.	desk_dwg1
APPROVED BY		SCALE	1:1
			SHEET 1 OF 1
			A3



ALL DIMENSIONS IN MM



**SIEMENS**

THIS DRAWING HAS BEEN PRODUCED USING AN EXAMPLE  
TEMPLATE PROVIDED BY SIEMENS PLM SOFTWARE

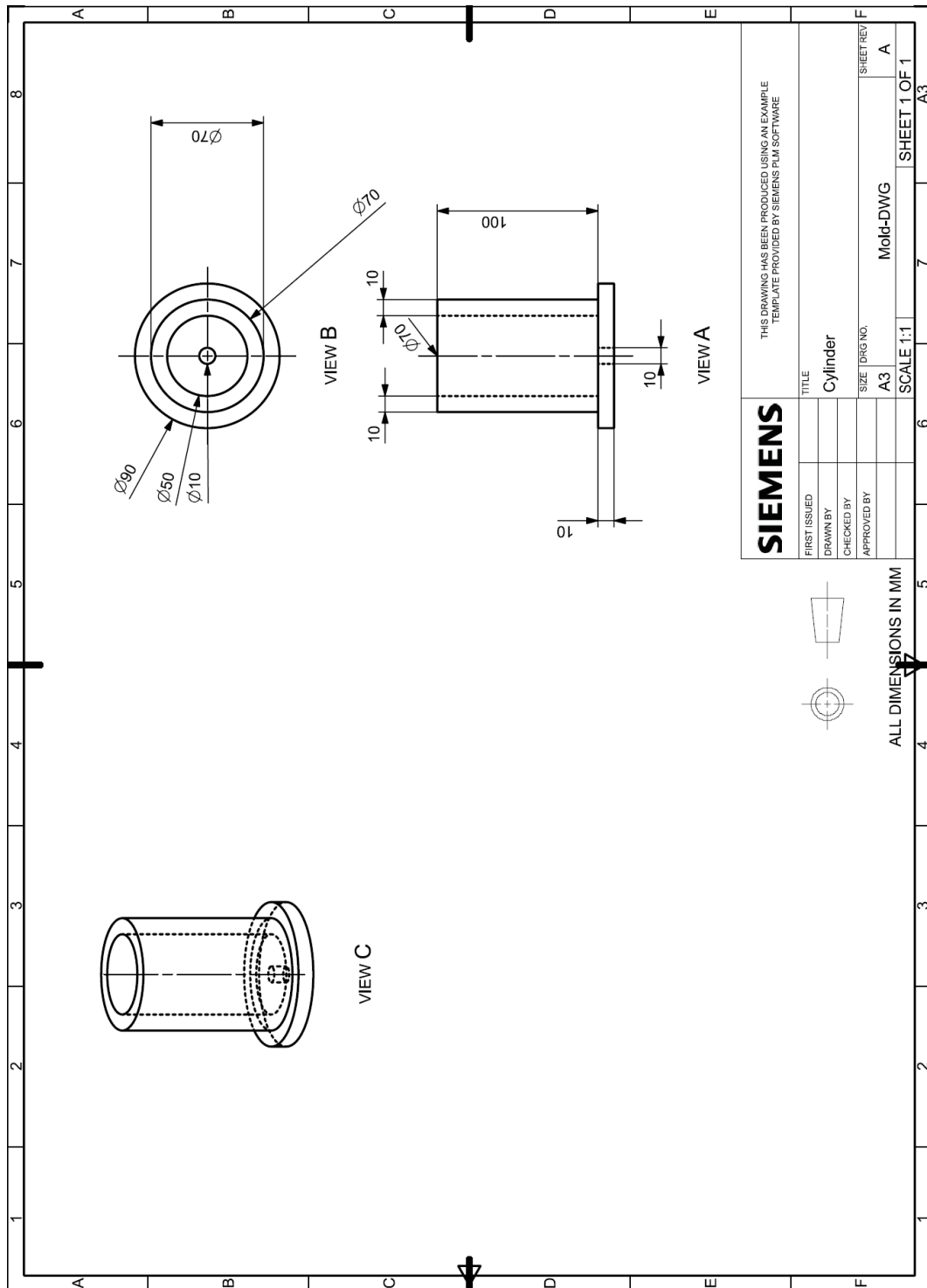
FIRST ISSUED	TITLE	DRAWN BY	Cylinder
CHECKED BY	SIZE (DRG NO.)	APPROVED BY	SHEET NO.
	A3		A
SCALE 1:1			SHEET 1 OF 1
			A3

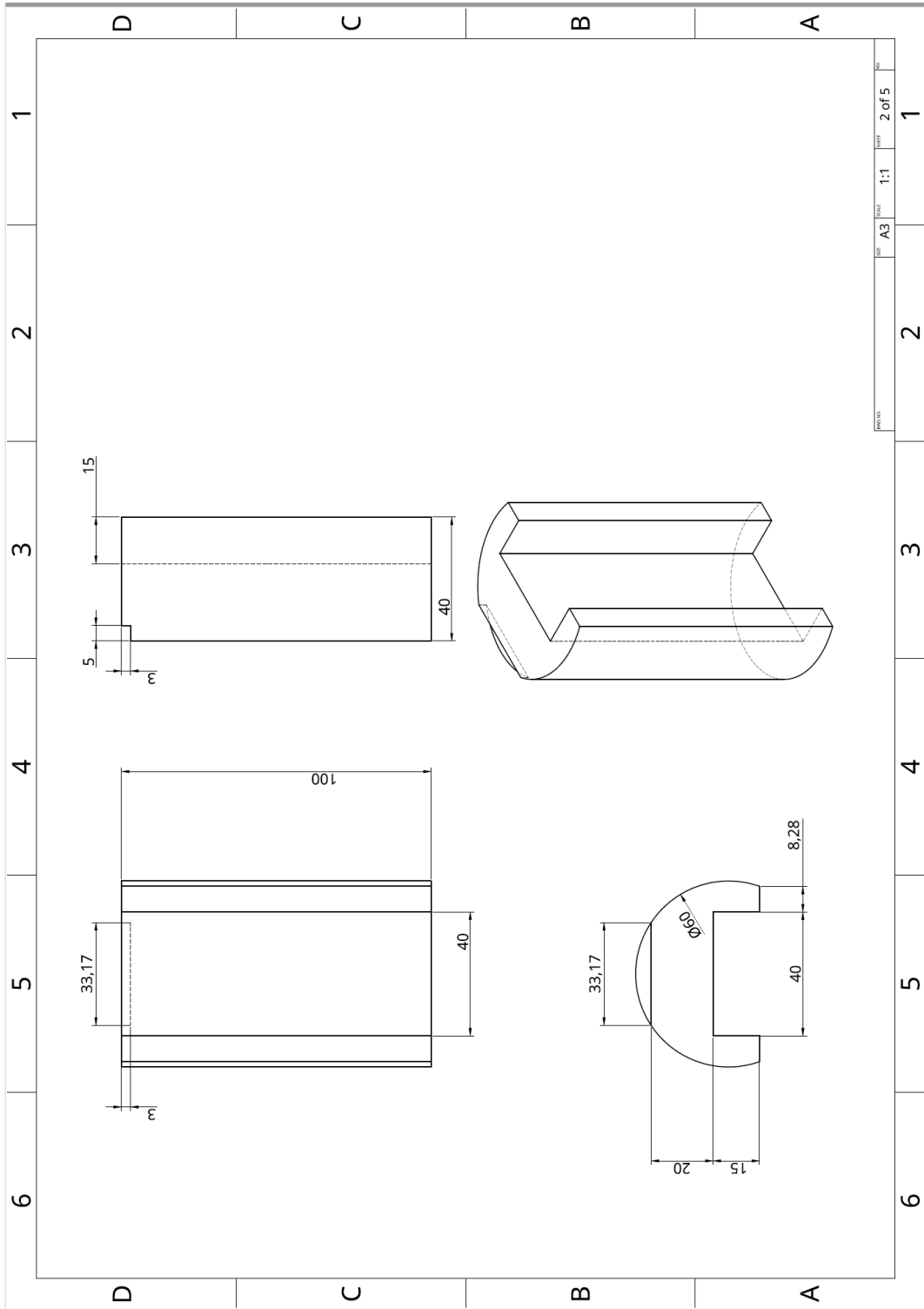


ALL DIMENSIONS IN MM

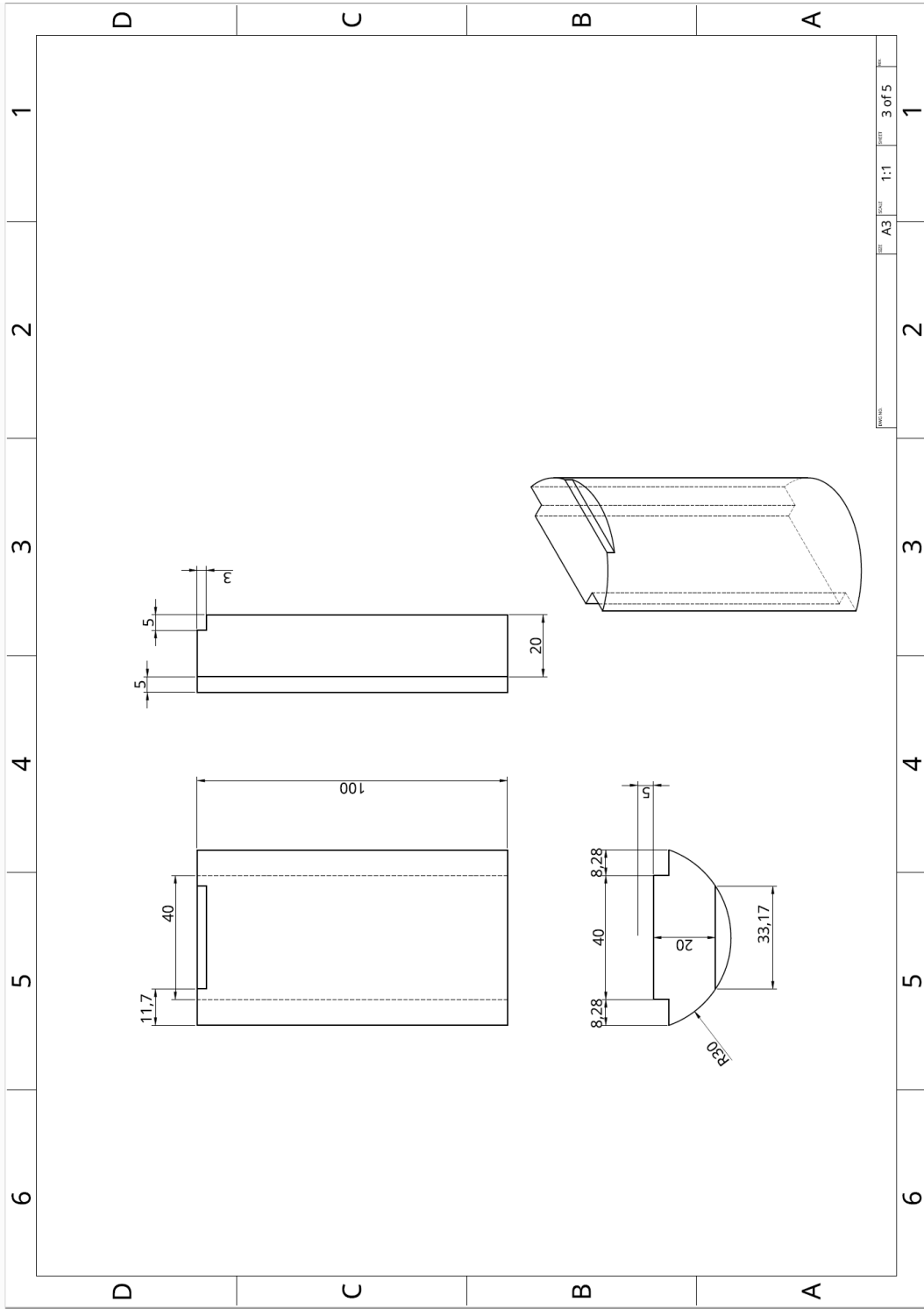
### 3- Design for Ramming Paste Extrusion Through a Nozzle

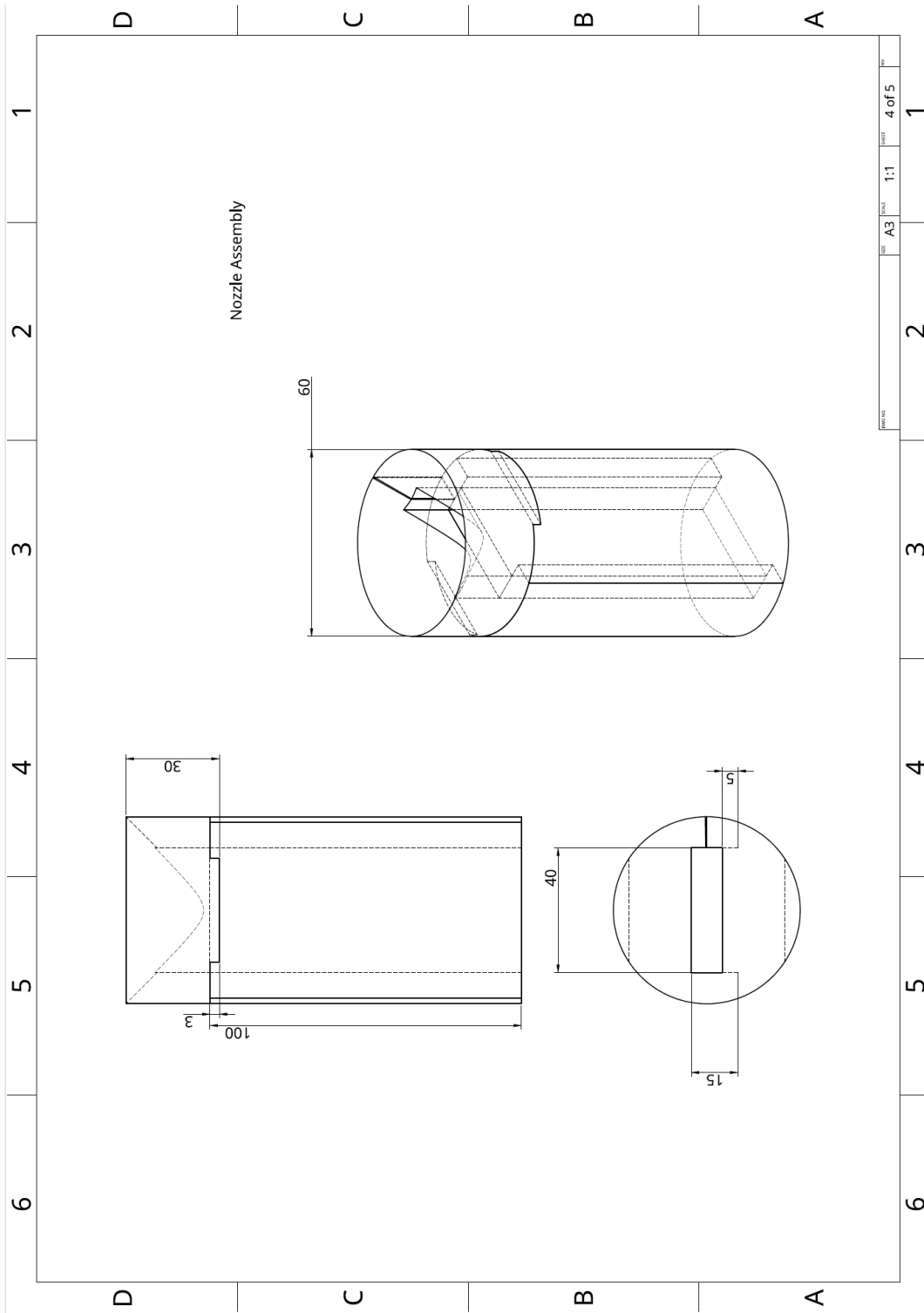
#### a. 45° Nozzle



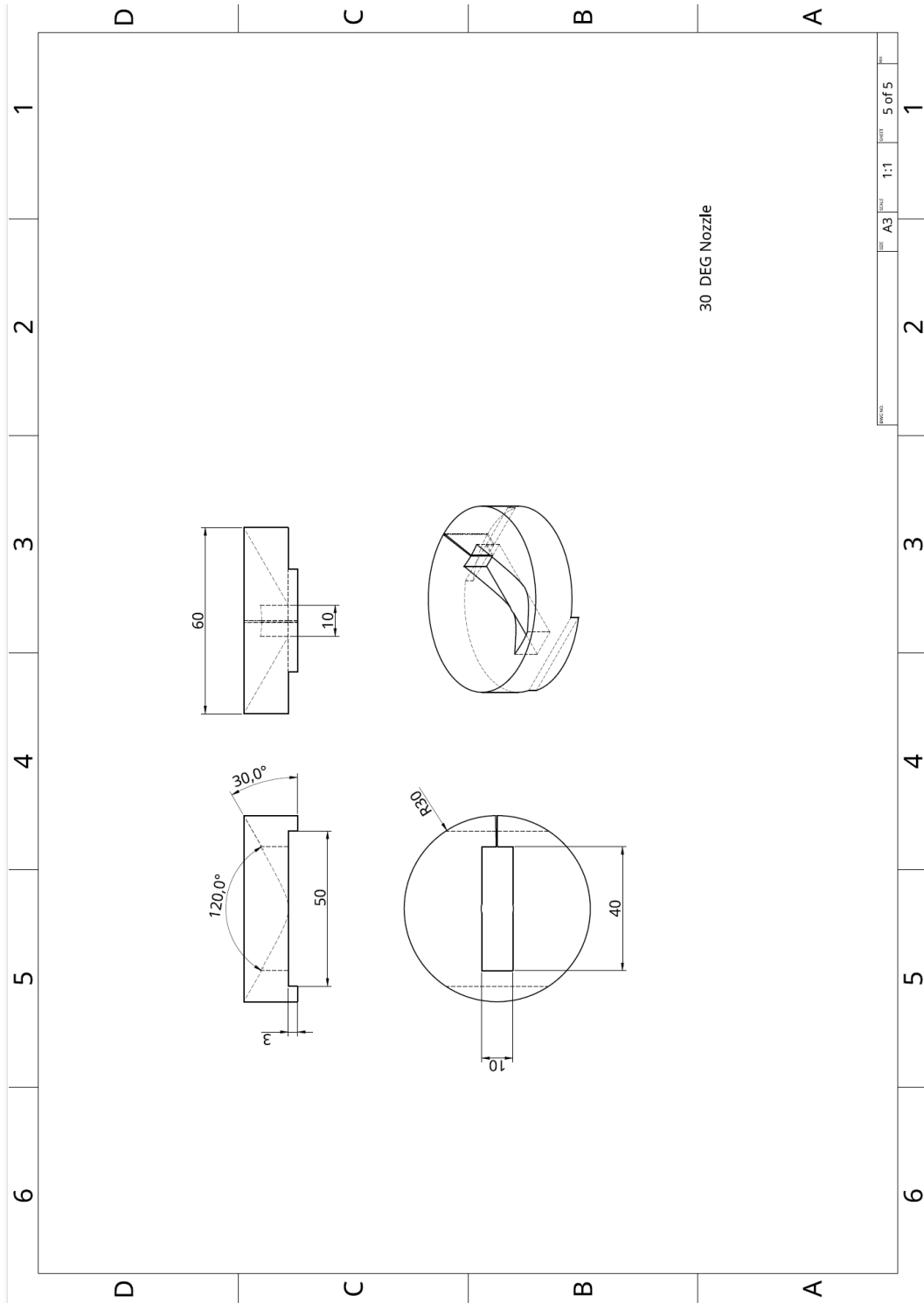


REV	A3	DATE	1:1	QUANTITY	2 of 5	NO.
1						



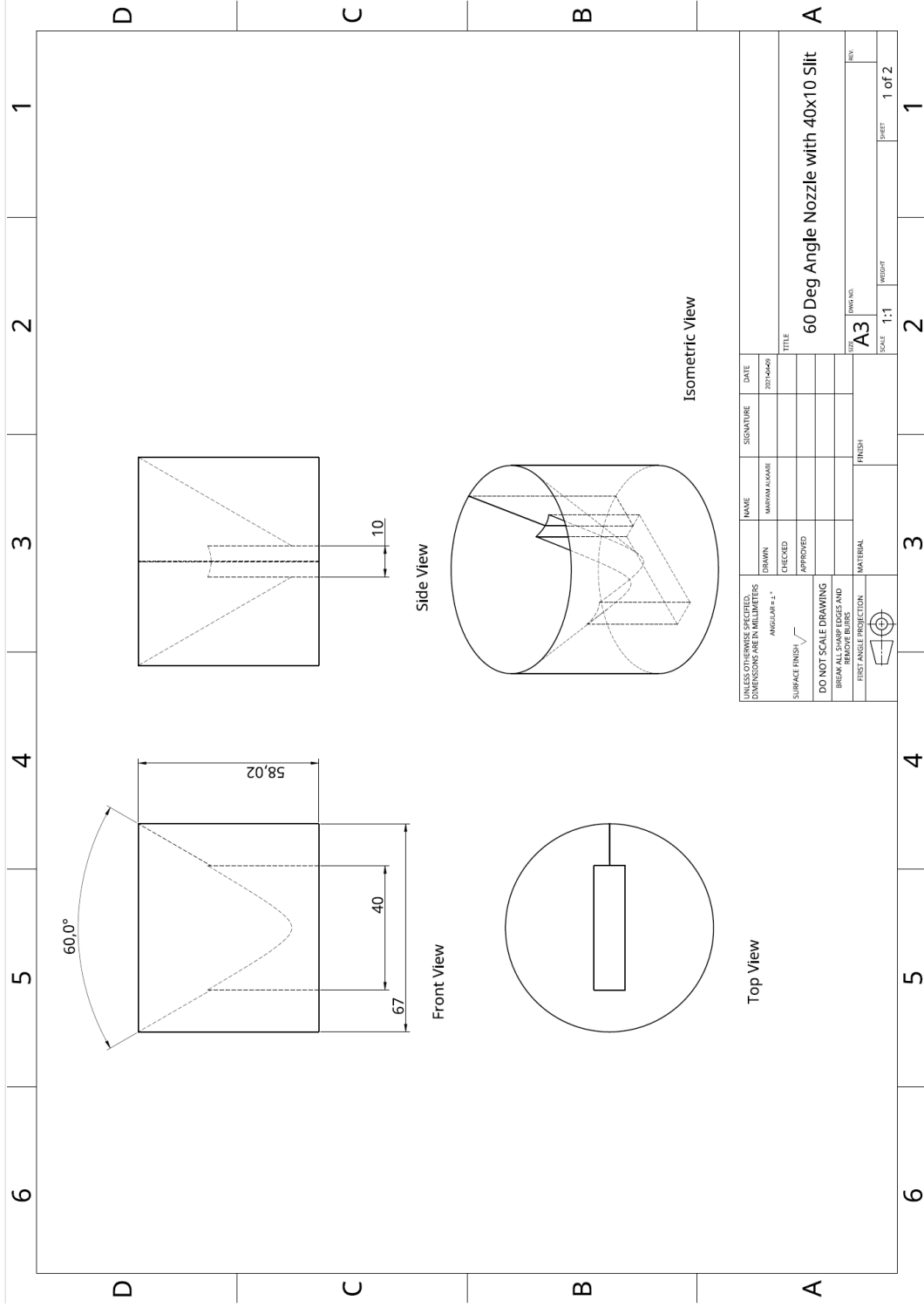


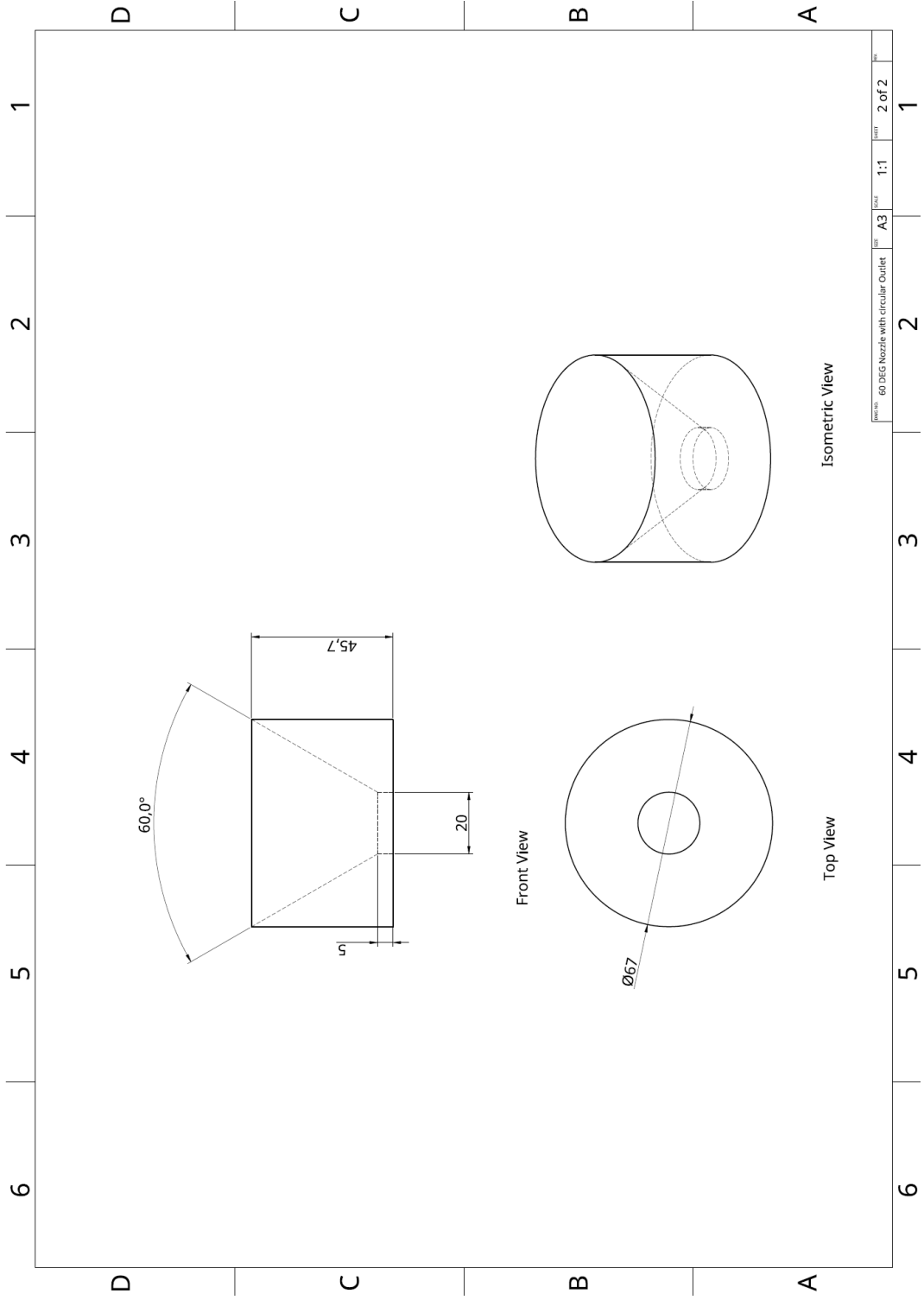
b. 30° Nozzle

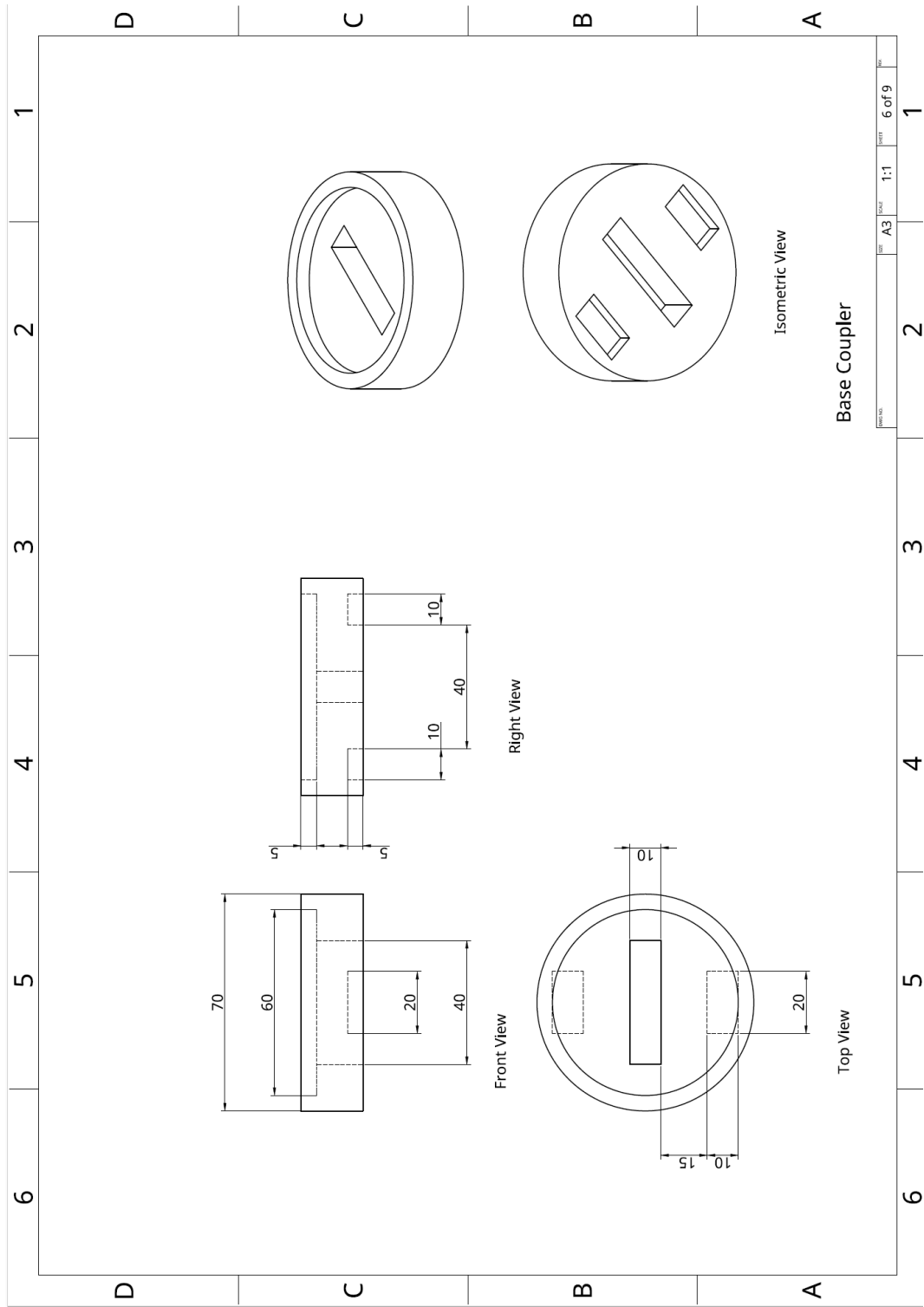


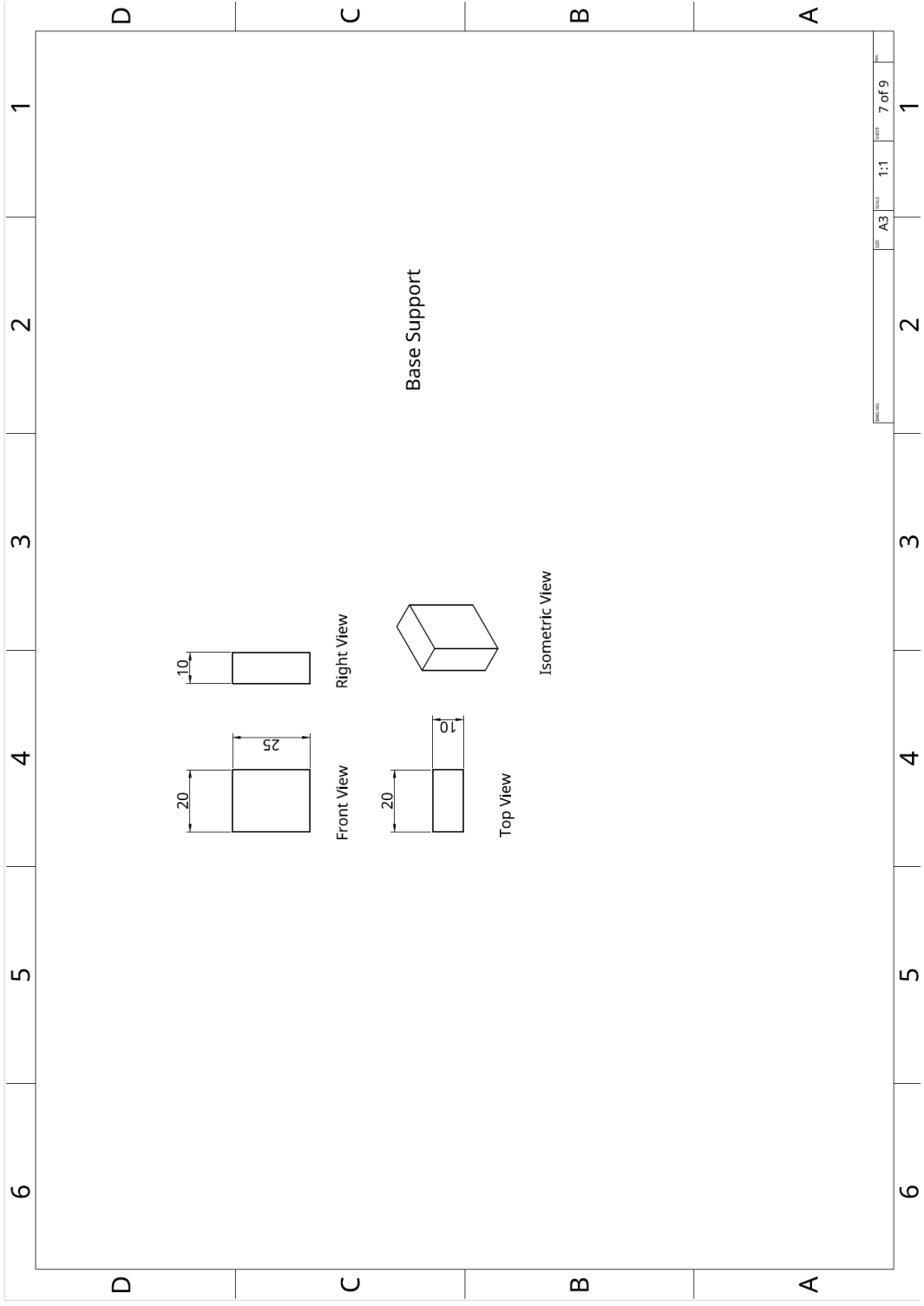


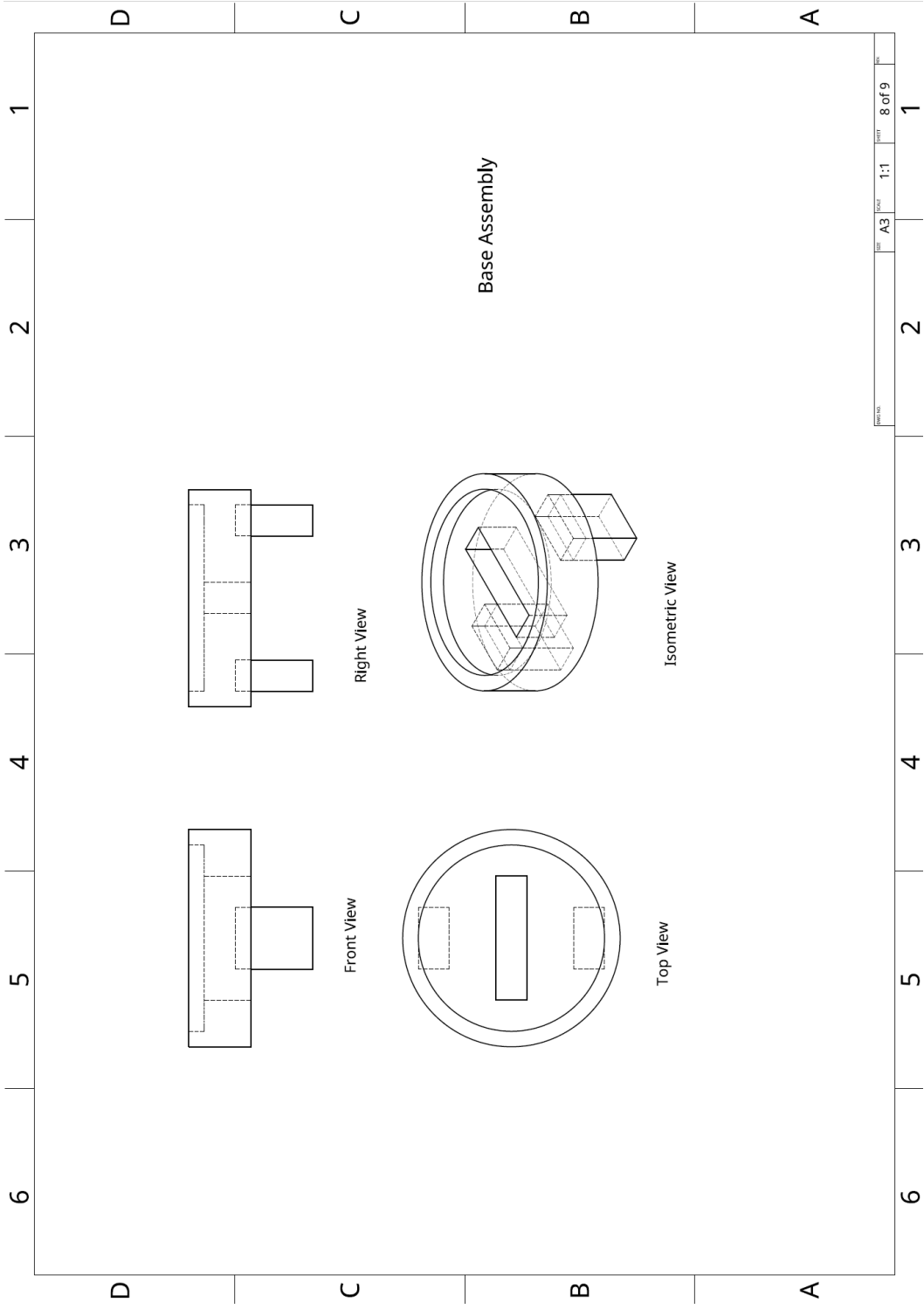


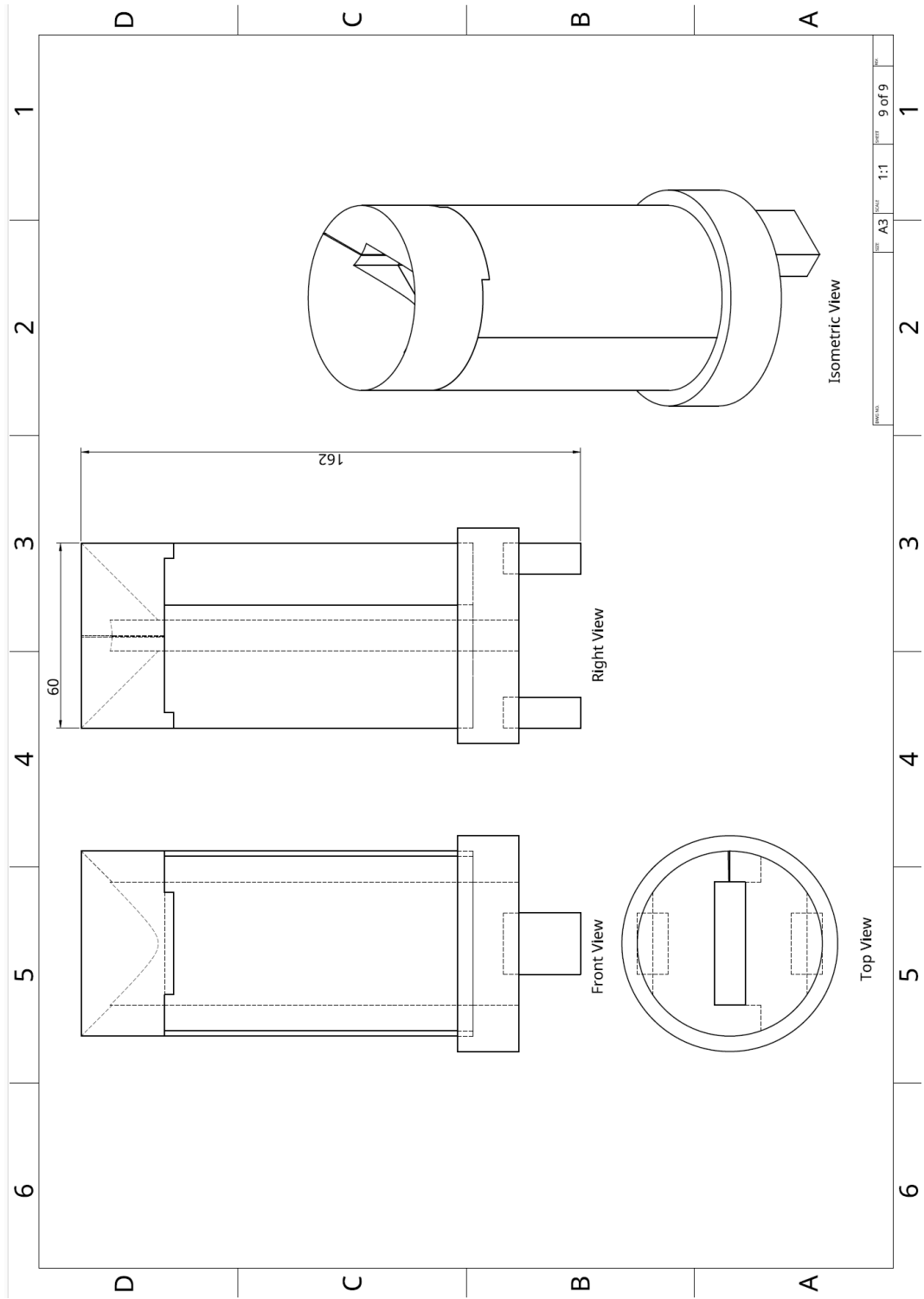






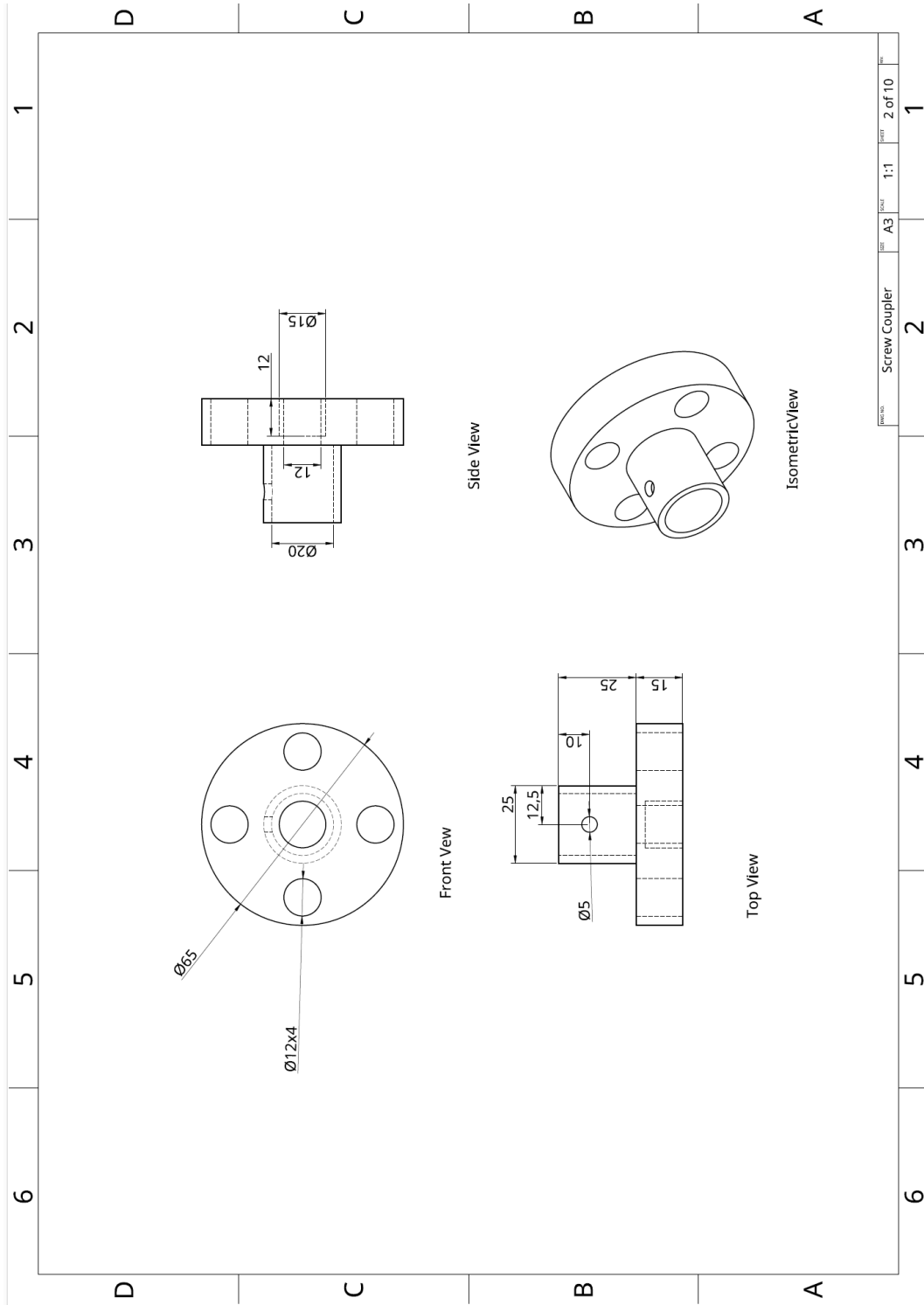


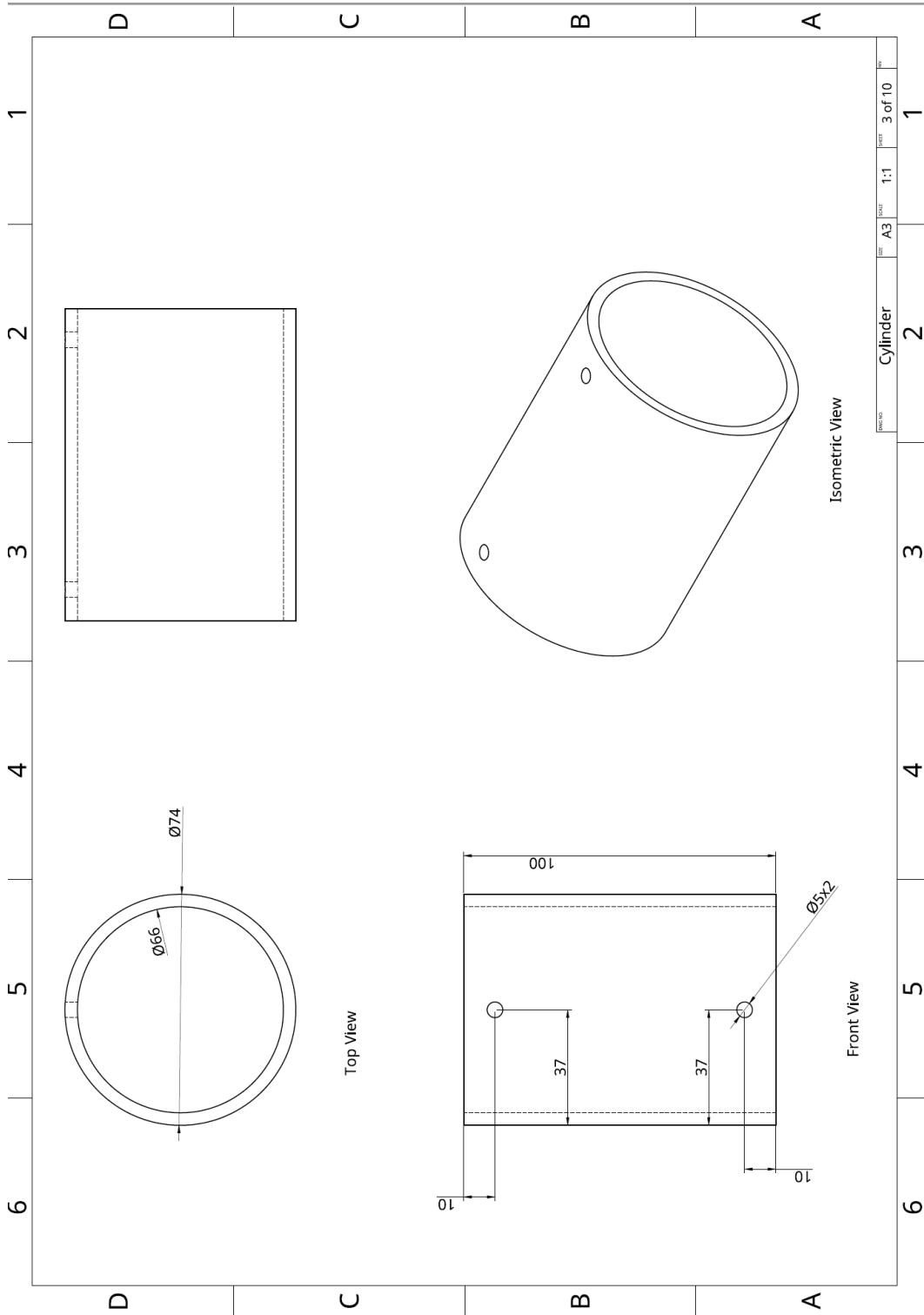












6

5

4

3

2

1

A

B

C

D

Isometric View

Front View

Top View

6

5

4

3

2

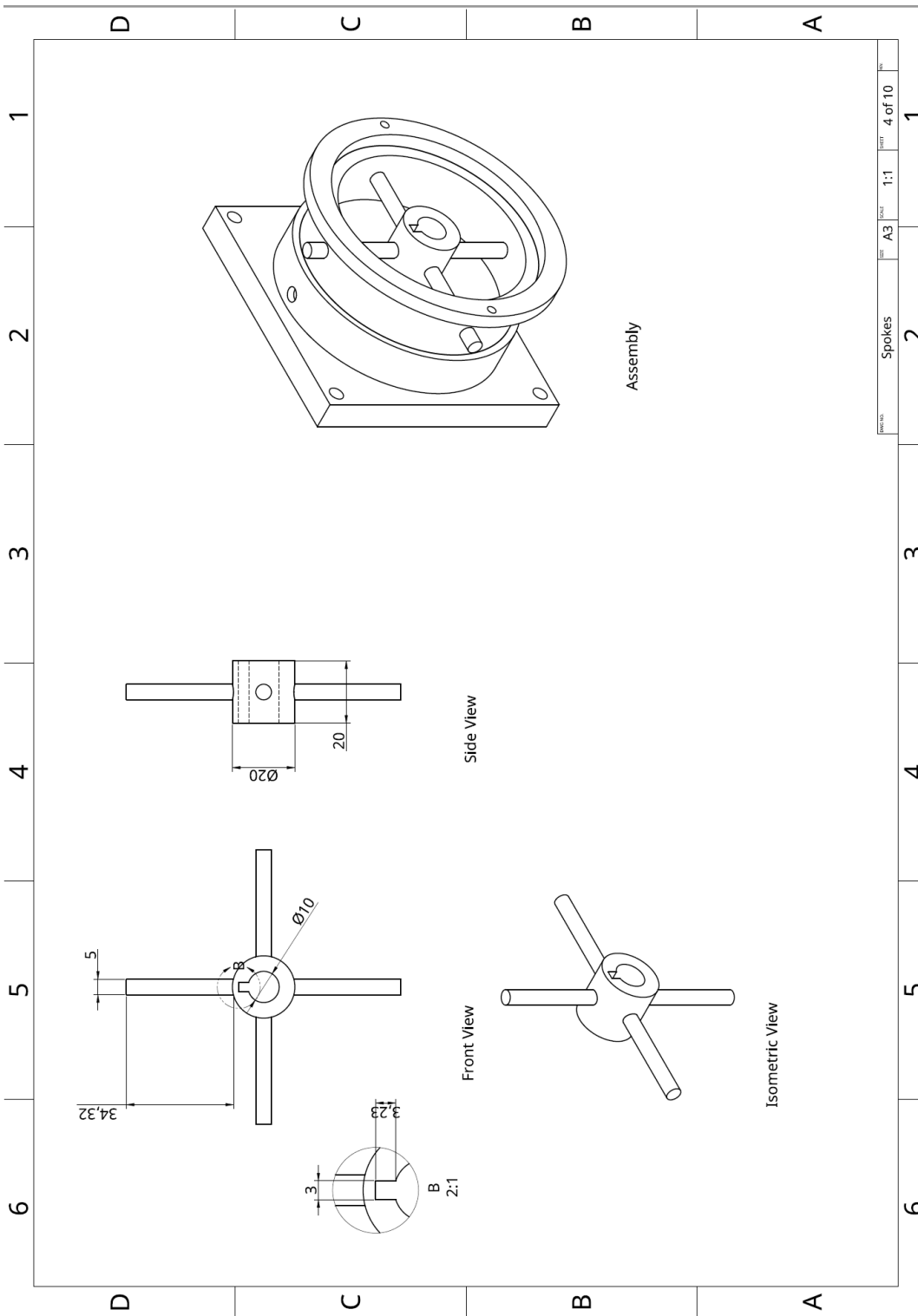
1

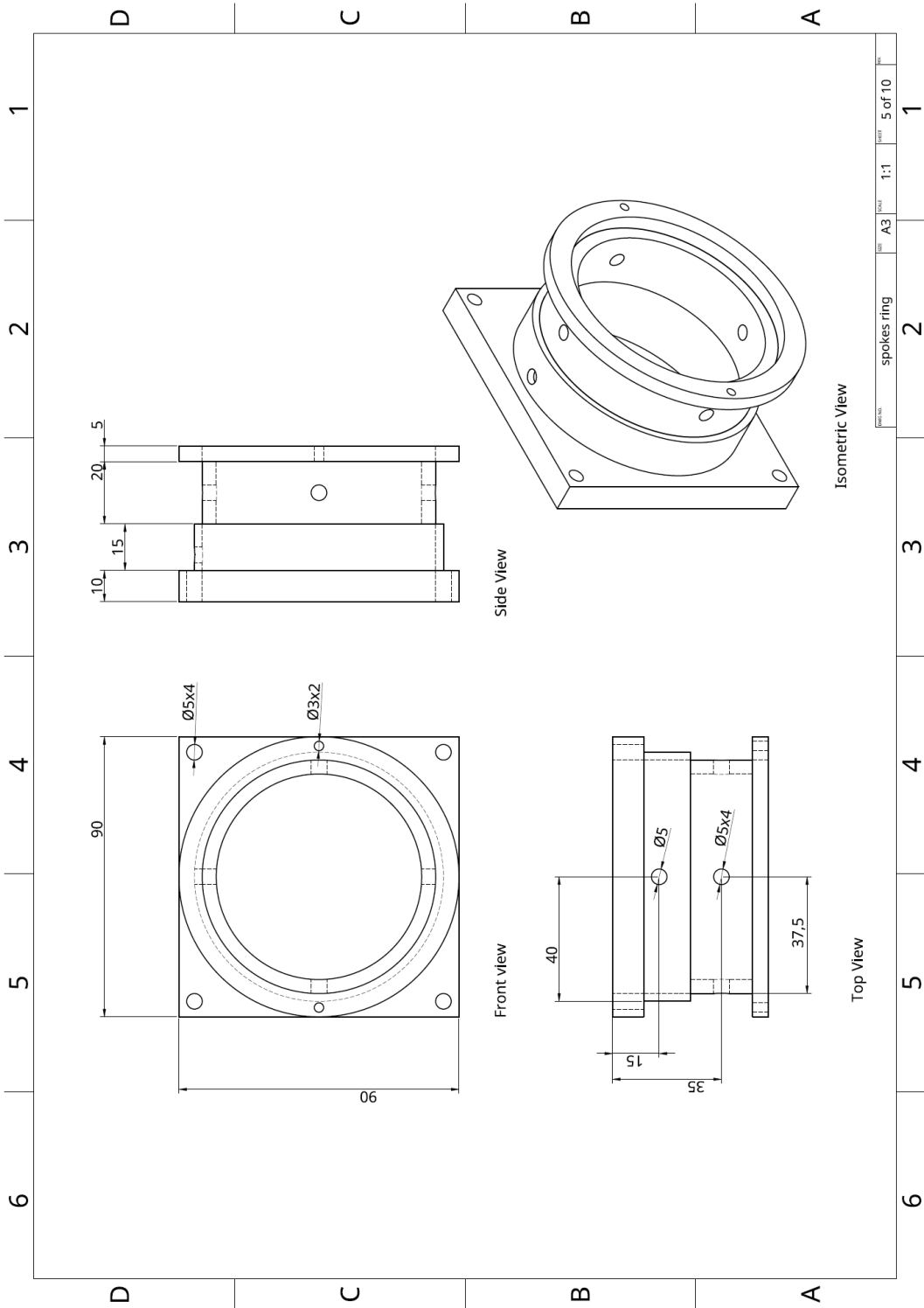
DATE	BY	CHKD	SCALE	SHEET	TOTAL
			1:1	3 of 10	10

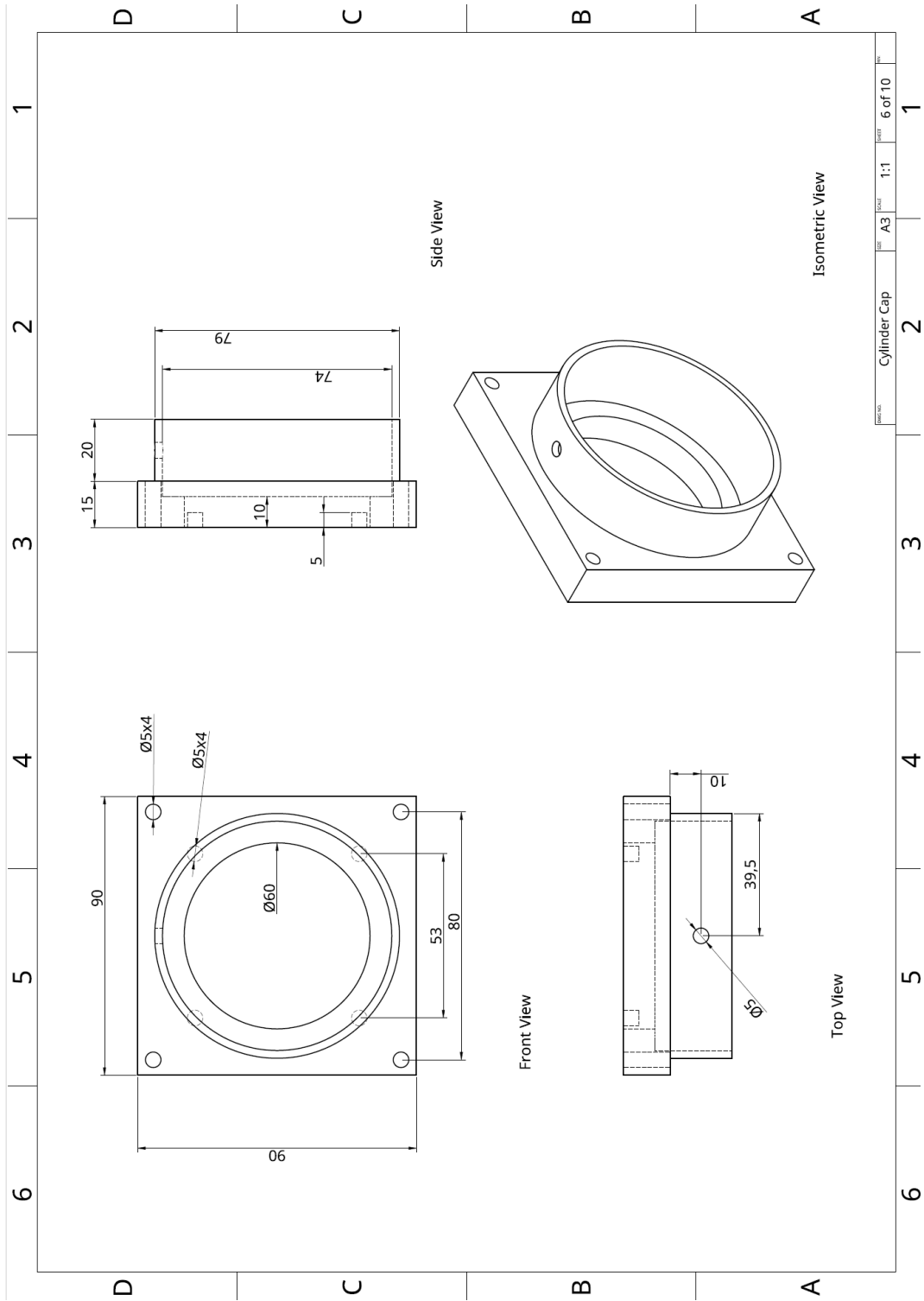
Cylinder

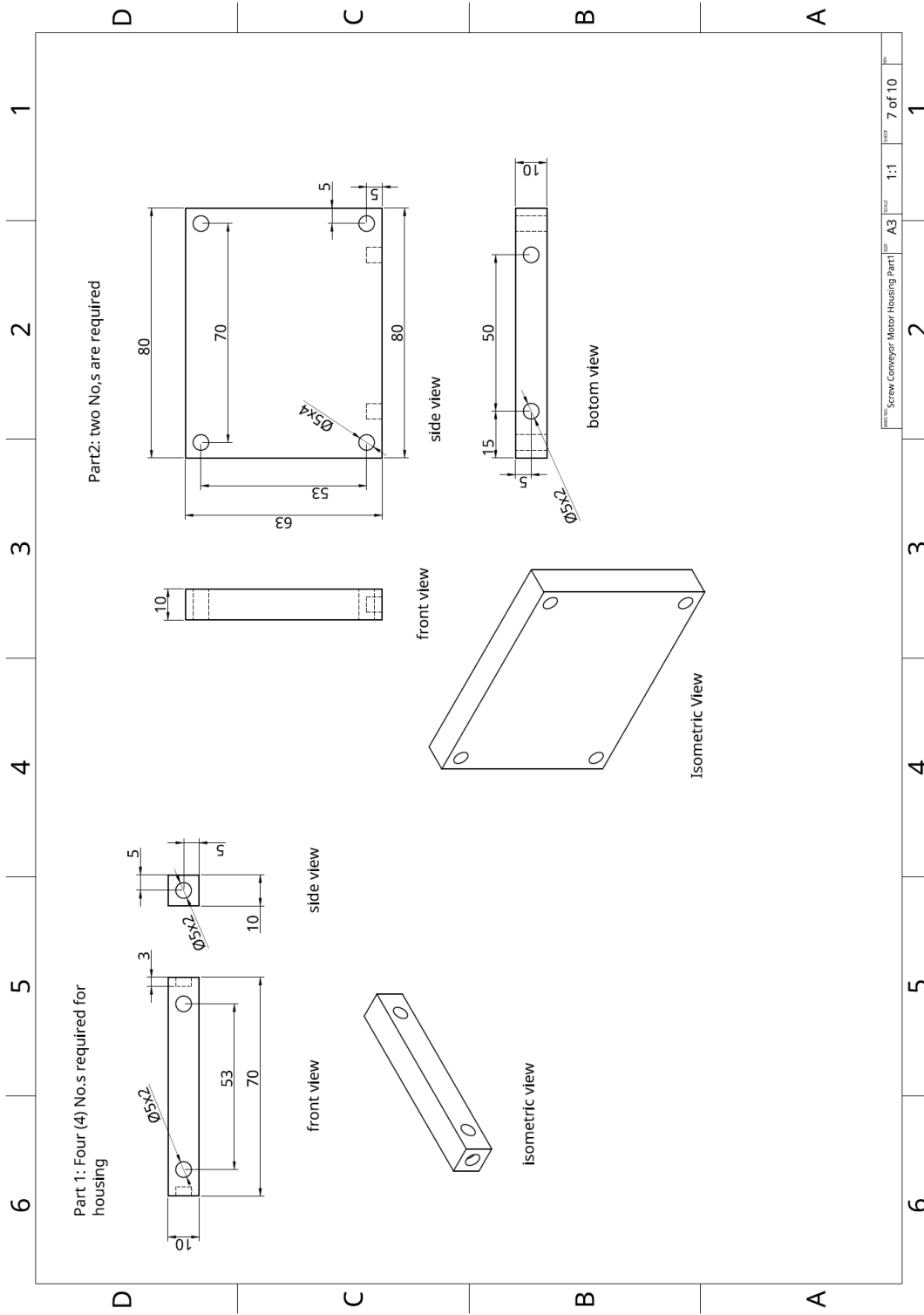
3 of 10

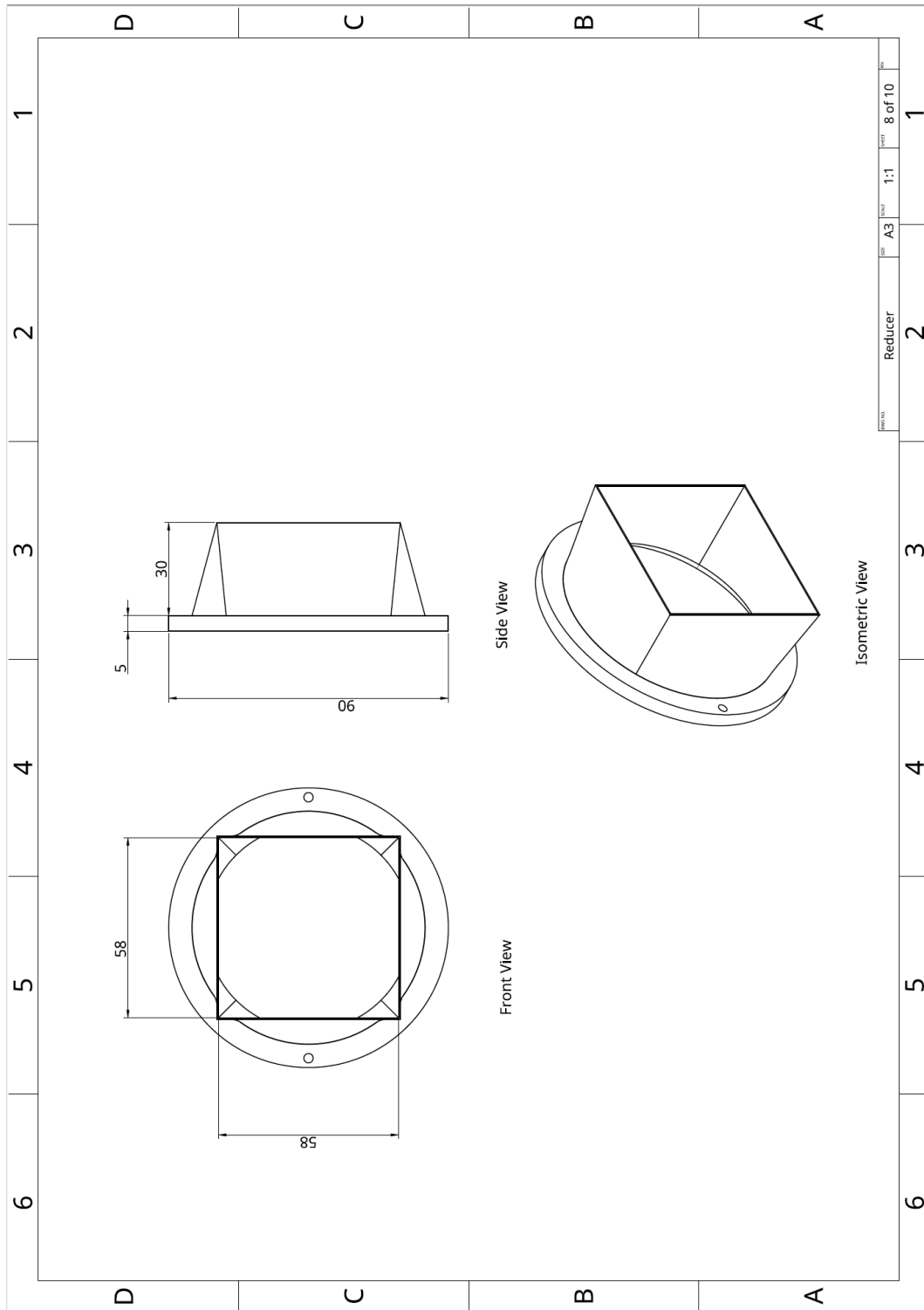
10

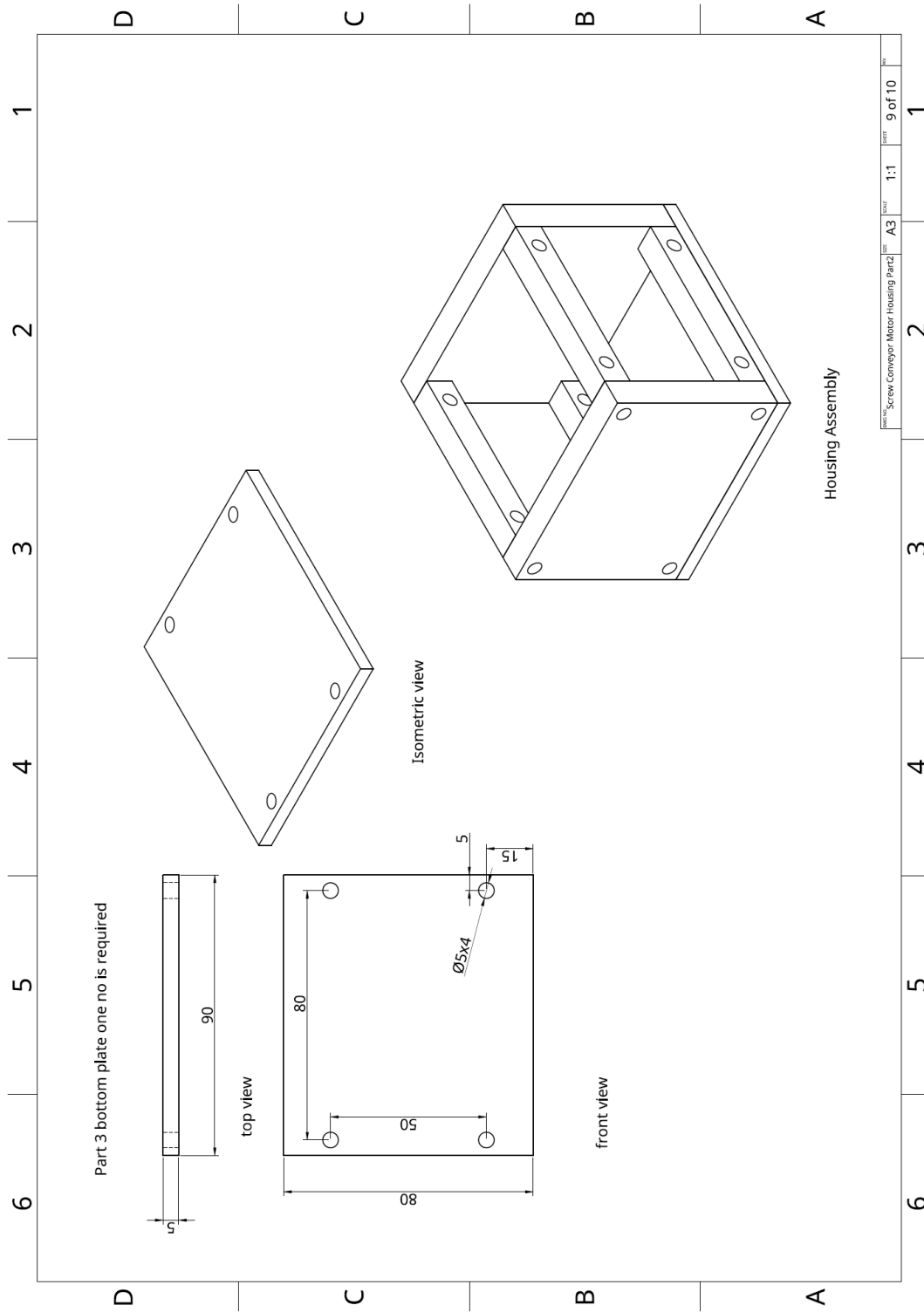




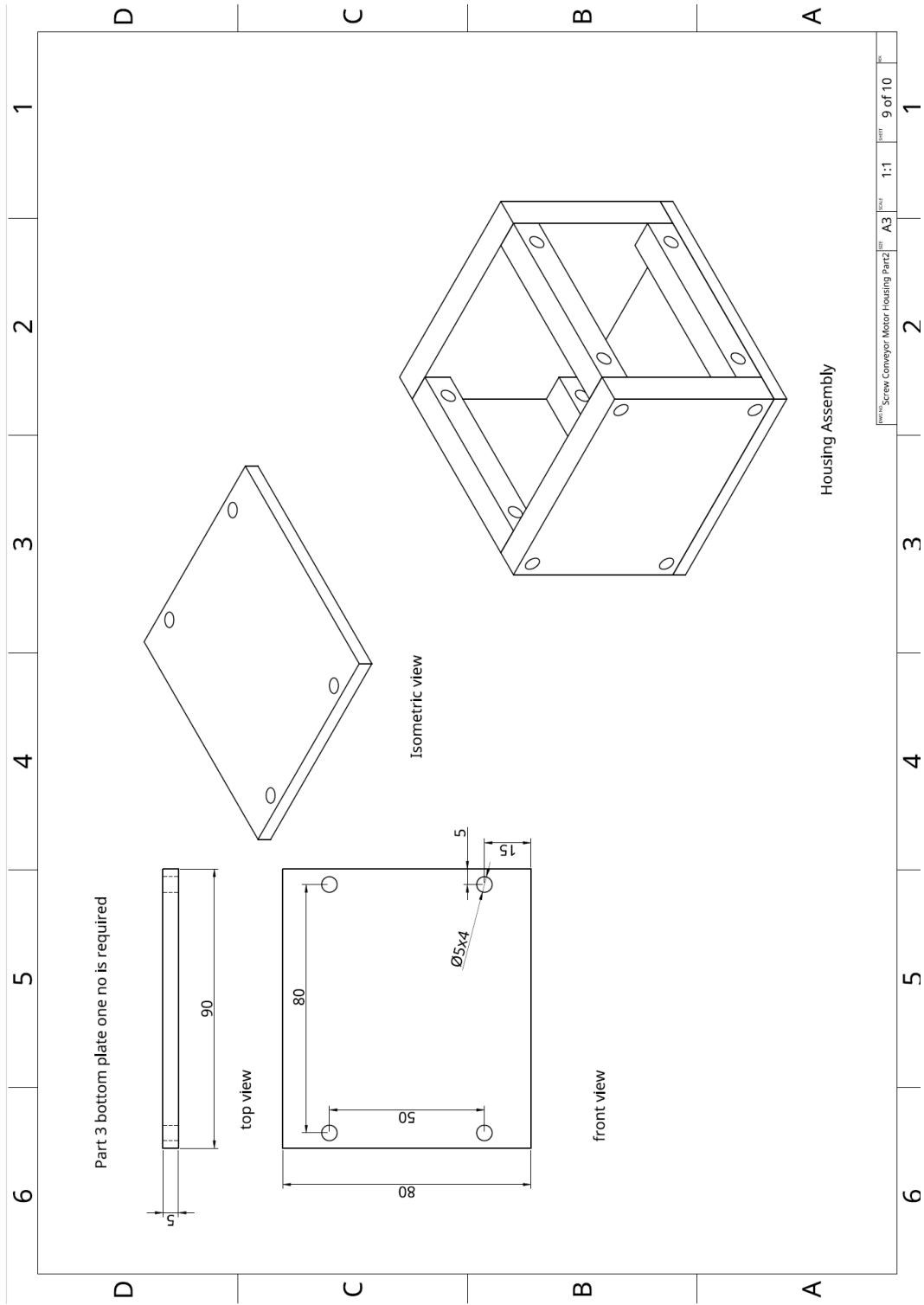


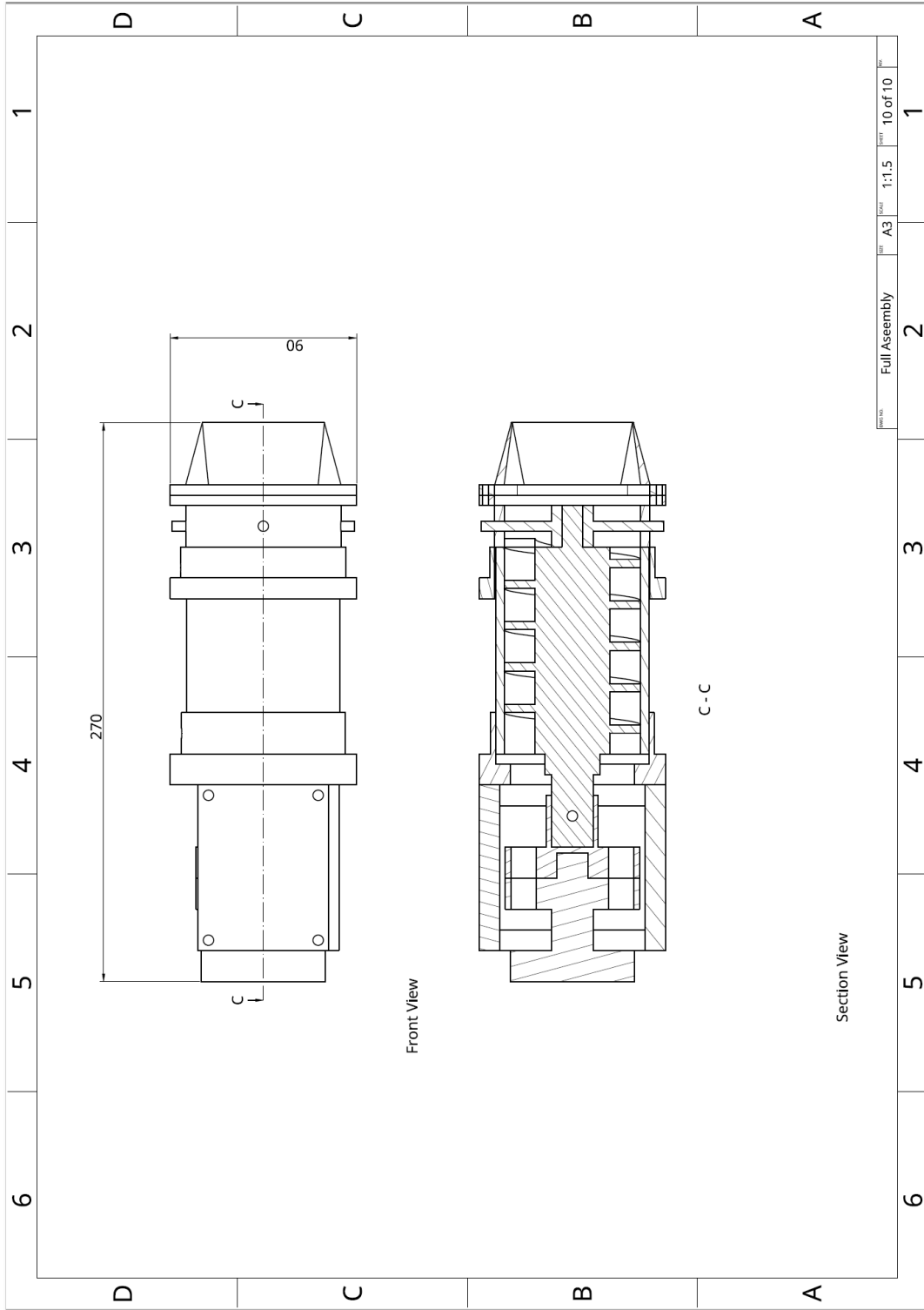






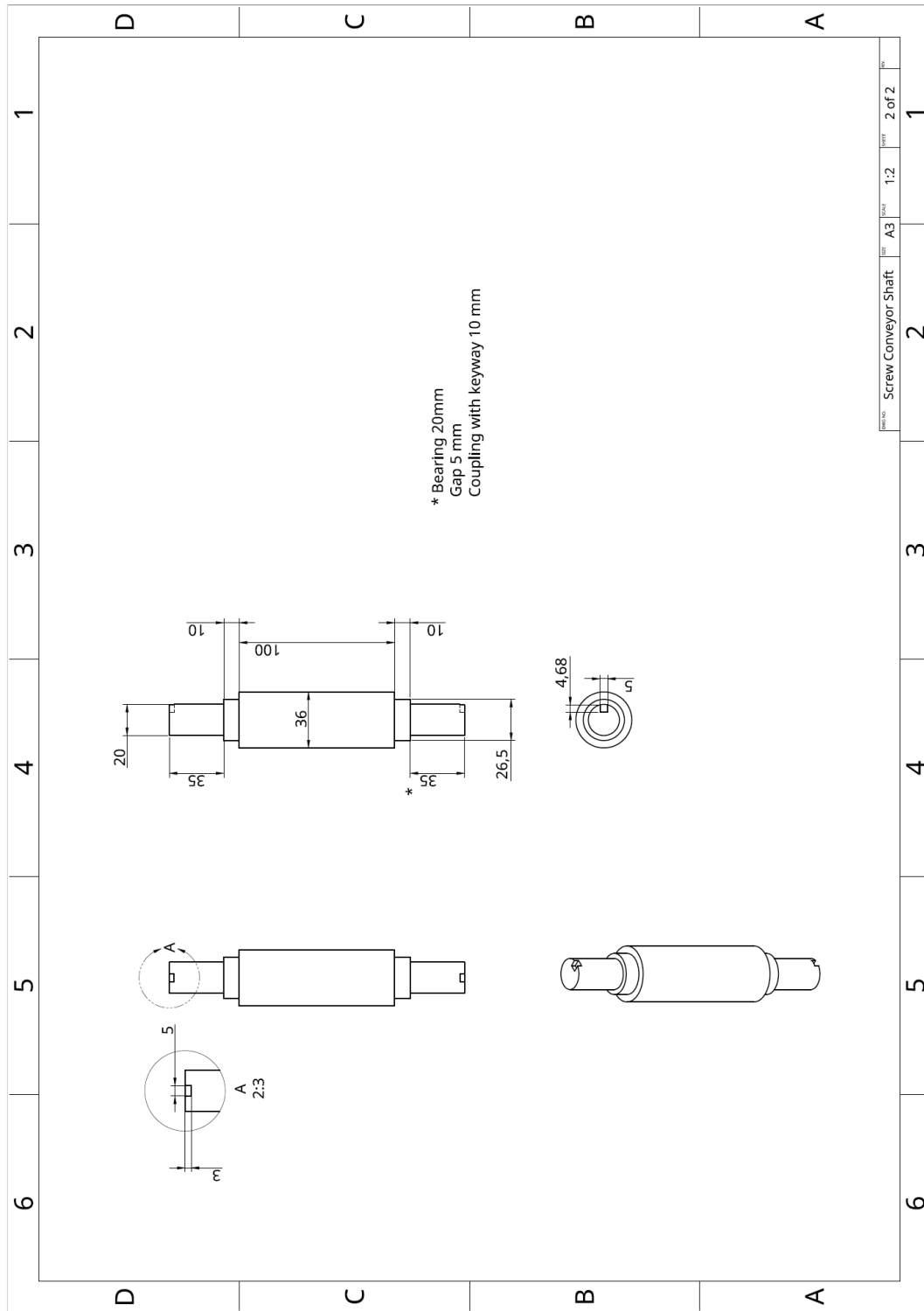






DATE	ISS	SCALE	SHEET	TOTAL
	A3	1:1.5	10 of 10	10

Full Assembly



Screw Conveyor Shaft A3 1:2 2 of 2

